Aus der Medizinischen Klinik und Poliklinik III
der Ludwig-Maximilians-Universität München
Direktor: Prof. Dr. Dr. Michael von Bergwelt
und der Abteilung Genvektoren des
Helmholtz Zentrums München

Functional Characterization of STAT6 Mutations in Follicular Lymphoma

Dissertation
zum Erwerb des Doktorgrades der Naturwissenschaften
an der Medizinischen Fakultät
der Ludwig-Maximilians-Universität München

vorgelegt von
Michael Bösl
aus Nürnberg
2018

Gedruckt mit Genehmigung der Medizinischen Fakultät der Ludwig-Maximilians-Universität München

Betreuerin: PD Dr. rer. nat. Ursula Zimber-Strobl

_____

(Ursula Zimber-Strobl)

Zweitgutachter: Prof. Dr. rer. nat. Gunnar Schotta

Dekan: Prof. Dr. med. dent. Reinhard Hickel

Tag der mündlichen Prüfung: 19.12.2018

Eidesstattliche Versicherung

Ich erkläre hiermit an Eides statt, dass ich die vorliegende Dissertation mit dem Thema

Functional Characterization of STAT6 Mutations in Follicular Lymphoma

selbständig verfasst, mich außer der angegebenen keiner weiteren Hilfsmittel bedient und alle Erkenntnisse, die aus dem Schrifttum ganz oder annähernd übernommen sind, als solche kenntlich gemacht und nach ihrer Herkunft unter Bezeichnung der Fundstelle einzeln nachgewiesen habe.

Ich erkläre des Weiteren, dass die hier vorgelegte Dissertation nicht in gleicher oder in ähnlicher Form bei einer anderen Stelle zur Erlangung eines akademischen Grades eingereicht wurde.

München, 25.07.2018 _____

(Michael Bösl)

To my wife Hannah and my family Irmgard, Michael and Fabian.

Abstract

Follicular lymphoma (FL) is among the most common Non-Hodgkin lymphomas (NHL) worldwide. Its highly variable clinical course is determined by the molecular heterogeneity of the tumor cells and complex interactions with the microenvironment. Interleukin (IL)-4 producing T follicular helper cells (TFH) have been identified as a key component of the malignant B-cell niche. Moreover, IL-4/STAT6 signaling is one of the most frequently dysregulated pathways, but the underlying molecular mechanisms and therapeutic vulnerabilities remain to be explored.

In a cohort of 258 patients with advanced stage FL, STAT6 mutations were detected in 13% of cases, all clustered within the DNA binding domain. Gene expression data and immunohistochemistry of primary patient samples showed upregulation of IL-4/STAT6 target genes in STAT6 mutant cases, including *FCER2*/CD23. Functional experiments revealed that IL-4 stimulated expression of *FCER2*/CD23 was enhanced in representative NHL cell lines stably expressing STAT6 mutants, and associated with increased nuclear accumulation of mutant phospho-STAT6. Of note, a STAT6 polymorphism-like variant within the DNA binding domain had a similar gain-of-function phenotype.

RNA sequencing of IL-4-stimulated STAT6 mutant and wild-type lymphoma cell lines identified PARP14, a transcriptional co-activator of STAT6, as the top differentially expressed gene. Bioinformatic analysis discovered PARP14 as a previously unidentified, mutation-specific STAT6 target gene. Reporter assays demonstrated increased transactivation activity of mutant STAT6 at the PARP14 promoter, suggesting a positive feed forward system. Inhibition of PARP and knockdown of PARP14 attenuated the STAT6 gain-of-function phenotype. In summary, these results suggest PARP14 as a novel therapeutic target in STAT6 mutant FL.

Zusammenfassung

Das Follikuläre Lymphom (FL) gehört zu den häufigsten Non-Hodgkin-Lymphomen (NHL) weltweit. Klinische Herausforderung der Erkrankung sind sein variabler klinischer Verlauf, welcher durch eine große molekulare Heterogenität der Tumoren und eine komplexe Interaktion zwischen den Tumorzellen und den umliegenden, benignen Immunzellen begründet ist. Die Interleukin (IL)-4 produzierenden follikulären T-Helferzellen (TFH) haben eine besondere Bedeutung, da die IL-4/STAT6 Signalkaskade im FL sehr häufig von malignen Veränderungen betroffen ist. Die zugrundeliegenden molekularen Mechanismen und Möglichkeiten für gerichtete Therapieoptionen innerhalb dieses Signalwegs sind jedoch noch nicht ausreichend erforscht.

In einer Kohorte von 258 Patienten mit fortgeschrittenem FL wurden in 13% der Fälle STAT6 Mutationen detektiert, wobei alle Mutationen in der DNA-Bindungsdomäne lokalisiert waren. Genexpressionsdaten und immunhistochemische Färbungen von primären Patientenproben zeigten in den Fällen mit mutiertem STAT6 eine Überexpression von IL-4/STAT6-regulierten Genen, darunter *FCER2*/CD23. In NHL Zelllinien, welche stabil mutiertes STAT6 exprimieren, war ebenfalls eine IL-4 induzierte Überexpression von *FCER2*/CD23 zu sehen. Dies ging mit einer verstärkten nukleären Akkumulation von mutiertem pSTAT6 im Vergleich zu Wildtyp pSTAT6 einher. Interessanterweise zeigte eine STAT6 Variante innerhalb der DNA-Bindungsdomäne, welche als STAT6 Polymorphismus bekannt ist, einen vergleichbaren, gain-of-function Phänotyp wie die STAT6 Mutationen.

Der Vergleich der RNA-Expressionsprofile von STAT6 mutierten und STAT6 Wildtyp NHL Zelllinien, die mit IL-4 stimuliert wurden, identifizierte PARP14 als das Gen, welches am signifikantesten differentiell exprimiert wurde. PARP14 wurde bereits als ein Co-Aktivator des STAT6 Transkriptionskomplexes beschieben. Die bioinformatische Untersuchung der PARP14 Promotor-Region identifizierte STAT6 Bindestellen innerhalb des PARP14 Promotors. Reportergen Assays zeigten, dass mutiertes STAT6 den Promotor besser als

wildtyp STAT6 aktiviert, was eine positive Rückkopplung nahe legte. Chemische Inhibition von PARP und Gen-Knockdown von PARP14 führten zu einer Aufhebung des IL-4 induzierten gain-of-function Phänotyps der STAT6 Mutationen. Diese Daten weisen darauf hin, dass die Inhibition von PARP14 als neuartige Therapieoption von FL mit mutierten STAT6 näher untersucht werden sollte.

Contents

List of Figures

List of Tables

Abbreviations

ANOVA	Analysis of variance
APC	Allophycocyanin
att	Attachment site
BCA	Bicinchoninic acid
BCCA	British Columbia Cancer Agency
BCR	B cell receptor
bp	Base pair
CCL	CC chemokine ligand
CD	Cluster of differentiation
cDNA	Complementary DNA
ChIP	Chromatin immunoprecipitation
CHOP	Cyclophosphamide, doxorubicin, vincristine, prednisone
CMV	Cytomegalovirus
Ct	Cycle threshold
CTL	Cytotoxic T lymphocytes
CVP	Cyclophosphamide, vincristine, prednisone
CXCL	CXC chemokine ligand
CXCR	CXC chemokine receptors
DAPI	4',6-diamidino-2-phenylindole
DASL	cDNA-mediated annealing, selection, extension, and ligation
DI	Deionized
DLBCL	Diffuse large B cell lymphoma
DNA	Deoxyribonucleic acid
ECL	Enhanced chemilumescent
ECOG	Eastern Cooperative Oncology Group
EMSA	Electrophoretic mobility shift assay

FACS	Fluorescence-activated cell sorting
FBS	Fetal bovine serum
FC	Fold change
FDC	Follicular dendritic cells
FDR	False discovery rate
FFPE	Formalin-fixed, paraffin-embedded
FFS	Failure-free survival
FL	Follicular lymphoma
FLIPI	Follicular Lymphoma International Prognostic Index
FRC	Fibroblastic reticular cells
GC	Germinal center
gDNA	Genomic DNA
GLSG	German Low-Grade Lymphoma Study Group
GSEA	Gene Set Enrichment Analysis
HL	Hodgkin lymphoma
Ig	Immunoglobulin
IHC	Immunohistochemistry
IL	Interleukin
IL4R	IL-4 receptor
IP	Immunoprecipitation
IRS	Insulin receptor substrate
JAK	Janus kinase
LB	Lysogeny broth
LDS	Lithium dodecyl sulfate
MeOH	Methanol
MHC	Major histocompatibility complex
MOPS	3-(N-morpholino)propanesulfonic acid
mRNA	Messenger RNA
NHL	Non-Hodgkin lymphoma
NTC	Non-target control
OS	Overall survival

PAGE	Polyacrylamide gel electrophoresis
PARP	Poly ADP-ribose polymerase
PCA	Principal components analysis
pCIG	pHAGE-CMV-MCS-IRES-ZsGreen
PCR	Polymerase chain reaction
PFS	Progression-free survival
PMBL	Primary mediastinal large B cell lymphoma
pSTAT6	Phospho-STAT6
PVDF	Polyvinylidene difluoride
qPCR	Quantitative PCR
RIPA	Radioimmunoprecipitation assay
RNA-seq	RNA sequencing
RT	Room temperature, reverse transcription
sCD23	Soluble CD23
SCRB-seq	Single cell RNA barcoding and sequencing
SDS	Sodium dodecyl sulfate
shRNA	Short hairpin RNA
SNV	Single-nucleotide variant
SOCS	Suppressor of cytokine signaling
STAT	Signal transducer and activator of transcription
TAM	Tumor-associated macrophage
TBS	Tris-buffered saline
TBS-T	TBS with 0.1% (V/V) Tween20
TD	T cell-dependent activation
TFH	T follicular helper cells
Th2	T helper cell type 2
TI	T cell-independent activation
Treg	Regulatory T cells
TSS	Transcription start site
VAF	Variant allele frequency

1 Introduction

1.1 Follicular lymphoma (FL): A clinical challenge

1.1.1 Epidemiology and clinical features

Follicular lymphoma (FL) is a malignant tumor arising from germinal center (GC) B lymphocytes. It is among the most common subtypes of Non-Hodgkin lymphoma (NHL) with an incidence rate of 3.18 cases per 100 000 people/year in the USA and 2.18 cases per 100 000 people/year in Europe.[1,2] The median age at diagnosis is 65 years and the incidence increases with age.[3]

Diagnosis of FL relies on assessment of lymphoma tissue by the pathologist. Typically, the tumor presents with a follicular growth pattern and consists of centrocytes and centroblasts. Similar to Hodgkin lymphoma (HL) and other NHL, FL is classified by the Ann Arbor staging system.[4] Stages I and II are referred to as early or limited stages of FL (figure 1.1). However, most patients (75-85%) are diagnosed with advanced stage disease (Stages III and IV), and are still considered incurable.[5]

1.1.2 Clinical course and prognosis of FL

The clinical course of the disease is highly heterogeneous. The current median overall survival (OS) of patients with FL is more than 18 years.[7] However, a 20% subpopulation has early progression of disease (defined as within 2 years after initial immunochemotherapy), aggressive clinical course, and short OS.[8] Moreover, 30-40% of FL cases undergo histologic transformation towards an aggressive lymphoma within 10 years (3% per year).[9] Identification of patients with high-risk FL is crucial and treatment stratification is one of the most pressing challenges today.

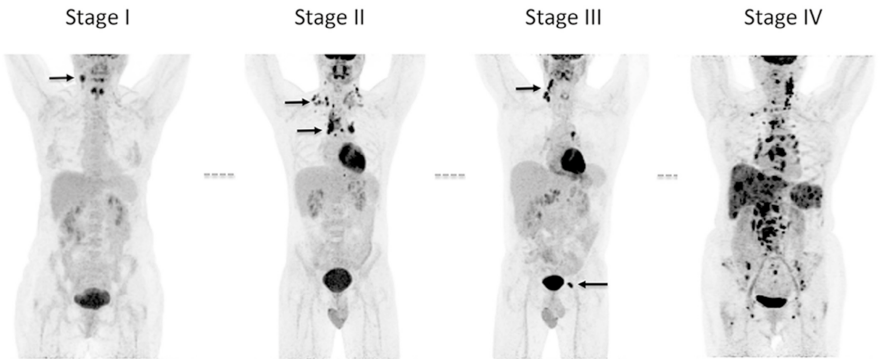

Figure 1.1
Ann Arbor staging of lymphoma. PET/CT (Positron emission tomography–computed tomography; allows to trace glucose metabolism, which is increased in tumors (using fluorodeoxyglucose (^{18}F))) images of four patients with Hodgkin lymphoma at stage I-IV. The grey dashed line illustrates the postion of the diaphragm. Black arrows mark the affected lymph node regions. In stage I one lymph node, in stage II multiple lymph nodes above the diaphragm, and in stage III multiple lymph nodes on both sides of the diaphragm are involved. Stage IV is characterized by involvement of extralymphatic organs (here: liver and bone marrow) in addition to diffuse or disseminated involvement of multiple lymph nodes. Figure from El-Galaly *et al.*[6]

The Follicular Lymphoma International Prognostic Index (FLIPI) is the most widely used and best established prognostic tool based on five clinical risk factors and divides patients with FL into three risk groups (table 1.1 and 1.2).[10]

Table 1.1
Adverse prognostic factors in FL

Age	>60 years
Involved nodal areas	>4
Ann Arbor stage	III or IV
Hemoglobin level	<12.0 g/dl
Serum lactate dehydrogenase level	above normal

Yet, the FLIPI has limitations. For example, it is solely based on clinical risk factors and cannot inform about the underlying tumor biology. In a recent study, Pastore *et al.* established a prognostic model called m7-FLIPI, which included the FLIPI, the Eastern Cooperative Oncology Group (ECOG) performance status, and the mutation status of seven genes (*EZH2*, *ARID1A*, *MEF2B*, *EP300*, *FOXO1*, *CREBBP*, and *CARD11*). In two independent cohorts, including patients with advanced stage disease and in need of treatment, from the German Low-Grade Lymphoma Study Group (GLSG) 2000 and the British Columbia Cancer Agency (BCCA), the m7-FLIPI outperformed risk-stratification by FLIPI alone, FLIPI and ECOG performance status combined, and a model that inclu-

Table 1.2
Risk groups as determined by the Follicular Lymphoma International Prognostic Index (FLIPI)

	Number of adverse factors	10-year OS	Hazard ratio
Low risk	0-1	71%	1.0
Intermediate risk	2	51%	2.3
High risk	>3	36%	4.3

ded only mutations. Overall, this study demonstrated that gene mutations are clinically relevant predictors of treatment outcome.[11]

1.1.3 Current treatment of FL

Treatment strategy of FL depends on the Ann Arbor stage at presentation. For limited stage disease standard treatment is radiation-based therapy, which is currently the only option to potentially cure FL.[12,13] In cases where radiation therapy is not applicable, approaches vary from *watch & wait*, treatment with anti-CD 20 antibody rituximab, or therapy regimes for advanced stage FL.[14]

Patients with advanced stage disease are treated according to the presence and severity of symptoms, tumor burden, as well as patient's condition (figure 1.2).[14] For most patients at this stage immunochemotherapy is indicated. Current chemotherapy regimens include: bendamustine; cyclophosphamide, doxorubicin, vincristine, and prednisone (CHOP); and cyclophosphamide, vincristine, and prednisone (CVP). The addition of rituximab to one of those chemotherapy regimens has been shown to increase response rate, progression-free survival (PFS), and OS compared to chemotherapy alone and is current standard treatment.[15,16] Moreover, two years of rituximab maintenance after initial immunochemotherapy further improves PFS.[17]

Despite these major improvements in therapy through rituximab, and other anti-CD20 antibodies, the majority of patients will ultimately relapse. Current treatment options for relapsed or transformed FL involve immunochemotherapy or stem cell transplantation. However, these aggressive therapies are not applicable for many patients, since they are elderly people with poor prognosis and significant comorbidities. Therefore, it is crucial to implement molecular targeted therapies, which hold promise to be less toxic and are better tolerated. This requires better understanding of the underlying FL biology.

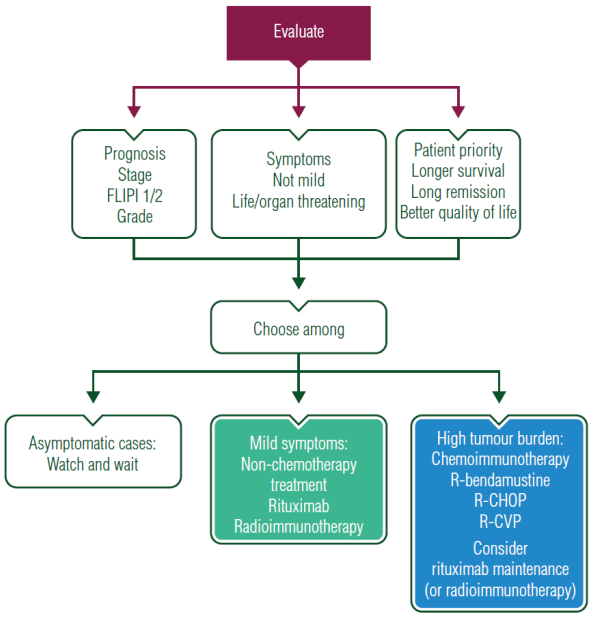

Figure 1.2
Initial treatment of advanced stage FL. Treatment decision depends on presence of symptoms, tumor burden, and patient's condition. Figure from Dreyling *et al.*[14]

1.2 The biology of follicular lymphoma

1.2.1 B lymphocyte development and activation

B lymphocytes derive from hematopoietic stem cells, which are located in the red bone marrow. Early B cell development involves several differentiation steps and aims to produce immature B cells expressing a functional B cell receptor (BCR). The most important step in this process is the V(D)J rearrangement in pre-B cells, which creates a highly diverse repertoire of BCRs by somatic recombination. To avoid autoimmunity, B cells are tested after V(D)J rearrangement if their BCRs are reactive to self-antigens. Immature B cells exit the bone marrow and mostly migrate to the spleen. Within the spleen these transitional B cells differentiate either into marginal zone B cells or follicular B cells. At this stage, B cells are considered mature B cells. Marginal zone B cells are noncirculating and stay within the spleen, whereas follicular B cells move to the peripheral blood and to other secondary lymphoid organs.[18,19]

B cell activation occurs following two principles: T cell-independent (TI) and T cell-dependent (TD) activation. Marginal zone B cells preferably undergo TI activation, which is initiated when a TI antigen binds to the BCR. This leads to secretion of mostly low-affinity immunoglobulin (Ig)M. Immune response via TI activation is very rapid, but rather

unspecific and is considered as a first response until production of high-affinity antibodies. Follicular B cells preferable undergo TD activation in secondary lymphoid organs, which is in turn initiated when a TD antigen binds to the BCR. This form of activation requires interaction of the B cell with a CD4+ T helper cell, which are in this case mostly T follicular helper cells (TFH). The BCR specifically binds to its TD antigen, which is internalized, digested, and peptides are presented at the cell surface through the histocompatibility complex (MHC) class II. TFH cells which were exposed to the same antigen, bind to the antigen-MHC class II complex via the T cell receptor-CD3 complex and the co-receptor CD4. This first signal is then confirmed by co-stimulatory molecules CD80 and CD86 on the B cell, which activate CD28 on the T cell. This initiates T cell activation and the TFH cell subsequently expresses and secretes multiple molecules to activate and support the B cell, like interleukin (IL)-4, IL-21, as well as CD40L. TD immunization results in GC formation, where somatic hypermutation and the Ig class switching recombination take place. Somatic hypermutation improves the affinity of the BCR by introduction of mutations in the deoxyribonucleic acid (DNA) of the Ig variable region. Ig class switching recombination on the other hand alters the constant region of Igs, which results in a change of the Ig isotype. B cells expressing Ig with the highest affinity are positively selected and differentiate to high affinity plasma cells and memory B cells. The formation of the GC is dynamic and the morphology changes during the GC reaction. It is characterized by a dark zone, a light zone, and a surrounding mantle zone. Clonal expansion of centroblasts and somatic hypermutation occur in the dark zone, class switching recombination and surface Ig selection occur in the light zone. Due to this highly mutagenic processes within the GC, the GC environment is involved in the development of many lymphomas, e.g. FL.[18,20]

1.2.2 FL pathogenesis

The molecular hallmark of FL is the t(14;18)(q32;q21) translocation, which puts the *BCL2* gene under control of *IGH* regulatory elements. The *BCL2* translocation is acquired during V(D)J recombination in the bone marrow and is traditionally considered the first event in FL pathogenesis. It leads to constitutive over-expression of the anti-apoptotic BCL2 protein and gives t(14;18)+ cells a survival advantage, e.g. during the GC reaction, where BCL2 expression is usually repressed.[21–23] At advanced stage disease, the *BCL2/IGH* translocation is present in 85% of FL cases, however it is neither necessary nor sufficient for lymphomagenesis.[24] Additional events are required for full

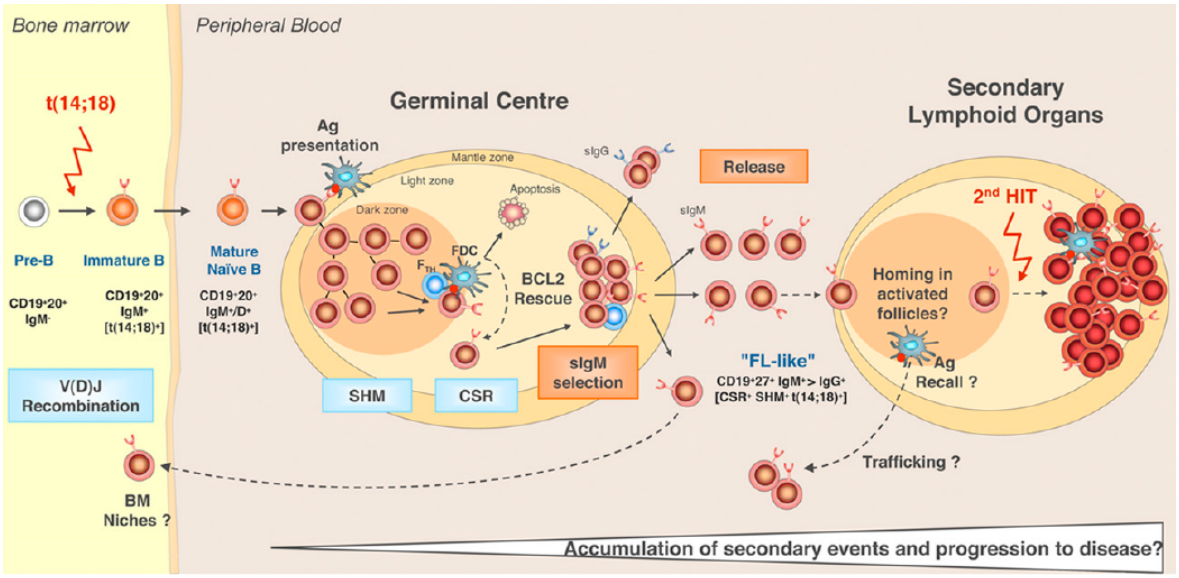

Figure 1.3
Follicular lymphoma pathogenesis. The *BCL2* translocation is considered to be the first hit in lymphomagenesis and occurs during rearrangement of the Ig genes. t(14;18)+ B cells exit the bone marrow and undergo GC reaction in secondary lymphoid organs. Due to their aberrant BCL2 expression, t(14;18)+ B cells escape apoptosis and GC selection. These "FL-like" B cells are then released and acquire additional genetic alterations, which are necessary to develop FL. BM: bone marrow, SHM: somatic hypermutation, CSR: class switching recombination, sIg: surface immunoglobulin. Figure from Kahl and Yang.[34]

malignant transformation.[25,26] Subsequent alterations are then acquired in secondary lymphoid organs during somatic hypermutation or class switching recombination (figure 1.3).[27] However, current research by various groups suggests that this model is oversimplifying and that the molecular ontogeny of FL is much more complex.[28–33]

1.2.3 FL microenvironment

FL is dependent on the crosstalk to its microenvironment (figure 1.4). This interaction between FL B cells and surrounding non-malignant immune cells or stromal cells has two major consequences: On the one side, it promotes tumor survival and growth, on the other side it contributes to the suppression of the anti-tumoral immune response.[35–37]
The presence of TFH cells is essential for the tumor, since they nurture the FL cells by various mechanisms, including secretion of IL-4 and IL-21, CD40L/CD40 stimulation, and interaction of the T cell receptor and MHC class II.[38,39] Stromal cells, especially fibroblastic reticular cells (FRC) and follicular dendritic cells (FDC) secrete CXC chemokine ligand (CXCL) 12 as well as CXCL13 and attract FL cells, which express high levels of

CXC chemokine receptor (CXCR) 4 and CXCR5. This interaction leads FL cells to home into the lymph nodes and mediates trafficking within the different zones of the lymph node. Cytotoxic T lymphocytes (CTL) are key players of anti-tumor immunity. However, their function is often impaired in FL by T cell exhaustion and a dysfunctional immunologic synapse.[40,41] Moreover, regulatory T cells (Treg) are attracted into the tumor microenvironment by CC chemokine ligand (CCL) 17 and CCL22, which are produced by FL B cells.[42] These Tregs contribute to tumor immune evasion in FL and other cancer entities by inhibition of CTL proliferation and degranulation.[43–46] Due to increased IL-4 levels produced by TFH cells (and CCL2 expression of stromal cells), the tumor microenvironment polarizes tumor-associated macrophages (TAM) to an alternatively activated M2 phenotype, whereas anti-tumoral M1 TAMs are not present.[47,48] M2-polarized TAMs are tumor-supportive by promotion of angiogenesis and secretion of immunosuppressive molecules.[37,49]

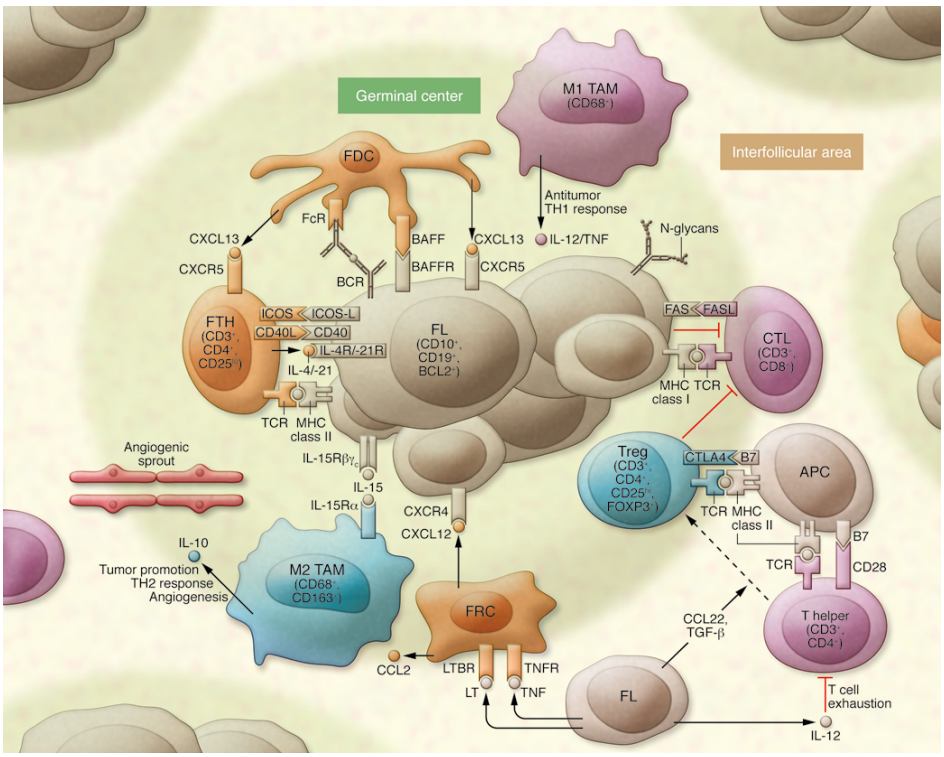

Figure 1.4
Overview of the FL microenvironment. Tumor supporting cells (orange) like T follicular helper cells (FTH or TFH), follicular dendritic cells (FDC), and fibroblastic reticular cells (FRC) foster tumor cells (FL) in various ways and promote tumor survival and growth. The regular anti-tumor immune response from tumor-associated macrophage (TAM) subtype M1, T helper cells, and cytotoxic T lymphocytes (CTL) (purple) is impaired by regulatory T cells (Treg) and M2 TAM (blue). Figure from Kridel *et al.*[36]

Novel treatment strategies aim to disrupt the tumor-supportive microenvironment. For

example, the immunomodulatory drug (IMiD) lenalidomide degrades the transcription factors Ikaros and Aiolos, which are both key regulators of lymphoid development and differentiation. This has various effects on the immune system, many of them still unknown. E.g. one study by Ramsay *et al.* could show that lenalidomide can revoke tumor immune evasion by repairing the dysfunctional T-cell immunologic synapse.[41,50,51] Lenalidomide is tested in several ongoing phase III clinical trails in combination with rituximab. Recent data from the RELEVANCE study showed that the combination of lenalidomide with rituximab performed almost identical in regards to PFS compared to rituximab in combination with chemotherapy in patients with untreated FL. The preliminary results of this study is encouraging, and it shows the great potential of targeting transcription factors and the microenvironment in lymphoma.[52]

1.2.4 The mutational landscape in FL

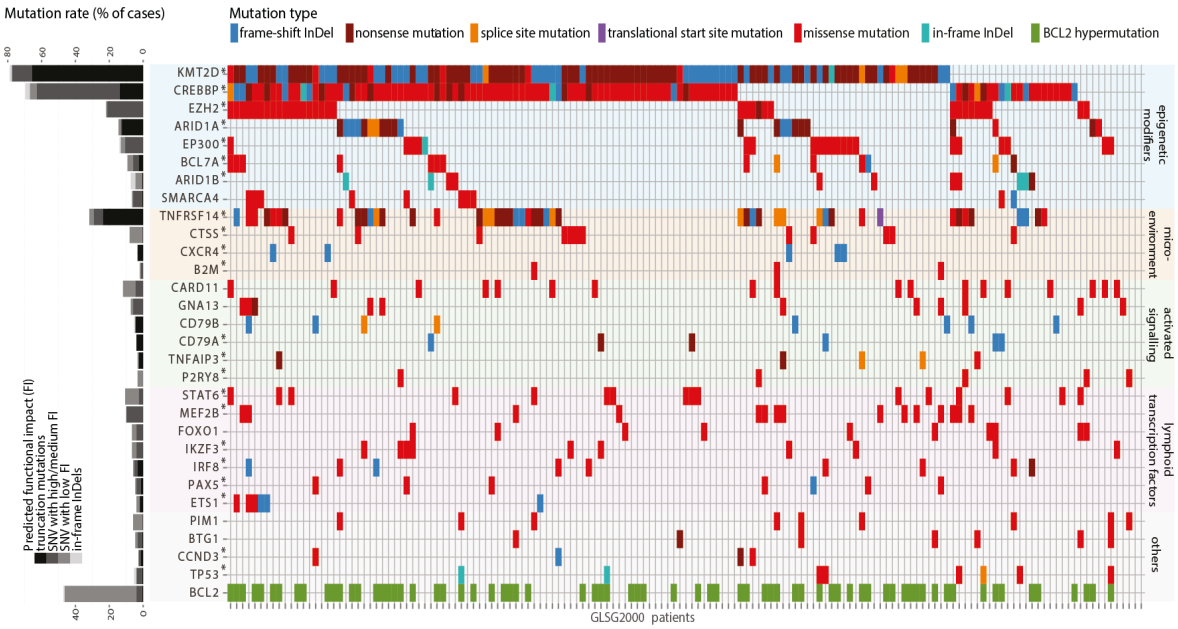

Figure 1.5
The targeted mutational landscape of FL from 151 patients of the GLSG2000 cohort. Virtually every patient carries at least one mutation in an epigenetic modifier. Additionally, transcription factors are recurrently altered in FL. Half of the patients with FL have alterations in that group of genes. Asterisks mark 22 significantly mutated genes by MutSigCV analysis. SNV: single-nucleotide variant. Figure from Pastore *et al.*[11]

Next-generation sequencing techniques over the past decade increasingly deciphered the mutational landscape in FL (figure 1.5).[11,31–33,53] The most frequently altered group of genes are the epigenetic modifiers, with virtually every patient harboring one or more

mutation in that category. The second largest group of genes altered in FL are the transcription factors. Fifty percent of FL cases carry mutations in that group of genes. Signal Transducer and Activator of Transcription (STAT) 6 is among the most frequently mutated transcription factors in FL.

1.3 Signal transducer and activator of transcription 6 (STAT6)

1.3.1 The IL-4/STAT6 signaling pathway

The STAT family consist of seven members and has a prominent role in cytokine signaling.[54] These proteins transduce signals from the cell membrane to the nucleus and are transcription factors. STAT6 is a 94 kDa protein which contains 847 amino acids and its gene is located on chromosome 12. In hematopoietic cells, STAT6 is activated by IL-4 which binds to the IL-4 receptor (IL4R) consisting of the IL4R alpha chain and the common gamma chain.[55] After IL-4 binding, Janus kinases (JAK) 1 and 3 are activated and phosphorylate tyrosine residues on the IL-4 receptor. Cytosolic STAT6 binds to the phosphorylated receptor via its src homology 2 domain, and gets phosphorylated itself by JAKs on the highly conserved position Y641. Phospho-STAT6 (pSTAT6) forms homodimers, which shuttle to the nucleus and bind to palindromic STAT6 binding sites $TTCN_4GAA$ or $TTCN_3GAA$ via the DNA-binding domain (figure 1.6).[49,56–58] Nuclear shuttling is mediated through the importin-α–importin-β1 system. Nuclear import and export of STAT6 is continuous and independent of Y641 phosphorylation. pSTAT6 accumulates primarily within the nucleus due to its binding to the DNA.[59] Afterwards, STAT6 binds transcriptional co-activators like poly ADP-ribose polymerase (PARP) 14, CBP/p300, NCoA1, and NCoA3 using the transactivation domain and initiates the transcription of STAT6 target genes (figure 3.1).[60,61]

STAT6 signaling is terminated either directly or indirectly. Direct termination includes STAT6 dephosphorylation by phosphatases like PTPN6, STAT6 proteolysis by calpains, and proteasomal degradation.[62–64] Suppressor of cytokine signaling (SOCS) proteins suppress STAT6 signaling indirectly. SOCS can inhibit the activity of JAKs, they are competing with STAT6 for phosphorylated binding sites on the IL4R, and they ubiquitinate bound signaling proteins for subsequent proteasomal degradation. Moreover, *SOCS1* is a target gene of STAT6, which forms a negative feedback loop.[65–67]

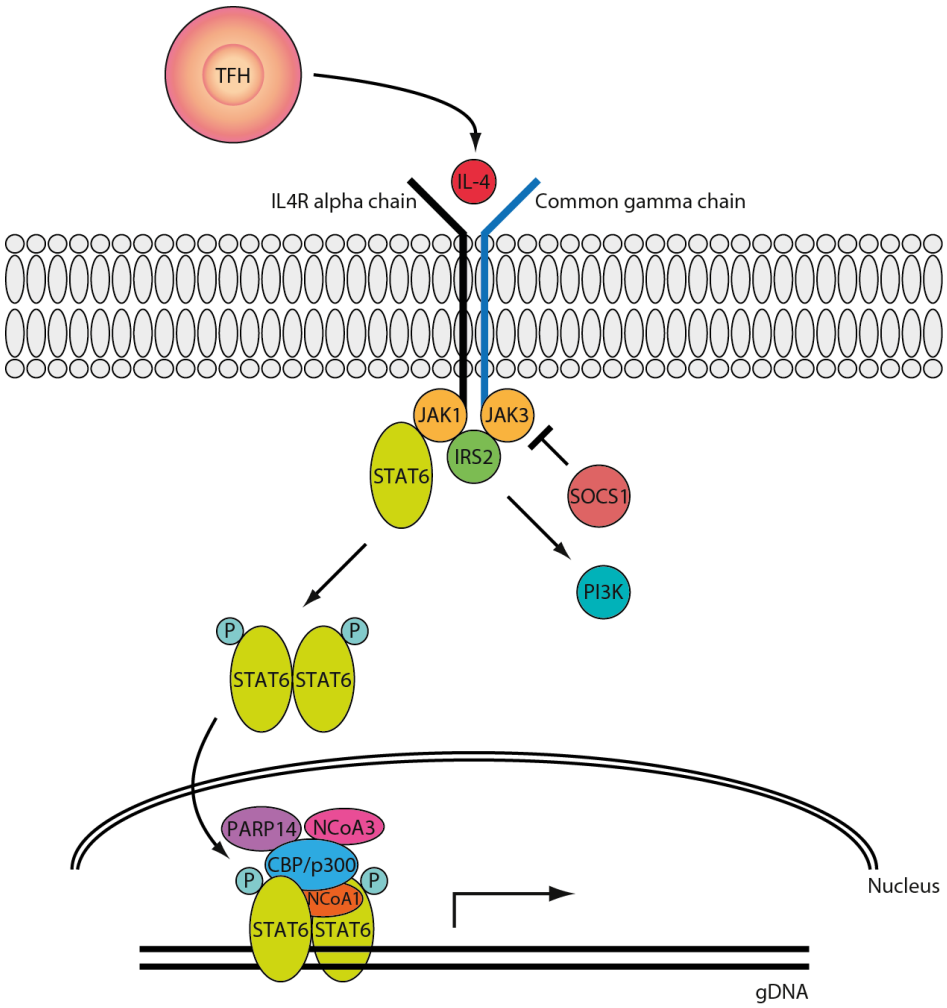

Figure 1.6
The IL-4/STAT6 signaling pathway. STAT6 is activated by IL-4. Upon phosphorylation at position Y641, pSTAT6 homodimers shuttle into the nucleus and initiate transcription.

Upon IL-4 stimulation, the IL-4 receptor also activates insulin receptor substrate (IRS) 2. Calvo *et al.* described that IL-4 via IRS2 also triggers the PI3K signaling pathway which activates AKT and the MAP kinase cascade which activates ERK in patients with FL.[68]

1.3.2 Physiological function and target genes of STAT6

The best-known function of STAT6 is the initiation of T helper cell type 2 (Th2) differentiation from naive CD4 T cells. Upon IL-4 stimulus, STAT6 regulates the expression of the GATA3 transcription factor, which is considered to be the master regulator of Th2 differentiation.[69] Studies in knockout mice revealed that STAT6 deficiency results in an

almost complete loss of Th2 cytokine production, including IL-4, IL-5, and IL-13. Additionally, STAT6 plays a crucial role in Ig class switching to IgG1 and IgE in B cells. For IgE class switching, a combined synergistic activation of IL-4/STAT6 and CD40L/nuclear factor-κB signaling leads to induction of the germline epsilon promoter.[70,71] In consequence, STAT6 deficient mice do not produce IgE and the immune response to helminth infection is strongly impaired.[72–74] STAT6 is also responsible for the expression of molecules involved in antigen presentation, like MHC class II, CD80, and CD86. Other cell surface molecules regulated by IL-4/STAT6 include the IL4R alpha chain, suggesting an autocrine positive feedback loop, and the low-affinity Fc receptor for IgE, alias CD23.[56,60] Cytokines, like *CCL17* and *CCL22* are target genes of STAT6, as well.[42,75,76] Outside of T and B cells, STAT6 mediates the IL-4 induced alternative activation of macrophages.[49] Therefore, hyperactive or constitutive STAT6 signaling results in increased Th2 differentiation plus Th2 cytokine production, elevated IgE levels, alternative activation of macrophages, recruitment of innate immune cells, like eosinophils and mast cells, and more. These processes cause allergic inflammation, asthma, as well as atopic dermatitis, they create a tumor-supportive microenvironment (chapter 1.2.3), and they promote lymphomagenesis.[77–79]

1.3.3 STAT6 in lymphoma

The first link between STAT6 and lymphoma has been found in 2002 by Skinnider *et al.* In their study, STAT6 was constitutively activated in 25 out of 32 (78%) classical HL cases.[80] Moreover, SOCS1 function is frequently impaired by disruptive mutations in HL.[81] Taken together, this data suggests that STAT6 plays an important role in HL biology and Natoli et *et al.* proposed to block the IL-4/STAT6 axis by inhibition of the IL-4 receptor.[82]

Another lymphoma entity in which STAT6 was found to be constitutively activated is primary mediastinal large B cell lymphoma (PMBL, a subtype of diffuse large B cell lymphoma (DLBCL)).[83] Ritz *et al.* first described recurrent *STAT6* mutations in the DNA binding domain in patients with PMBL.[84]

STAT6 mutations are rarely present in DLBCL at diagnosis. On the other hand, Morin *et al.* found *STAT6* mutations in 36% of patients with relapsed or refractory DLBCL of the GC B cell type and transformed FL.[85] This striking increase of mutation frequency indicates that STAT6 mutations play a crucial role in the progression of some lymphomas.

In recent years, various groups have described *STAT6* mutations in FL and histologic transformed FL.[32] Moreover, Okosun *et al.* found mutations in *STAT6* were clonal events in a 100% of FL and transformed FL cases, suggesting that they are early events and drivers of lymphomagenesis.[31] In 2015, Yildiz *et al.* reported the first functional data on *STAT6* mutations, demonstrating that they are activating and result in increased STAT6 target gene expression. Mechanistically, they reported increased nuclear STAT6 in cell lines expressing mutant STAT6. Of note, Yildiz *et al.* showed increased DNA binding of mutant STAT6 to oligonucleotides having a STAT6 binding site by electrophoretic mobility shift assays (EMSA).[53] This is in contrast to data published by Ritz *et al.* who reported decreased DNA binding of mutant STAT6 compared to wild-type STAT6 in their EMSAs.[84]

Interestingly, Siddiqi *et al.* described a small cohort of patients with FL, which were negative for the t(14;18) *IGH*/*BCL2* and expressed CD23. Nine out of eleven patients also had mutations in *STAT6*. When performing immunohistochemistry, all patients with STAT6 mutations also stained positive for nuclear phospho-STAT6.[86]

To summarize the current state of the research on mutant *STAT6* in FL: STAT6 mutations are gain-of-function and are clonal/early events in lymphomagenesis. Moreover, mutant *STAT6* is involved in the histologic transformation of FL and in the biology of t(14;18) negative FL.

1.4 Previous results

Pastore *et al.* described *STAT6* to be recurrently mutated in FL and MutSigCV algorithm identified *STAT6* as significantly mutated in the GLSG2000 cohort (figure 1.5).[11] MutSigCV is a mathematical approach to identify genes in which mutations occur more often than by random chance.[87]

As part of her Bachelor thesis, Elisa Osterode validated *STAT6* mutational calls in seven primary patient samples from the GLSG2000 cohort by Sanger sequencing. In two cases matched normal DNA was available and the somatic status of those mutations could be confirmed. In all other cases, the variant allele frequency suggested somatic status of the mutation.

1.5 Aims of this study

Taken together, the IL-4/STAT6 axis plays a critical role in lymphoma biology. Moreover, STAT6 is recurrently as well as significantly mutated in patients with FL and STAT6 mutations are somatically acquired.

However, the underlying mechanism of how mutant STAT6 contributes to FL biology remains incompletely understood. Furthermore, potential therapeutic vulnerabilities have not been investigated. Therefore, this study aims to address the following topics:

- Correlate STAT6 mutations in primary FL and IL-4/STAT6 pathway activation
- Identify an appropriate cell line model for the functional characterization of *STAT6* mutants
- Examine STAT6 target gene expression in cell lines expressing wild-type and mutant STAT6 in the presence and absence of IL-4
- Investigation of the underlying mechanism of mutant *STAT6* gain-of-function phenotype
- Explore therapeutic vulnerabilities for patients with aberrant IL-4/STAT6 signaling

2 Material and Methods

2.1 Material

2.1.1 Reagents and chemicals

Table 2.1
List of used reagents and chemicals

Reagent	Supplier	Product number
2-Propanol	AppliChem	A3928
Agarose Molecular Grade	Bioline	BIO-41026
Albumin Fraction V (pH 7.0)	AppliChem	A1391
Ampicillin	Sigma-Aldrich	A9518
Anti-Anti (100x)	Gibco	15240-062
BD™ CompBeads Anti-Mouse Ig, κ	BD Biosciences	552843
Bolt™ Antioxidant	Novex	BT0005
Bolt™ LDS Sample Buffer 4x	Novex	B0007
Bolt™ MES SDS Running Buffer 20x	Novex	B0002
Bolt™ MOPS SDS Running Buffer 20x	Novex	B0001
Bolt™ Sample Reducing Agent 10x	Novex	B0009
Bolt™ Transfer Buffer 20x	Novex	BT00061
BsrGI	New England Biolabs	R0575L
Buffer RLT	Qiagen	79216
Ciprofloxacin	Sigma-Aldrich	17850
Chloroform	Sigma-Aldrich	C2432
CutSmart® Buffer	New England Biolabs	B7204S
Cycloheximide solution	Sigma-Aldrich	C4859
DAPI dilactate	Promocell	PKCA70740009
DMSO	Sigma-Aldrich	472301
DNase I recombinant, RNase-free	Roche	04716728001
DpnI	New England Biolabs	R0176S
Dulbecco's MEM	Biochrom	F0445
EDTA 0.5 M, pH 8.0	Merck	324506

Reagent	Supplier	Product number
Ethanol	Merck	1.00983
Fast SYBR™ Green Master Mix	Applied Biosystems	4385612
FBS Superior	Biochrom	S0615
Formaldehyde 37%	Merck	8.18708
Gel Loading Dye Purple (6x), no SDS	New England Biolabs	B7025S
Glycerol $\geq$ 99%	Sigma-Aldrich	G5516
HEPES Buffer 1M	Biochrom	L1613
HindIII-HF®	New England Biolabs	R3104L
Human IL-4 premium grade	Miltenyi Biotec	130-093-921
IMDM	PAN™ BIOTECH	P04-20450
Kanamycin Sulfate	Sigma-Aldrich	K1377
L-Alanyl-L-Glutamine 200 mM	Biochrom	K0302
LB-Agar (Lennox)	Carl Roth	X964.1
LB-Medium (Lennox)	Carl Roth	X965.1
MagicMark™ XP	Invitrogen	LC5602
Milk powder blotting grade	Carl Roth	T145.1
Methanol	AppliChem	141091.1211
NEBuffer™ 2.1	New England Biolabs	B7202S
NP40 Substitute	AppliChem	A1694
Nuclease-Free-Water	Ambion	AM9937
One Shot® *ccd*B Survival™ 2 T1^R Competent Cells	Invitrogen	A10460
One Shot® TOP10 Chemically Competent *E. coli*	Invitrogen	C404003
Passive Lysis Buffer, 5X	Promega	E194
PBS Dulbecco w/o Mg^{2+}, Ca^{2+}	Biochrom	L1820
Phosphatase Inhibitor Cocktail 2	Sigma-Aldrich	P5726
Phosphatase Inhibitor Cocktail 3	Sigma-Aldrich	P0044
Pierce® ECL Western Blotting Substrate	Thermo Scientific	32106
PJ34 Hydrochlorid	Selleckchem	S7300
Polybrene Infection / Transfection Reagent	Merck millipore	TR-1003-G
Pre-Diluted Protein Assay Standards: Bovine Serum Albumin (BSA) Set	Thermo Scientific	23208
Protein G-Agarose	Roche	11243233001
Protease Inhibitor Cocktail	Sigma-Aldrich	P8340
Purified BSA 100x, 10 mg/ml	New England Biolabs	B9001S
Quick-Load® 2-log DNA ladder	New England Biolabs	N0469S
Quick-Load® Purple 50bp ladder	New England Biolabs	N0556S
Restore™ Plus Western Blot Stripping Buffer	Thermo Scientific	46430

Reagent	Supplier	Product number
RNase AWAY®	Carl Roth	A998.4
Roti-Safe Gel Stain	Carl Roth	3865.1
RPMI 1640	PAN™ BIOTECH	P04-16500
SeeBlue® Plus 2 Prestained Standard	Invitrogen	LC5925
Sodium Deoxycholate	Sigma-Aldrich	D6750
Sodium Fluoride	Sigma-Aldrich	S7920
Sodium Orthovanadate	Sigma-Aldrich	450243
S.O.C Medium	Invitrogen	15544-034
TAE Buffer 10x	Promega	V4271
TBE Buffer 10x	Invitrogen	15581-028
TBS Buffer 10x, pH 8.0	In-house	T03290
Tris	Carl Roth	5429.3
TRIzol® Reagent	Ambion	15596026
Trypan Blue stain 0.4%	Invitrogen	T10282
Trypsin/EDTA solution	Biochrom	L2143
Tween20	Carl Roth	9127.2
ViaFect™ Transfection Reagent	Promega	E498A
XhoI	New England Biolabs	R0146S

2.1.2 Antibodies

Table 2.2
List of used antibodies

Antibody	Supplier	Product number	Dilution
Primary antibody			
Anti-HA High Affinity Clone 3F10	Roche	11867423001	1:2500
Anti-Lamin B1 antibody [EPR8985(B)]	Abcam	ab133741	1:2500
Anti-PARP9 antibody	Abcam	ab53796	1:150
Anti-PARP14	Sigma	HPA012063	1:250
APC Mouse anti-Human CD23 Clone M-L233	BD Biosciences	558690	1:50
APC Mouse IgG1, κ Isotype Control	BD Biosciences	555751	1:50
GAPDH Antibody (6C5)	Santa Cruz Biotechnology	sc-32233	1:200000
Jak2 Antibody	Cell Signaling Technology	3773	1:1000
Monoclonal Anti-α-Tubulin Clone DM1A	Sigma-Aldrich	T6199	1:20000
Monoclonal ANTI-FLAG® M2	Sigma-Aldrich	F3165	1:2500
Phospho-Stat6 (Tyr641) Antibody	Cell Signaling Technology	9361	1:2000
Stat1 p84/p91 Antibody (E-23)	Santa Cruz Biotechnology	sc-346	1:500
Stat6 Antibody	Cell Signaling Technology	9362	1:2000
Secondary antibody			
Anti-Rabbit IgG (H+L), HRP Conjugate	Promega	W4011	1:5000
Anti-Mouse IgG (H+L), HRP Conjugate	Promega	W4021	1:5000
Peroxidase-conjugated AffiniPure Goat Anti-Rat IgG + IgM (H+L)	Jackson Immuno Research Laboratories	112-035-044	1:5000

2.1.3 Primers

Table 2.3
List of used primers

Name	Sequence (5' to 3')	Application
STAT6_GW_fw	G GGG ACA ACT TTG TAC AAA AAA GTT GGC CACC ATG TCT CTG TGG GGT CTG GTC TCC AAG	Addition of *att*B site & Kozak sequence
STAT6_GW_rv	GGG GAC AAC TTT GTA CAA GAA AGT TGG CTA CTT GTC ATC GTC ATC CTT GTA GTC GAT GTC ATG ATC TTT ATA ATC ACC GTC ATG GTC TTT GTA GTC CCA ACT GGG GTT GGC CCT TAG GTC C	Addition of *att*B site, Stop codon, & 3xFlag sequence
STAT6_GW_HA_rv	GGG GAC AAC TTT GTA CAA GAA AGT TGG CTA AGC GTA ATC TGG AAC ATC GTA TGG GTA CCA ACT GGG GTT GGC CCT TAG GTC C	Addition of *att*B site, Stop codon, & HA sequence
STAT6_D419G_fw	GGC AAC CAA GGC AAC AAT GCC AAA GCC AC	Site-directed mutagenesis
STAT6_D419G_rv	CAT TGT TGC CTT GGT TGC CAT GGA CGA TG	Site-directed mutagenesis
STAT6_D419N_fw	GGC AAC CAA AAC AAC AAT GCC AAA GCC AC	Site-directed mutagenesis
STAT6_D419N_rv	CAT TGT TGT TTT GGT TGC CAT GGA CGA TG	Site-directed mutagenesis
STAT6_N421K_fw	GAC AAC AAA GCC AAA GCC ACT ATC CTG TGG	Site-directed mutagenesis
STAT6_N421K_rv	TGG CTT TGG CTT TGT TGT CTT GGT TGC CAT G	Site-directed mutagenesis
STAT6_D519V_fw	GCA GTG GTT TGT TGG TGT CCT GGA CCT CAC	Site-directed mutagenesis
STAT6_D519V_rv	AGG ACA CCA ACA AAC CAC TGC CAA AAG GTG AAG	Site-directed mutagenesis

Name	Sequence (5' to 3')	Application
qPCR_CD23_ST240_F	CTG GGA CAC CAC ACA GAG TC	qPCR
qPCR_CD23_ST240_R	GAC ACC TGC AAC TCC ATC CT	qPCR
GAPDH_ex9&ex10_f	CAC CCA CTC CTC CAC CTT TG	qPCR
GAPDH_ex9&ex10_r	TCT CTC TCT TCC TCT TGT GCT CTT G	qPCR
qPCR_IFI27_FP	GCC TCT GGC TCT GCC GTA GTT	qPCR
qPCR_IFI27_RP	ATG GAG GAC GAG GCG ATT CC	qPCR
qPCR_JAK2_FP	TTC AGC AAT TCA GCC AAT GC	qPCR
qPCR_JAK2_RP	TTC TTT ATG TTT CCC TCT TGA CCA C	qPCR
qPCR_PARP9_FP	CTC ATT GAG GTG GTT ATG AAC ATT G	qPCR
qPCR_PARP9_RP	CTT GAG TTG GAG GCA CAG GAC	qPCR
qPCR_PARP14_FP	GAC TGT CGC TAT GTG CTT CAC	qPCR
qPCR_PARP14_RP	GGA CAA GCT CTC AGT GAT CTC C	qPCR
qPCR_STAT1_FP	CTT TCT GCT GTT ACT TTC CCT GAC	qPCR
qPCR_STAT1_RP	GGC TCT GGT GCT TCC TTT G	qPCR
M13-FP	TGT AAA ACG ACG GCC AGT	Sanger sequencing
M13-RP	CAG GAA ACA GCT ATG ACC	Sanger sequencing
pDONOR-FP	TAA CGC TAG CAT GGA TCT C	Sanger sequencing
pDONOR-RP	CAA TGT AAC ATC AGA GAT	Sanger sequencing
STAT6_1600_fw	TGG TTT GAT GGT GTC CTG GAC	Sanger sequencing
STAT6_1800_rv	ATG GCT GGA TGT TCT CTA TCT GTG	Sanger sequencing
RVprimer3_FP	CTA GCA AAA TAG GCT GTC CC	Sanger sequencing
GLprimer2_RP	CTT TAT GTT TTT GGC GTC TTC CA	Sanger sequencing

Name	Sequence (5' to 3')	Application
PARP14prom_ 1+2_FP	CCG CTC GAG GCA GAC ATG GGC TGT TAC ATT AAG	Luciferase reporter assay
PARP14prom_ 1+2_RP	CCC AAG CTT GTC TTG AAA GCC AAG GAA AGA AAG	Luciferase reporter assay
PARP14prom_ 3+4_FP	CCG CTC GAG GCT GAT CTC TCT GCC TCC ACT C	Luciferase reporter assay
PARP14prom_ 3+4_RP	CCC AAG CTT CCA TGC ACT CAC TCA CTG AAC C	Luciferase reporter assay
PARP14prom_ 5+6_FP	CCG CTC GAG GGA TGA CTC TGC CAT TCC TG	Luciferase reporter assay
PARP14prom_ 5+6_RP	CCC AAG CTT CAG AAA ACG ATC GAG GGA TAA AG	Luciferase reporter assay
PARP14prom_ 7+8+9_FP	CCG CTC GAG GAG GTG ATC TGC TGG CTC AAG	Luciferase reporter assay
PARP14prom_ 7+8+9_RP	CCC AAG CTT TCT GAA GTC AAA GTG GGG AAA AC	Luciferase reporter assay
PARP14prom_ 10+11+12FP	CCG CTC GAG TTC AGT TTC CTA CTT GAG GAA CCA C	Luciferase reporter assay
PARP14prom_ 10+11+12RP	CCC AAG CTT CTG ATG TCC AAC CTC CCT TAC C	Luciferase reporter assay
PARP14prom_ comp_FP	CCG CTC GAG AAG CAA AAT GAG GTG GAG TGG	Luciferase reporter assay
PARP14prom_ comp_RP	CCC AAG CTT GGG GAT TGA GGA CTG GAT AGG	Luciferase reporter assay 5' overhang XhoI restriction site HindIII restriction site

2.1.4 Short hairpin RNA plasmids

Table 2.4
List of used shRNA plasmids

Name / Sequence	Supplier	TRC number
MISSION® pLKO.1-puro Non-Target shRNA Control	Sigma-Aldrich	SHC016-1EA (catalog number)
CCGGGCGCGATAGCGCTAATAATTTCTCGAGAAATTATTAGCGCTATCGCGCTTTTT		
MISSION® pLKO.1-puro PARP14 shRNA #1	Sigma-Aldrich	TRCN0000053162
CCGGGCACCATTTGAAGAGTCACTACTCGAGTAGTGACTCTTCAAATGGTGCTTTTTG		
MISSION® pLKO.1-puro PARP14 shRNA #2	Sigma-Aldrich	TRCN0000296754
CCGGGATTGAGTTTGATACACTTAACTCGAGTTAAGTGTATCAAACTCAATCTTTTTG		
MISSION® pLKO.1-puro PARP14 shRNA #3	Sigma-Aldrich	TRCN0000290897
CCGGGCACCATTTGAAGAGTCACTACTCGAGTAGTGACTCTTCAAATGGTGCTTTTTG		
MISSION® pLKO.1-puro PARP14 shRNA #4	Sigma-Aldrich	TRCN0000053158
CCGGCGGAACTTCATTCTTCACAAACTCGAGTTTGTGAAGAATGAAGTTCCGTTTTTG		
MISSION® pLKO.1-puro PARP14 shRNA #5	Sigma-Aldrich	TRCN0000053159
CCGGGCAGATTGTATCAGTGAGTTTCTCGAGAAACTCACTGATACAATCTGCTTTTTG		

2.1.5 Kits

Table 2.5
List of used kits

Kit	Supplier	Product number
CD23 (soluble) Human ELISA Kit	Invitrogen	KAS0251
Dual-Glo® Luciferase Assay System	Promega	E2920
Gateway® BP Clonase™ II	Invitrogen	11789-020
Gateway® LR Clonase™ II	Invitrogen	11791-020
KOD Xtreme™ Hot Start DNA Polymerase	Novagen	71975-3
Phusion® High-Fidelity PCR Kit	New England Biolabs	E0553S
Pierce™ BCA Protein Assay Kit	Thermo Scientific	23227
PureYield™ Plasmid Midiprep System	Promega	A2492
PureYield™ Plasmid Miniprep System	Promega	A1222
QIAamp® DNA Blood Mini Kit	QIAGEN	51104
QIAquick® Gel Extraction Kit	QIAGEN	28706
QIAquick® PCR Purification Kit	QIAGEN	28106
Qproteome® Nuclear Protein Kit	QIAGEN	37582
Quick Ligation™ Kit	New England Biolabs	M2200S
SuperScript® III First-Strand Synthesis System for RT-PCR	Invitrogen	18080-051

2.1.6 Buffers

Table 2.6
List of used buffers

Name	Composition
Co-IP buffer *	HEPES pH 7.4, 50mM NaCl 150 mM NP40 0.5% (V/V) Sodium Deoxycholate 0.25% (m/V)
Co-IP washing buffer	HEPES pH 7.4, 50mM NP40 0.1% (V/V) Sodium Deoxycholate 0.05% (m/V)
RIPA cell lysis buffer *	Tris pH 8.0, 50 mM NaCl 150 mM EDTA pH 8.0, 5 mM NP40 1.0% (V/V) Sodium Deoxycholate 0.5% (m/V) SDS 0.1% (V/V)
Transfer buffer	50 ml 20x Bolt™ Transfer Buffer 100 ml MeOH 1 ml Bolt™ Antioxidant to 1l DI water
* Fresh inhibitors were added to Co-IP buffer and RIPA buffer before use	Na_3VO_4 1 mM NaF 5 mM 1x Protease inhibitor cocktail 1x Phosphatase inhibitor cocktail 2 1x Phosphatase inhibitor cocktail 3

2.1.7 Cell lines

Table 2.7
List of used cell lines

Name	Species	Cell type	Culture Properties	Medium	References
293T	human	Embryonic kidney cells	Adherent	90% DMEM + 10% FBS + 2.0 mM L-Alanyl-L-Glutamine	[88–90]
DB	human	B lympho-blast	Suspension	90% RPMI 1640 + 10% FBS	[91–93]
DG-75	human	B lympho-blast	Suspension	90% RPMI 1640 + 10% FBS	[94,95]
HeLa	human	Epitheloid cervix carcinoma	Adherent	90% DMEM + 10% FBS + 2.0 mM L-Alanyl-L-Glutamine	[96–98]
Karpas 422	human	B cell lymphoma	Suspension	90% RPMI 1640 + 10% FBS	[99–112]
Namalwa	human	B cell lymphoma	Suspension	90% RPMI 1640 + 10% FBS	[113–117]
OCI-Ly1	human	B cell lymphoma	Suspension	80% IMDM + 20% FBS	[91,118–122]
OCI-Ly8	human	B cell lymphoma	Suspension	80% IMDM + 20% FBS	[100–104,118,121]
OCI-Ly18	human	B cell lymphoma	Suspension	90% RPMI 1640 + 10% FBS	[120,123,124]
SU-DHL-4	human	B cell lymphoma	Suspension	90% RPMI 1640 + 10% FBS	[91,125–130]
SU-DHL-5	human	B cell lymphoma	Suspension	90% RPMI 1640 + 10% FBS	[91,126,128,129]
WSU-FSCCL	human	B cell lymphoma	Suspension	90% RPMI 1640 + 10% FBS	[131–133]

2.1.8 Consumables

Table 2.8
List of used consumables

Consumable	Supplier	Product number
5 ml Round Bottom Polystyrene Test Tube	Falcon®	352058
5 ml Round Bottom Polystyrene Test Tube with Cell Strainer Snap Cap	Falcon®	352235
5 ml Stripette® Serological Pipets	Corning	4487
10 ml Stripette® Serological Pipets	Corning	4488
25 ml Serological Pipets	Greiner Bio-One	760180
96-well PCR plate	Brand	781400
96-well Solid White Microplate	Corning	07-200-628
Bacterial cell spreaders	Carl Roth	AY19.1
Bolt™ 4-12% Bis-Tris Plus Gels, 10-well	Invitrogen	NW04120BOX
Bolt™ 4-12% Bis-Tris Plus Gels, 15-well	Invitrogen	NW04125BOX
Combitips advanced® 0.5 ml	Eppendorf	0030089634
Combitips advanced® 1.0 ml	Eppendorf	0030089642
Combitips advanced® 5.0 ml	Eppendorf	0030089669
Combitips advanced® 10.0 ml	Eppendorf	0030089677
CryoPure Tube 1.8 ml	Sarstedt	72.379
Disposal bags	Brand	759710
DURAN® beaker	Schott	21 106
DURAN® GL 45 Lab Bottles	Schott	21 801
DURAN® Erlenmeyer flask	Schott	21 216
MicroAmp™ Fast Optical 96-Well Reaction Plate	Applied Biosystems	4346906
MicroAmp™ Optical Adhesive Film	Applied Biosystems	4311971
Micro tube 1.5 ml SafeSeal	Sarstedt	72.706.400
Micro tube 2.0 ml SafeSeal	Sarstedt	72.695.400
Millex-GV, 0.22 μm, PVDF filter	Millipore	SLGV033RS
Millex-HV, 0.45 μm, PVDF filter	Millipore	SLHV033RB
PARAFILM® M	Sigma	P7793
PCR tubes, strips of 8	Brand	781332
Perfusion syringe 50 ml	BD Medical	300137
Petri dish with vents	Greiner Bio-One	633180
Safe-Lock Tubes, 0.5 ml	Eppendorf	0030121023
SafeSeal SurPhob filter tips 10 μl	Biozym	VT0200
SafeSeal SurPhob filter tips 100 μl	Biozym	VT0230
SafeSeal SurPhob filter tips 200 μl	Biozym	VT0240
SafeSeal SurPhob filter tips 1250 μl	Biozym	VT0270

Consumable	Supplier	Product number
SurPhob pipette tips 10 μl	Biozym	VT0001X
SurPhob pipette tips 200 μl	Biozym	VT0003X
SurPhob pipette tips 1000 μl	Biozym	VT0005X
TC Dish 100, Standard	Sarstedt	83.3902
TC Flask T25, Standard, Vent. Cap	Sarstedt	83.3910.002
TC Flask T75, Standard, Vent. Cap	Sarstedt	83.3911.002
TC Flask T175, Standard, Vent. Cap	Sarstedt	83.3912.002
TC Flask T25, Suspension, Vent. Cap	Sarstedt	83.3910.502
TC Flask T75, Suspension, Vent. Cap	Sarstedt	83.3911.502
TC Flask T175, Suspension, Vent. Cap	Sarstedt	83.3912.502
TC Plate 6 Well, Standard	Sarstedt	83.3920
TC Plate 12 Well, Standard	Sarstedt	83.3921
TC Plate 24 Well, Standard	Sarstedt	83.3922
TC Plate 48 Well, Standard	Sarstedt	83.3923
TC Plate 96 Well, Standard	Sarstedt	83.3924
TC Plate 6 Well, Suspension	Sarstedt	83.3920.500
TC Plate 12 Well, Suspension	Sarstedt	83.3921.500
TC Plate 24 Well, Suspension	Sarstedt	83.3922.500
TC Plate 48 Well, Suspension	Sarstedt	83.3923.500
TC Plate 96 Well, Suspension	Sarstedt	83.3924.500
Tube 13 ml, PP, Vent. Cap	Sarstedt	62.515.006
Tube 15 ml, PP	Sarstedt	62.554.502
Tube 50 ml, PP	Sarstedt	62.547.254
Vasco® Nitril blue	B. Braun	9209833

2.1.9 Equipment

Table 2.9
List of used equipment

Device	Specification	Supplier
Analytical balance	ABJ 220-4NM	Kern & Sohn
Autoclave	VX-150	Systec
	VARIOKLAV® Typ 500	HP Medizintechnik
Benchtop shaker	neoLab® shaker DRS-12	neoLab Migge
	Titramax 101	Heidolph Instruments
	LD76160011	Rotator
	RS-TR 5 tuberoller	Phoenix instrument
Blotting module	Mini Blot Module	Life Technologies
Cell counting and cell viability	Vi-CELL™ XR	Beckman Coulter
	Countess II	Life Technologies
Centrifuge	5415D	Eppendorf
	5424R	Eppendorf
	Heraeus™ Multifuge™ X1R	Thermo Scientific
	Sprout® Mini Centrifuge	Heathrow Scientific
CO_2 incubator	CB 220	Binder
Cold chamber	TC 207	Tritec
Drying and heating chamber	FD 115	Binder
Flow cytometers	FACSAria™ III	BD Biosciences
	FACSCanto™ II	BD Biosciences
Fluorescence microscope	DMi8	Leica
Freezer	GNP 3056 Premium	Liebherr
	HERAfreeze™ HFU240BV	Thermo Scientific
Freezing container	Mr. Frosty™ Cryo 1°	Nalgene
Fridge	7085638-01	Liebherr
Gel electrophoresis	Gel System Mini S	Peqlab
	Gel System Mini L	Peqlab
	Bolt™ Mini Gel Tank	Life Technologies
Gel chamber power supply	PowerPac™ Basic	Bio-Rad
Gel scanner	Fusion SL4	Vilber Lourmat
	E-BOX VX2	Vilber Lourmat
Heating block	Thermomixer compact	Eppendorf
	BT 1302	HLC
Ice machine	FM-170AKE	Hoshizaki
Incubator	Multitron II	Infors
	Mini Incubator	Labnet
Laminar Flow Cabinet Class2	FlowSafe® B-[MaxPro]^2-130	Berner Safety
Magnetic stirrer	IKAMAG® RET	IKA-Werke

Device	**Specification**	**Supplier**
Microscope	ID03	Carl Zeiss
Microplate reader	GloMax® Discover	Promega
Milligram scale balance	Kern PCB 2500-2	Kern & Sohn
PCR Workstation	Peqlab PCR Workstation Pro	VWR
pH meter	inoLab® pH 7110	WTW
Pipettes	Research plus (100-1000 μl, 20-200 μl, 10-100 μl, 2-20 μl, 0.5-10 μl, 0.1-2.5 μl)	Eppendorf
Pipette controller	pipetus®	Hirschmann
Real-Time PCR System	7900HT Fast	Applied Biosystems
Spectrophotometer	NanoDrop 1000	Thermo Scientific
Thermocycler	peqSTAR 96 Universal Gradient	Peqlab
Ultrapure water system	Milli-Q™ Reference System	Millipore
	Q-POD® Remote Dispenser	Millipore
Vortex	Vortex-Genie 2	Scientific Industries
Water bath	Typ 1003	GFL

2.1.10 Software

Table 2.10
List of used software

Application	Software	Developer
FACS data analysis	FlowJo 10.0.8	FlowJo, LLC
Flow cytometer setup and data acquisition	FACSDiva™ 8.0.1	BD Biosciences
Gel documentation	E-Capt 15.06	Vilber Lourmat
Gene set enrichment analysis	GSEA 3.0	Broad Institute
Graphics editor	Adobe Illustrator CC 2015 19.2.0	Adobe
Molecular biology software	Serial Cloner 2.6.1	SerialBasics
nCounter data analysis	nSolver 2.6.43	NanoString Technologies
Promoter analysis	MatInspector Version June 2017	Genomatix
qPCR data analysis	SDS 2.4.1	Applied Biosystems
Reference management	EndNote X7.7.1	Thomson Reuters
Sanger trace viewer	FinchTV 1.4	Geospiza, Inc.
Statistical analysis and data visualization	GraphPad Prism 6.07	GraphPad Software
	R 3.3.3	The R Foundation
	RStudio 1.0.136	RStudio, Inc.
Western blot analysis	FusionCapt Advance 16.11	Vilber Lourmat
Word processing	MikTex 2.9	Christian Schenk
	Texmaker 4.5	Pascal Brachet

2.2 Methods

2.2.1 Patients of the GLSG2000 and BCCA cohorts

Hybrid-capture target sequencing data of 151 patients from the GLSG2000 and 107 patients from the BCCA were available from Pastore *et al.* and were reanalyzed.[11] Patients had advanced stage FL and were in need of treatment. Further patient characteristics and patient flow charts for both cohorts are depicted in figure A.1 and A.2 in the appendix.

2.2.2 Gene expression profiling of primary patient samples

For 107 BCCA patients with known STAT6 status, genome-wide gene expression profiling data, analyzed using the Illumina complementary DNA (cDNA)-mediated annealing, selection, extension, and ligation (DASL) assay, were available. This work has been done by Dr. Robert Kridel in the laboratory of Prof. Dr. Randy Gascoyne and has previously been published (GEO repository: GSE66166).[11] Gene expression data from one patient did not meet quality criteria and were excluded (n=106). Data were reanalyzed for differential gene expression analysis using limma (3.32.2) package, Gene Set Enrichment Analysis (GSEA, chapter 2.2.3), as well as unsupervised, hierarchical clustering according to patients' STAT6 mutational status.

Moreover, gene expression data of 138 patients from the GLSG2000 cohort was available. Nanostring® nCounter® technology was used to analyze primary patient material according to the manufacturer's protocol. This technology allows direct detection of mRNA from FFPE samples using a capture probe, which has a biotin label as well as a 35-50 base pair (bp) sequence complementary to the target gene, and a reporter probe, which contains a color code and also a 35-50 bp sequence complementary to the target gene. For the GLSG2000 cohort a customized panel of probes covering 184 candidate genes was designed. This data was kindly provided by Dr. Anette Staiger and Prof. Dr. German Ott.

2.2.3 Gene Set Enrichment Analysis

GSEA was performed for the OCI-Ly1 STAT6 cell line and for the BCCA cohort gene expression data.[134,135] Compared were STAT6 wild-type and STAT6 mutant phenotype. 1000 permutations were performed to assess the statistical significance of the enrichment score. Permutation type was set to *phenotype*. Datasets already included gene symbols, so Collapse dataset to gene symbol was selected *false*. For all other parameters default values were used.

2.2.4 Kaplan–Meier estimator

Patients were stratified by STAT6 mutation status (n=221 wild-type versus n=37 with a DNA binding variant, n=151 from GLSG2000 and n=107 from BCCA). Survival curves were plotted using prodlim (1.6.1) and survival (2.41-3) packages. Kaplan-Meier curves were compared using the log-rank test. The prognostic value of the STAT6 mutational status was assessed using a multivariate cox-regression model with adjustment for high-risk FLIPI and ECOG performance status 2-4.

2.2.5 Immunohistochemistry

Immunohistochemistry (IHC) staining of OCI-Ly1 cell lines and patient biopsies was performed by the Department of Pathology, University of Kiel, under the supervision of Prof. Dr. Wolfram Klapper. For formalin-fixed, paraffin-embedded (FFPE) blocks cell lines were fixed in 4.5% formalin solution, mixed with isopropanol and glycerin. The pellet was embedded using standard procedures for tissues. The applied staining procedures for cell block slides or tissue sections are listed in table 2.11.

2.2.6 Cloning of STAT6 expression vectors

STAT6-pENTR223 plasmid was purchased from PlasmID (Harvard Medical School, HsCD 00365550), containing the wild-type STAT6 cDNA sequence. The Gateway® technology from Invitrogen, which is based on site-specific recombination system of the lambda phage, was used to move the STAT6 sequence into the expression vector. In a first step, the attachment (*att*) sites (DNA recombination sequences), a Kozak sequence, a

Table 2.11
Immunohistochemistry staining procedures

Antibody **Staining procedure**	**Supplier**	**Product number**	**Dilution**
CD23 Novocastra Clone 1B12	Leica biosystems	PA0169	1:20
Laica BOND automated stainer, antigenretrival program ER1			
PE Mouse Anti-Stat6 (pY641) Clone 18	BD Biosciences	562078	1:1000
Heat-induced antigen retrieval with pressure cooker (3 min, citrate buffer pH 6.0) Manual staining using CSA-Kit (Dako, Glostrup, Denmark)			

3xFlag tag, and a stop codon were added to the STAT6 sequence by polymerase chain reaction (PCR). Afterwards, the STAT6 sequence was transferred into pDONR222 vector by BP reaction. Site-directed mutagenesis was performed to create mutant STAT6 sequences. Finally, STAT6 wild-type and mutant sequences were moved to pHAGE-CMV-MCS-IRES-ZsGreen (pCIG, EvNO00061605, PlasmID, Harvard Medical School, vector map in appendix A.4) expression vector by LR reaction (figure 2.1).

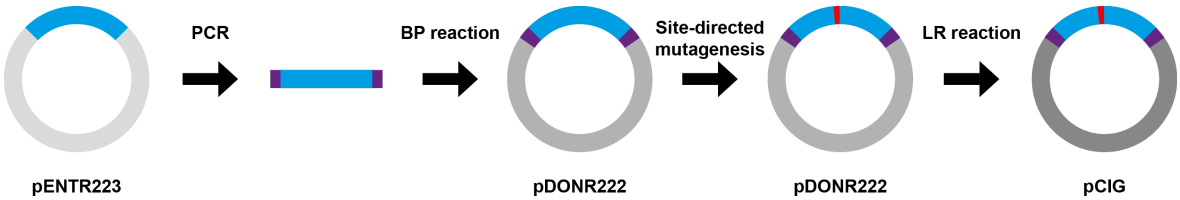

Figure 2.1
Cloning strategy to create STAT6 expression vectors.
Cyan: STAT6 cDNA sequence, purple: attachments (*att* sites, Kozak sequence, 3xFlag tag, stop codon), red: point mutation, grey: vector backbone.

Transformation of *E. coli*

For propagation of DNA plasmids, chemically competent *E. coli* were transformed by heat shock. Twenty-five μl of One Shot® TOP10 Chemically Competent *E. coli* were transferred to a 13 ml tube with ventilation cap and mixed with 1.0 μl plasmid solution or 20 ng of DNA plasmid. Tubes were then incubated for 30 min on ice. Heat shock was performed by placing the tubes in a water bath at 42°C for 30 sec. Afterwards, tubes were placed on ice for 2 min and 500 μl of preheated S.O.C medium was added to each tube. Samples were incubated at 37°C for 1 h in a horizontal shaker, before plated on

Lysogeny broth (LB) agar plates with appropriate antibiotic. Agar plates were incubated overnight at 37°C.

Preparation of plasmid DNA

For preparation of plasmid DNA, four to six single colonies were picked with a pipette tip from the agar plate and each was transferred to 2 ml LB medium supplemented with the suitable antibiotic in a 13 ml tube with ventilation cap. After overnight incubation at 37°C in a shaking incubator, the PureYield™ Plasmid Miniprep System was used for miniprep plasmid isolation according to the manufacturer's protocol. For midiprep plasmid isolation, 150 μl of bacterial suspension used for miniprep plasmid isolation were transferred to an Erlenmeyer flask with 150 ml LB medium supplemented with the appropriate antibiotic. After overnight incubation at 37°C in a shaking incubator, isolation of plasmid DNA was performed using PureYield™ Plasmid Midiprep System according to the manufacturer's protocol.

Restriction digest

Restriction digest of DNA was performed using enzymes and buffers from New England Biolabs according to the manufacturer's protocol. To analyze any Gateway® vector, BsrGI restriction digest was performed. This enzyme cuts within the *att* sites, but not in STAT6 sequence. Reagents from table 2.12 were mixed together and incubated for 1 h at 37°C. 10 μl from the reaction mix were used for agarose gel electrophoresis.

Table 2.12
Restriction enzyme reaction

Name	Amount
DNA	1.0 μg
10x NEBuffer™ 2.1	2.0 μl
BsrGI (10,000 U/ml)	1.0 μl
Nuclease-free water	x μl
Final volume	20.0 μl

Agarose gel electrophoresis

Agarose was dissolved in the appropriate buffer (see table 2.13) by heating in a microwave. Roti-Safe Gel Stain was used 1:5000 for in-gel staining of DNA. Samples were mixed with Gel Loading Dye (6x) and loaded on the gel together with Quick-Load® 2-log DNA ladder or Quick-Load® Purple 50 bp ladder, respectively.

Table 2.13
Agarose gels used in this work

DNA size	Amount agarose	Buffer
50 - 500 bp	2.0 % (m/V)	0.5x TBE
200 - 1000 bp	1.5 % (m/V)	1.0x TAE
$\geq$1000 bp	0.7 % (m/V)	1.0x TAE

DNA extraction from agarose gels

For extraction of DNA fragments from an agarose gel, the appropriate bands were excised under UV-light and DNA was extracted using the QIAquick® Gel Extraction Kit according to the manufacturer's protocol.

Polymerase chain reaction

Primers used for PCR were designed with Primer 3 program and are listed in table 2.3.[136,137] *att* sites were were added upstream and downstream of the STAT6 sequence to allow cloning into vectors containing the Gateway® cassette. Furthermore, a Kozak consensus sequence was included for more efficient translation. A 3xFlag tag followed by a stop codon was added C-terminal. This allows detection of ectopically expressed STAT6 and discrimination from endogenous STAT6 in cell lines. Moreover, a STAT6 wild-type HA tag construct was created, for dimerisation assays (chapter 2.2.8).

PCRs were carried out using KOD Xtreme™ Hot Start DNA Polymerase and HsCD00365550 as DNA template. A 3-step stepdown PCR program was run as listed in table 2.14, the according reaction mix is depicted in table 2.15. Afterwards, the PCR reactions were applied to agarose gel electrophoresis. The 2630 bp STAT6 wild-type HA product and the 2670 bp STAT6 wild-type 3xFlag product were excised from the gel and DNA was extracted (QIAquick® Gel Extraction Kit).

Table 2.14
3-step stepdown PCR program for STAT6 constructs

Step	Temperature [°C]	Duration [sec]	Cycles
Initial denaturation	95	120	
Denaturation	95	30	
Annealing	74 ▶ 70 ▶ 66 ▶ 62 ▶ 58	40	3/Temp
Extension	68	180	
Denaturation	95	30	
Annealing	54	40	15
Extension	68	180	
Final extension	68	300	
Store	12	∞	

Table 2.15
PCR mix for KOD polymerase

Reagent	Volume [μl]	Final
Nuclease-free water	4.2	
2x Xtreme Buffer	10.0	1.0x
2 mM dNTPs	4.0	0.4 mM
10 μM Forward primer	0.6	0.3 μM
10 μM Reverse primer	0.6	0.3 μM
Template DNA (50 ng/μl)	0.2	10.0 ng
KOD polymerase	0.4	0.4 Units

BP recombination reaction

To create STAT6 wild-type pDONR entry clones, *att*B-flanked PCR products were cloned into pDONR222 vector (vector map in appendix A.3) by BP reaction. The 5 μl reaction mix was pipetted as listed in table 2.16. Samples were incubated at 25°C for 2 h. The reaction was stopped by addition of 0.5 μl proteinase K and incubation at 37°C for 10 min. Samples were either stored at -20°C or 1 μl of each sample was used for transformation.

Site-directed mutagenesis

Mutations to the STAT6 sequence were introduced by site-directed mutagenesis. PCR was performed using Phusion® High-Fidelity polymerase and STAT6 wild-type 3xFlag

Table 2.16
BP reaction mix

Reagent	Volume [μl]	Final
attB PCR product (30 ng/μl)	1.5	25 fmol
pDONR222 (100 ng/μl)	0.75	25 fmol
TE buffer pH 8.0	1.75	
BP clonase enzyme mix	1.0	

pDONR construct as template. Primers used in this PCR are listed in table 2.3, reaction mix in table 2.18, and PCR program in table 2.17. Afterwards, samples were purified using QIAquick® PCR Purification Kit according to the manufacturer's protocol. To eliminate STAT6 wild-type 3xFlag pDONR template, samples were digested with DpnI restriction enzyme before transformation.

Table 2.17
PCR program for site-directed mutagenesis

Step	Temperature [°C]	Duration [sec]	Cycles
Initial denaturation	98	30	
Denaturation	98	10	
Annealing	66 ▶ 62 ▶ 58	30	3/Temp
Extension	72	150	
Denaturation	98	10	
Annealing	54	20	20
Extension	72	150	
Final extension	72	1200	
Store	12	∞	

Table 2.18
PCR mix for Phusion polymerase

Reagent	Volume [μl]	Final
Nuclease-free water	11.8	
5x HF Buffer	4.0	1.0x
10 mM dNTPs	0.4	0.2 mM
10 μM Forward primer	1.0	0.5 μM
10 μM Reverse primer	1.0	0.5 μM
Template DNA (20 ng/μl)	1.0	20.0 ng
DMSO	0.6	3.0%
Phusion polymerase	0.2	0.4 Units

LR recombination reaction

To create expression clones from STAT6 pDONR constructs, LR recombination reaction was performed to transfer STAT6 wild-type and mutant sequences into pCIG expression vector. It is a lentiviral vector with cytomegalovirus (CMV) promoter, thus suitable for transduction and expression in mammalian cells. As fluorescent marker the vector features ZsGreen, a GFP variant, which is expressed simultaneously to STAT6 due to the internal ribosome entry site upstream of ZsGreen. For Gateway® cloning, a Gateway® cassette was inserted to the multiple cloning site. The LR reaction mix is listed in table 2.19, otherwise the reaction is performed analogous to the BP reaction.

Table 2.19
LR reaction mix

Reagent	Volume [μl]	Final
STAT6 pDONR (500 ng/μl)	0.4	200 ng
pCIG GW (1000 ng/μl)	0.3	300 ng
TE buffer pH 8.0	3.3	
LR clonase enzyme mix	1.0	

Sanger sequencing

Correct sequences for all STAT6 constructs was confirmed by Sanger sequencing (Lightrun sequencing, GATC Biotech). Five μl of purified Plasmid DNA (80-100 ng/μl) were mixed together in a 1.5 ml reaction tube with 5 μl of sequencing primer (5 μM). Sanger sequencing traces were analyzed using FinchTV software and the DNA sequence was aligned to a reference sequence using Serial Cloner software. Table 2.20 lists all successfully cloned STAT6 constructs. The 3xFlag-tagged STAT6 wild-type, D419G, N421K, and D519V pDONR constructs were cloned by Elisa Osterode as part of her Bachelor thesis.

2.2.7 Cell culture

Cell lines used for this work are listed in table 2.7. The identity of those cell lines was verified by short tandem repeat analysis (Eurofins) before this study. Thawing, cultivation and passage of cells were performed under sterile conditions in a laminar flow cabinet class 2.

Table 2.20
Cloned STAT6 constructs

STAT6	Tag	Vector
wild-type	3xFlag	pDONR
wild-type	3xFlag	pCIG
wild-type	HA	pDONR
wild-type	HA	pCIG
D419G	3xFlag	pDONR
D419G	3xFlag	pCIG
D419N	3xFlag	pDONR
D419N	3xFlag	pCIG
N421K	3xFlag	pDONR
N421K	3xFlag	pCIG
D519V	3xFlag	pDONR
D519V	3xFlag	pCIG

Thawing of cells

The cells were thawed at RT in a cryovial until a little ice block remained. In the next step, they were transferred to precooled 13 ml cultivation medium in a 15 ml Falcon tube. Cells were spun down at 300 x g, 5 min, RT and the cell pellet was resuspended in 5 ml preheated (37°C) culture medium. Afterwards, the cells were seeded at high density (2.0 x 10^6/ml) in a T25 flask. After two days medium was added and the cells were transferred to a T75 flask for further cultivation.

Cultivation and passage

Cells were incubated in a humidified incubator at 37°C and 5% CO_2. Culture flasks were checked via light microscopy and on nutrition consumption indicated by the pH indicator on a daily basis. Suspension cell lines were maintained at a cell density between 0.1 - 2.0 x 10^6/ml. Cells were diluted 1:10-1:20 twice a week. Adherent cells were passaged when reaching 80-90% confluency. Therefore, cells were washed once with PBS and afterwards incubated with Trypsin/EDTA solution for max. 5 min at 37°C. Trypsinization was stopped by addition of culture medium and cells were diluted as needed.

Freezing of cells

One day before freezing, the cell's medium was changed. Cells were counted and their viability was checked by Vi-CELL^{TM} XR. 10.0 x 10^6 viable cells were frozen per vial. Cells were transferred into a 50 ml Falcon tube and washed in PBS. Cells were resuspended in 1.0 ml of ice cold freezing medium (50% fetal bovine serum (FBS), 40% cultivation medium, 10% DMSO) and aliquoted into cryovails. Cryovials were stored overnight at -80°C in freezing containers and then transferred into liquid nitrogen for long term storage.

Cell stimulation

Unless indicated otherwise, cells were seeded at a concentration of 1.0 x 10^6 viable cells/ml and stimulated with human, recombinant IL-4, at a final concentration of 10 ng/ml, for the indicated time. During stimulation, cells were kept in a humidified incubator at 37°C. For the *pulse* condition, cells were stimulated with IL-4 for 20 min. After one wash in PBS, cells were resuspended in fresh, preheated growth medium and plated on a new flask/plate. The cells were incubated for another 8 h at 37°C in the absence of IL-4, before further analysis.

Transient transfection of 293T and HeLa

Transfection of cells was carried out by using the cationic lipid delivery reagent ViaFect^{TM}, which forms complexes with anionic nucleic acids and mediates the uptake of DNA plasmids into the cell. Twenty-four hours prior to transfection, 7.0 x 10^6 293T cells were plated on a 10 cm dish in 10 ml growth medium. On the day of transfection, cells were checked for subconfluency (80-90%). Cells were washed with PBS and 8 ml of DMEM + 2.0 mM L-Alanyl-L-Glutamine without FBS was added. Plates were put back in the incubator during preparation of transfection solution. This solution contained 12-20 μg DNA plasmid and was mixed with serum-free DMEM to a final volume of 500 μl. ViaFect^{TM} Transfection Reagent was used at a ratio of 2.5:1 (μl reagent:μg DNA). Again, serum-free DMEM was added to the transfection reagent to a final volume of 500 μl. The two solutions were mixed and incubated for minimum 5 min to max. 10 min to form DNA-cationic lipid complexes. Afterwards, the complex solution was added to the cells. After 4-6 h incubation, 1 ml FBS was added. Twenty-four hours after transfection, the transfection efficiency was checked by fluorescence microscopy.

Lentivirus production

For production of recombinant, replication-deficient lentivirus, 293T cells, expressing SV40 large T antigen, were used as packaging cell line. 293T cells were cotransfected with 15 μg STAT6 pCIG expression vector, containing SV40 origin of replication, 15 μg psPAX2 packaging vector, containing Gag, Pol, Rev, and Tat virus proteins, and 1.5 μg of VSV-G envelope vector using the ViaFect™ transfection protocol (see chapter 2.2.7). Two 10 cm dishes were co-transfected for each construct. Twenty-four hours after transfection, the medium was replaced with 12.5 ml DMEM with 2.0 mM L-Alanyl-L-Glutamine and 10% FBS. Forty-eight hours after transfection, the virus supernatant was collected and 12.5 ml fresh medium was added to the cells. Seventy-two hours after transfection, the virus supernatant was collected for the second time. Remaining cells were removed by one centrifugation step and afterwards the supernatants were filtered through a 0.45 μm syringe filter. The virus was pelleted by 24 h centrifugation at 5000 x g, 4°C. The virus pellet was resuspended in 200 μl growth medium and aliquoted at 50 μl. Virus aliquots were either used for immediate transduction of human cell lines or stored at -80°C for max. 12 months.

Co-transfected packaging cell lines and the resulting replication incompetent lentivirus are classified biosafety level 2 (S2). All S2 operations were performed in a biosafety level 2 laboratory. All waste was collected separately and special decontamination procedures were executed, following S2 regulations. Transduced cell lines were handled as biosafety level 1, after their cell culture supernatant was tested negative for infecting virus particles.

Lentiviral transduction of human lymphoma cell lines

OCI-Ly1 and OCI-Ly8 cell lines were counted and their viability was checked by Vi-CELL™ XR before spin infection. Five hundred thousand cells were seeded in a 24-well plate in 1 ml regular growth medium. Fifty μl concentrated virus and Polybrene (final concentration: 1.0 μg/ml) were added to the cells. The plate was sealed with parafilm and afterwards centrifuged for 90 min at 1174 g, 37°C. Cells were incubated for 4 h, before cells were spun down, resuspended in preheated medium and seeded on a fresh 24-well plate. Forty-eight hours after transduction, the transduction rate was tested by measuring ZsGreen fluorescence using flow cytometry (chapter 2.2.9). In case of a sufficient transduction efficiency, cells were further expanded for cell sorting.

Cell sorting

After lentiviral transduction of OCI-Ly1 and OCI-Ly8, ZsGreen positive cells were sorted. Ten to twenty million cells were washed twice in 1.0 ml PBS with 5% (V/V) FBS. Cells were resuspended in 2.0 ml PBS with 5% (V/V) FBS and passed through a cell strainer cap into a new tube. For live-dead discrimination, 4',6-diamidino-2-phenylindole (DAPI) was added to a final concentration of 50 ng/ml shortly before measurement. Cells were sorted on a FACSAria^{TM} III using a 100 μm nozzle. Cells were collected in 2.0 ml PBS with 5% (V/V) FBS, 1x Anti-Anti, and 10 μg/ml ciprofloxacin. After sorting, cells were washed once with 1.0 ml PBS with 5% (V/V) FBS and resuspended in 500 μl growth medium in a 24-well plate. The medium was supplemented with 1x Anti-Anti and 10 μg/ml ciprofloxacin for 14 days after cell sorting.

2.2.8 Protein methods

Cell lysis for protein analysis

Before cell lysis, a new aliquot of radioimmunoprecipitation assay (RIPA) buffer was thawed and Sigma protease plus phosphatase inhibitors were added (see table 2.6). For adherent cell lines, the cell medium was discarded and the plate was washed once with icecold PBS. The cells were scraped in 1 ml PBS and transferred to a 1.5 ml micro tube. For suspension cell lines, 10.0 x 10^6 cells were transferred to a 15 ml Falcon tube and centrifuged to remove the growth medium. Cells were washed with PBS, the pellet was resuspended in 1 ml PBS, and transferred to a 1.5 ml micro tube. Cells were pelleted by centrifugation and resuspended in RIPA buffer by pipetting up and down several times. Approximately 100 μl RIPA buffer was used to lyse 10.0 x 10^6 cells. The samples were incubated for 20 min on ice and vortexed every 5 min. To remove unsoluble cell debris, micro tubes were centrifuged at 17,115 x g for 30 min at 4°C. Afterwards, the supernatant was transferred to a fresh, labelled micro tube and the pellet was discarded. All steps were performed on ice and cell lysates were always kept on ice. Lysates were used immediately in subsequent experiments or stored at -80°C.

BCA assay

To determine the protein concentration of cell lysates a bicinchoninic acid (BCA) assay was performed using the Pierce™ BCA Protein Assay Kit according to the manufacturer's protocol. Briefly, the lysates were diluted 1:10 in ultrapure water and 25 μl of sample or pre-diluted BSA standard were pipetted into a 96-well plate. Two hundred μl freshly prepared working reagent was added to each well. After 30 min incubation time at 37°C, a microtiter plate reader was used to measure the absorption at 560 nm in triplicates. A BSA standard curve was plotted to determine the protein concentration of the cell lysates.

Immunoblotting

SDS-PAGE

For separation of proteins sodium dodecyl sulfate (SDS)-polyacrylamide gel electrophoresis (PAGE) was performed using Bolt™ precast gels and the Bolt™ Mini Gel Tank according to the manufacturer's protocol. Briefly, 10 μg of protein was loaded, when using a 15-well gel and 30-40 μg for a 10-well gel, respectively. Samples were diluted to 6.5 μl with ultrapure water. Two and a half μl of lithium dodecyl sulfate (LDS) sample buffer (4x) and 1.0 μl of reducing agent (10x) were added, following 10 min incubation at 70°C to denature and reduce the samples. A 4-12% Bis-Tris gel was placed in the gel tank and the chamber was filled with 1x 3-(N-morpholino)propanesulfonic acid (MOPS) SDS running buffer. Samples were added to the wells, including 10 μl SeeBlue® Plus 2 Prestained Standard and 5 μl MagicMark™ XP Western Standard. The run time was 2 h at a constant voltage of 120 V.

Protein transfer

To blot the proteins to a polyvinylidene difluoride (PVDF) membrane (0.45 μm) the Bolt™ Mini Blot Module was used. Before transfer, the PVDF membrane was activated in methanol (MeOH) and sponge pads and filter papers were soaked in transfer buffer (table 2.6). The gel was trimmed and the blot sandwich was assembled with the membrane facing the anode and the gel facing the cathode core, followed by one filter paper and one sponge pad each. Any bubbles were removed and the blot sandwich was placed into the Mini Gel Tank. Deionized (DI) water was added into the chamber to the level of

the electrodes and additional transfer buffer was poured to the module core. The transfer time was 1 h at 20 V.

Chemiluminescent detection

After protein transfer, the membrane was washed once for 5 min in tris-buffered saline (TBS) with 0.1% (V/V) Tween20 (TBS-T) and transferred to a 50 ml Falcon tube. Blocking was performed in 5% (m/V) milk powder in TBS-T for 1 h, followed by one wash in TBS-T. Incubation of the primary antibody was carried out overnight at 4°C in 5 ml of 5% (m/V) milk powder in TBS-T at the appropriate concentration (see table 2.2). After washing (three times, 5 min in TBS-T) the secondary antibody was incubated for 1 h at RT in 5 ml of 5% (m/V) milk powder in TBS-T at a 1:5000 concentration. Subsequently the membrane was washed three times for 5 min in TBS-T and after adding 2 ml of fresh enhanced chemilumescent (ECL) substrate the membrane was visualized using the Fusion SL4 imaging system. Afterwards the ECL was washed away by TBS-T and the membrane was stored in TBS-T at 4°C.

Isolation of nuclear proteins

For isolation of nuclear proteins the Qproteome® Nuclear Protein Kit was used according to the manufacturer's protocol. Half of the recommended volume of lysis buffer NL and extraction buffer NX1 was used to extract nuclear proteins from 15.0 x 10^6 cells. The histone fraction was not extracted. Subsequently, cytosolic and nuclear fractions were applied to immunoblot analysis.

In vitro dimerisation assay

Five μg STAT6 wild-type HA and 5 μg STAT6 mutant 3xFlag construct were co-transfected into 293T cells using ViaFect™ Transfection Reagent (chapter 2.2.7). Twenty-four hours after transfection, cells were treated with IL-4 (10 ng/ml) for 20 min to initiate dimerisation. Afterwards, cells were lysed in RIPA buffer (chapter 2.2.8) and lysates were used to perform protein complex immunoprecipitation (Co-IP). Lysates from native 293T cells, 293T STAT6 wild-type HA only, and 293T STAT6 wild-type 3xFlag only were included as controls. All buffers used in this experiment are listed in table 2.6 and all steps were done on ice or at 4°C. Protein G beads were washed three times in 1 ml Co-IP buffer (centrifugation at 587 x g for 5 min at 4°C) and a 50:50 bead/buffer slurry was made.

For pre-clearing, 900 μl Co-IP buffer, 40 μl bead slurry, 2 μg normal rat IgG, and 600 μg lysate were mixed in a 1.5 ml microcentrifuge tube. For antibody-beads interaction, 900 μl Co-IP buffer, 40 μl bead slurry, and 2 μg anti-HA 3F10 antibody were mixed in a 1.5 ml microcentrifuge tube. Both sets were rotated for 1 h at 4°C. Sixty μg of each lysate was saved as input control, and the experiment included a normal IgG control. After centrifugation, the supernatants from the pre-clearing samples were mixed with the antibody-bead complexes and samples were rotated overnight at 4°C. Beads from pre-clearing and supernatants from antibody-beads interaction were discarded. After overnight incubation, the beads were washed twice with Co-IP buffer and twice with washing buffer. Ten μl 4x LDS sample buffer and 4 μl 10x reducing agent were added and samples were heated at 70°C for 10 min. Afterwards the beads were pelleted by spinning at 9,391 x g for 5 min at RT. Fifteen μl sample was loaded on a gel and immunoblot was performed (chapter 2.2.8). Protein bands were quantified and normalized to the phospho-STAT6 signal (loading control) using the FusionCapt Advance software.

2.2.9 Flow cytometry

To perform flow cytometry experiments, 0.5 x 10^6 cells were seeded in 1.0 ml growth medium in a 12-well plate. Cells were stimulated with IL-4 (10 ng/ml) for 24 h, unstimulated cell lines were included for baseline reference. In experiments which included use of PARP inhibitor PJ34, cells were treated with 50 μM inhibitor 30 min prior to IL-4 stimulation. Cells were transferred to fluorescence activated cell sorting (FACS) tubes and were washed twice in 1.0 ml PBS with 5% (V/V) FBS. Cells were resuspended in 98 μl PBS with 5% (V/V) FBS and 2 μl anti-CD23 allophycocyanin (APC) antibody was added. Samples were incubated for 45 min at 4°C in the dark. After two washing steps, cells were resuspended in 400 μl PBS with 5% (V/V) FBS and samples were applied to FACS analysis. For live-dead discrimination, DAPI was added to a final concentration of 500 ng/ml shortly before measurement. Unstained native cells, native cells plus DAPI, ZsGreen positive cells, and CD23 APC stained CompBeads Anti-Mouse Ig, κ were included as compensation controls. Compensation was calculated automatically by FACSDiva™ software. The applied gating strategy is depicted in figure 2.2 and the cytometer configuration is listed in table A.1 in the appendix. Data was exported and analyzed with FlowJo software. The geometric mean of the ZsGreen and APC double positive population was determined and applied to further statistical analysis (chapter 2.2.15). To maximize the signal and reduce the noise, the optimal concentration of FACS

antibody was determined by titration prior to experiments (table 2.2). Gating boundary for ZsGreen fluorescence was identified using ZsGreen negative OCI-Ly1 and OCI-Ly8 native cell lines. Gating boundary for APC fluorescence was identified using APC mouse IgG1, κ isotype control.

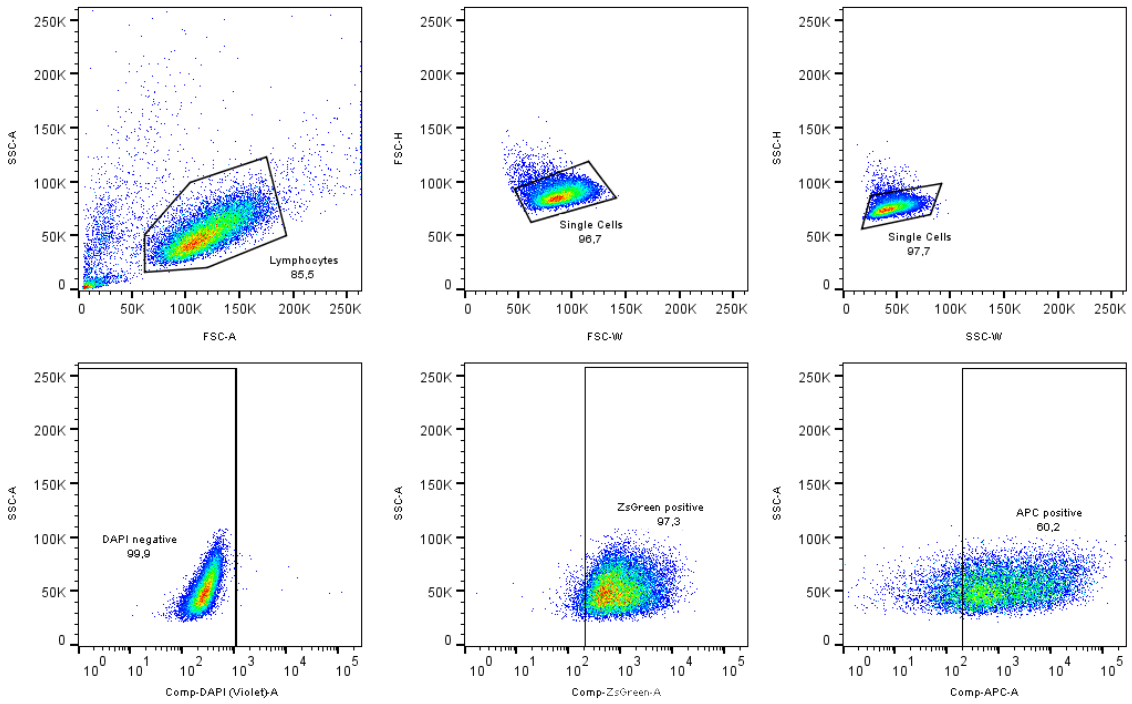

Figure 2.2
FACS gating strategy. Representative dot plots of OCI-Ly1 STAT6 D419G cell line to illustrate the applied gating strategy. Cells were stimulated with IL-4 (10 ng/ml) for 24 h before experiment.

2.2.10 Quantitative reverse transcription PCR

Isolation of total RNA

Total RNA was isolated by single-step acid guanidinium thiocyanate-phenol-chloroform extraction.[138,139] Therefore, 10.0 x 10^6 cells were transferred to a 15 ml Falcon tube and centrifuged. The medium was removed and the cell pellet was lysed in 500 μl TRIzol® reagent by pipetting up and down several times. Samples were either stored at -80°C (maximum 2 months) or RNA isolation procedure was continued immediately. For phase separation, 100 μl chloroform was added and tubes were shaken by hand for

15 sec. After centrifugation (12,000 x g, 15 min, 4°C), the upper, aqueous phase was removed into a fresh tube. To precipitate the RNA, 250 μl 100% isopropanol was added and samples were incubated at RT for 10 min. The RNA was pelleted by centrifugation at 12,000 x g for 10 min at 4°C and the supernatant was discarded. The RNA was washed in 500 μl 75% EtOH by vortexing, then centrifuged at 7,500 x g for 5 min at 4°C. Afterwards, the wash was removed, the RNA pellet was resuspended in 44 μl nuclease-free water, and tubes were incubated in a heat block at 55°C for 10 min. To remove genomic DNA (gDNA) contaminations from the samples, Deoxyribonuclease I digestion was performed using Roche DNase I kit. Therefore, 5 μl of the provided 10x incubation buffer and 1 μl enzyme solution (equates to 10 units) were added to the RNA samples and incubated at 37°C for 20 min. The enzyme was inactivated by addition of EDTA (pH 8.0) to a final concentration of 8 mM and heating to 75°C for 10 min. Afterwards, RNA concentration was determined by NanoDrop. RNA was stored at -80°C for maximum 2 months.

Working with RNA is challenging, mainly because of the ubiquitous presence of RNases and its chemical instability. Adequate precautions were taken when working with RNA. All RNA work was performed under a PCR Workstation. All surfaces, pipettes, racks etc. were treated with RNase AWAY® prior to work. Only nuclease-free filter tips, tubes, and water were used. RNA-containing samples were kept on ice whenever possible. Clean gloves and lab coat were worn and gloves were changed frequently.

Synthesis of complementary DNA

To synthesize first-strand cDNA from total RNA, the SuperScript® III First-Strand Synthesis System was used according to the manufacturer's protocol. Starting material was 1 μg of total RNA and the reaction was primed using random hexamers provided with the kit. cDNA synthesis reactions were used for subsequent quantitative PCR (qPCR) or stored at -20°C.

SYBR™ Green quantitative PCR

To quantify IL-4 mediated transcription of CD23 SYBR™ Green qPCR was performed. The components of the reaction mix were combined as displayed in table 2.21 in a MicroAmp® Optical 96-Well Reaction Plate.

Table 2.21
qPCR reaction mix

Name	Amount
cDNA synthesis reaction	1.0 μl
Forward primer (10 μM)	1.0 μl
Reverse primer (10 μM)	1.0 μl
Nuclease-free water	7.0 μl
Fast SYBR^{TM} Green Master Mix	10.0 μl

Controls in this experiment included cDNA from unstimulated cell lines and no template controls (negative control). GAPDH levels were measured for housekeeping. All used primers are listed in table 2.3 and every primer pair was tested for primer efficiency before use. Samples were run in technical duplicates. After pipetting, the plate was sealed with a clear adhesive film and the plate was stored in the dark until measurement. The program for DNA amplification and detection of SYBR^{TM} Green fluorescence is depicted in table 2.22. To validate the assay specificity, melting curves were recorded and analyzed for each sample. Furthermore, the PCR products were loaded on a 1.5% agarose gel in 0.5x TBE buffer to check for unspecific bands and primer dimers. Data analysis was performed using the provided SDS 2.4.1 software. The delta Cycle threshold (Ct) value was calculated by subtraction of Ct(GAPDH) values from the corresponding Ct(CD23) values. The mean of the two technical replicates was calculated. Average delta Ct values were log2 transformed (= $2^{\text{-delta Ct}}$), and data was normalized for IL-4 stimulated, wild-type STAT6. Subsequent statistical analysis is described in section 2.2.15.

Table 2.22
qPCR program

Step	Temperature [°C]	Duration [sec]	Cycles
Enzyme activation	95	20	1
Denaturation	95	1	40
Annealing/Extension	63	20	
Dissociation stage	95	15	1
	63	15	1
	95	15	1

2.2.11 ELISA

To measure soluble CD23 (sCD23) levels in cell culture supernatants, 0.5 x 10^6/ml cells were seeded in a 6-well plate, the total volume was 3.0 ml. Cells were stimulated with IL-

4 (10 ng/ml) for 48 h, for each cell line an unstimulated control was included. Afterwards, cells were counted and their viability was checked by Vi-CELL™ XR in duplicates. 2.0 ml of cell suspension was centrifuged and the supernatant was filtered through a 0.22 μm syringe filter to remove cell debris. Supernatants from native 293T HEK cells (with and without IL-4 stimulation) were included as negative controls. Supernatants were assayed with the CD23 (soluble) Human ELISA Kit, according to the manufacturer's protocol. Anti-sCD23 coated wells were pre-incubated in 20 μl diluent, before 180 μl cell culture supernatant was added. Absorbances were read with the GloMax® Discover at 450 nm in technical triplicates. Absorbance values were corrected by viable cell count before statistical analysis.

2.2.12 RNA sequencing of OCI-Ly1 STAT6 cell lines

RNA sequencing (RNA-seq) experiment included messenger RNA (mRNA) from OCI-Ly1 (STAT6 wild-type, D419G, D419N, and N421K). To reach the same sample size between STAT6 wild-type and STAT6 mutant samples, three independent STAT6 wild-type samples were included. Furthermore, the experiment involved three different time points and all samples had three biological replicates (54 samples in total). The experiment was performed blind to the genotype. Cells were cultivated separately one week before IL-4 treatment. On the day of IL-4 stimulation, cells were counted with Vi-CELL™ XR, randomized, and 1.0 x 10^6 viable cells were seeded in 1 ml growth medium on a 12-well plate. Cells were treated with IL-4 (10 ng/ml) for 20 min at 37°C and then transferred to a 1.5 ml microcentrifuge tube. After one wash in preheated PBS, cells were resuspended in 1 ml growth medium and plated onto a fresh 12-well plate. Stimulated cells were incubated at 37°C for 2 h, 4 h, and 8 h, respectively. After incubation, 10 μl cell suspension (or 10,000 cells) were transferred to a 96-well PCR tray and mixed with 100 μl Qiagen RLT buffer. For better handling, IL-4 stimulation was performed separately for each time point, and samples were frozen in three separate plates at -80°C.

Library preparation was performed in the laboratory of Prof. Dr. Wolfgang Enard by Christoph Ziegenhain following the single cell RNA barcoding and sequencing (SCRB-seq) protocol as described previously.[140,141] Briefly, RNA was extracted using the Direct-zol™ RNA MiniPrep Plus kit (Zymo Research) according to the manufacturer's protocol. cDNA was synthesized using Maxima H Minus Reverse Transcriptase, universal E5V6NEXT primer, and E3V6NEXT barcoded oligo-dT primer. E3V6NEXT primers contained a 6 bp barcode, which is well-specific, and a 10 bp unique molecular identifier,

which allows identification of individual mRNA molecules and their quantification.[142] Universal E5V6NEXT primer induced 2nd strand cDNA synthesis and template switching. Full length cDNA from all samples were pooled and concentrated using magnetic beads. Excessive primers were removed by Exonuclease I digestion. The cDNA pool was amplified by a single primer (SINGV6) PCR using KAPA HiFi HotStart polymerase. Afterwards, Nextera XT library preparation kit (Illumina) was used to create the sequencing library. The kit used transposomes for Tagmentation of DNA. This reaction fragments the full length cDNA and adds Illumina adaptor sequences to the fragments. Adaptor sequences are required for enrichment of adapter-ligated fragments, binding to the flow cell, and for multiplexing. The manufacturer's protocol was modified and a custom primer (P5NEXTPT5) was used. This results in 3' enrichment, since the 5' end is not able to bind to the flow cell. 3' enrichment is desired when aiming for transcriptome quantification and differential gene expression analysis. Finally, the sequencing library was size selected on a 2% E-Gel EX Gel (300-800 bp), DNA was extracted and quantified.

Libraries were sequenced in the laboratory of Dr. Helmut Blum by Dr. Stefan Krebs on an Illumina HiSeq 1500 system. Sequencing was performed paired-end on two lanes of an Illumina flow cell. Read one (16 bp) covered the well-specific barcode and UMI, an index read (8 bp) decoded the Nextera i7 barcode, and read two (50 bp) sequenced the cDNA fragment.

Raw sequence data was processed by Christoph Ziegenhain following the Drop-seq data pipeline.[143] Briefly, index reads were demultiplexed using deML, and reads were trimmed to 45 bp by cutadapt.[144,145] Afterwards, reads were aligned to the human genome (hg38, Ensemble release 84) using STAR 2.5.2b with standard parameters.[146] To count gene transcripts, unique UMI sequences were counted for each gene, within each sample. The output was a gene expression matrix with UMI counts for 31835 unique ENSG IDs (Ensembl genes) in 54 samples.

2.2.13 Bioinformatic analysis

This data was further analyzed using DESeq2 (1.16.1) package.[147] The count matrix was imported and samples were unblinded and annotated to from *DESeqDataSets*. Further data analysis was performed for the whole dataset and for each time point separately. Compared were samples according to their STAT6 mutational status. Data from STAT6 D419G, D419N, and N421K samples were pooled and were compared to STAT6 wild-type.

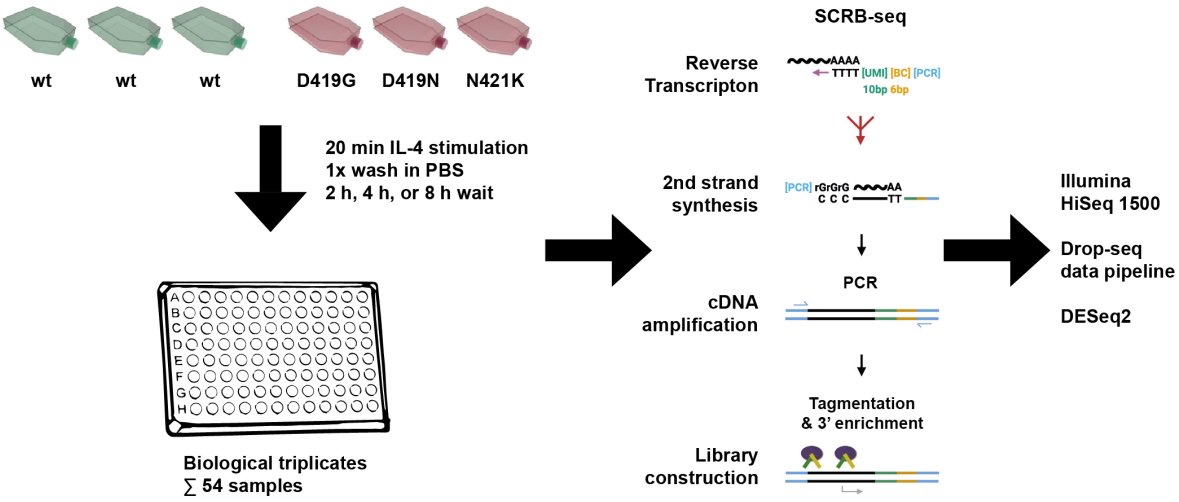

Figure 2.3
RNA sequencing workflow. The experiment included mRNA from OCI-Ly1 STAT6 D419G, D419N, and N421K mutant and three independent STAT6 wild-type samples. All samples had three biological replicates. Cells were treated with IL-4 for 20 min. After cytokine washout, cells were incubated for 2 h, 4 h, and 8 h, respectively. Library preparation was performed following SCRB-seq protocol. Libraries were sequenced on an Illumina HiSeq 1500 system and raw sequence data was processed following the Drop-seq data pipeline. Differential gene expression analysis was done using DESeq2 package. wt: wild-type. Figure modified from Ziegenhain *et al.*[140]

DESeqDataSets were pre-filtered by removing ENSG IDs with no counts, or only a single count. For data quality evaluation, sample-to-sample distances were visualized by doing principal components analysis (PCA) using regularized log transformed data. DESeq2 differential expression pipeline was run, false discovery rate (FDR) threshold was lowered to 5%. HGNC gene symbols were added using *useMart* function. ENSG IDs which received no HGNC symbol were filtered. Differential expression was statistically verified by Wald test and corrected for multiple testing using the Benjamini-Hochberg adjustment. Adjusted p-values and log2 fold change (FC) values were extracted to draw heatmaps and volcano plots. Heatmaps were generated using pheatmap (1.0.8) package, all other plots were created using ggplot2 (2.2.1).[148] The RNA-seq workflow is summarized in figure 2.3.

2.2.14 Luciferase reporter assay

The DNA sequence of the the PARP14 promoter region (ENSR00000305844) was uploaded to MatInspector software (Genomatix). The software identified twelve putative

STAT binding sites (figure 3.29). Eight constructs were designed covering the twelve sites (figure 3.30).

PARP14 promoter constructs were cloned from OCI-Ly8 gDNA by PCR using KOD polymerase (table 2.15). The primers used in this experiment are displayed in table 2.3 and the programs is listed in table 2.23 and 2.24. Forward primers contained XhoI restriction sites and reverse primers contained HindIII restriction sites for cloning of PARP14 promoter regions into the multiple cloning site of pGL3-Basic luciferase reporter vector (vector map in the appendix A.5).

Table 2.23
3-step stepdown PCR program for PARP14 promoter constructs. 45 sec extension time was applied for constructs #1-#5 (293 bp - 621 bp), 145 sec for contructs #6-#7 (1537 bp - 1609 bp).

Step	Temperature [°C]	Duration [sec]	Cycles
Initial denaturation	95	120	
Denaturation	95	30	
Annealing	74 ▶ 70 ▶ 66 ▶ 62 ▶ 58	40	3/Temp
Extension	68	45 or 145	
Denaturation	95	30	
Annealing	54	40	20
Extension	68	45 or 145	
Final extension	68	300	
Store	12	∞	

Table 2.24
2-step stepdown PCR program for full-length PARP14 promoter

Step	Temperature [°C]	Duration [sec]	Cycles
Initial denaturation	94	120	
Denaturation	98	10	
Annealing/Extension	74 ▶ 72 ▶ 70	340	5/Temp
Denaturation	98	10	
Annealing/Extension	68	340	20
Final extension	68	420	
Store	12	∞	

PCR products were run on an agarose gel, correct size bands were cut from the gel, and DNA was extracted. DNA was eluted in 40 μl nuclease-free water, which was mixed with 2.5 μl XhoI, 2.5 μl HindIII HF, and 5 μl CutSmart® Buffer for an double digest (overnight, 37°C). Samples were purified using PCR purification kit and quantified with NanoDrop 1000 Spectrophotometer. In parallel, five times 2 μg pGL3-Basic vector were digested accordingly (20 μl reactions). Linearized vector was cut from the agarose gel and extracted. A second digest was performed (3 h, 37°C) before samples were pooled, purified, and quantified. Ligation was done 5 min at RT using NEB Quick Ligation™ kit. Thirty ng of linearized vector was used, the insert to vector ratio was 3:1. Two and a half μl of the ligation reaction was mixed with 25 μl One Shot® TOP10 Chemically Competent *E. coli* for transformation. Constructs were verified by Sanger sequencing. Constructs #2, #3, and #6 were successfully cloned and tested. Only construct #3 showed induction of luciferase and was therefore selected for further analysis (data not shown).

Luciferase reporter assay was performed by transient transfection of PARP14 promoter pGL3 constructs in 293T HEK cells as described before (chapter 2.2.7). 293T HEK cells were particular suitable, since they lack endogenous STAT6, yet express all other components of the IL-4 signaling cascade.[149] One day prior transfection, 150,000 cells per well were plated in 500 μl cell culture medium on 24-well plates. 200 ng PARP14 promoter pGL3 were co-transfected with 40 ng pRL Renilla luciferase control reporter vector and 1 ng, 10 ng, or 50 ng STAT6 wild-type or mutant pCIG expression vector. Controls included reactions without STAT6 pCIG construct and reactions with pGL3-Basic vector without PARP14 promoter region. To ensure comparable transfection efficiency across all reactions, equal amounts of DNA (290 ng) were transfected. Therefore, 50 ng, 49 ng, or 40 ng pCIG empty vector were transfected, as well. Table 2.25 lists all plasmids used in this experiment.

Table 2.25
Plasmids used in luciferase reporter assays

Name	Function
PARP14 promoter pGL3	Luciferase reporter vector, *luc+* gene is under control of PARP14 promoter fragment
STAT6 wild-type / mutant pCIG	STAT6 expression vector
pRL	Renilla luciferase control reporter vector
pCIG empty vector	To transfect same amounts of DNA across reactions

FBS was added to the cells after 4-6 h. 24 h after transfection, cells were stimulated with 10 ng/μl IL-4 for 6 h. Afterwards, the cell medium was removed and cells were washed

with PBS. Hundred μl Promega passive lysis buffer (1x), which does not interfere with luciferase enzyme activity, was added to each well and plates were incubated for 10 min at RT on a horizontal shaker. Twenty μl lysate was transferred to a white 96-well plate and mixed with 50 μl Dual-Glo® Luciferase reagent. The assay was performed according to Promega Dual-Glo® Luciferase Assay System manual. Luminescence was measured in triplicates using the GloMax® Discover plate reader. Experiments were done on two separate days, each included samples in experimental triplicates and each sample was analyzed in technical duplicates. Data analysis started with averaging repeated measurements and subtraction of background. Technical replicates were also averaged and normalizing ratios of firefly luminescence and Renilla luminescence were calculated. Finally, fold changes were calculated based on the control sample with PARP14 promoter pGL3, pRL, and pCIG empty vector co-transfected (without STAT6 pCIG). Statistical analysis was assessed using GraphPad Prism software, performing ordinary two-way ANOVA and Dunnett's multiple comparisons test (chapter 2.2.15).

The PARP14 knockdown experiments were performed accordingly. Therefore, 200 ng PARP14 promoter pGL3 #3 construct were co-transfected with 50 ng STAT6 wild-type or mutant pCIG expression vector, 100 ng PARP14 short hairpin RNA (shRNA) plasmid (#4, #5, and non-target control, table 2.4) and 40 ng pRL Renilla Luciferase control reporter vector into HeLa cells, which express endogenous PARP14. Transfection protocol and Promega Dual-Glo® Luciferase assay protocol were identical. The assay was performed in experimental triplicates, on separate days and each samples was analyzed in technical duplicates.

2.2.15 Statistical analysis

Data from at least three independent experiments were collected and displayed as mean value $\pm$ SD. Ordinary two-way ANOVA followed by Dunnett's multiple comparisons test using GraphPad Prism software was performed. The number of analyzed families was two (with and without IL-4 Stimulation). Within each family, every mutant STAT6 was compared to wild-type STAT6 data. Multiplicity adjusted p-values for each comparison are reported. Statistical significance was defined as $p<0.05$. Before performing two-way ANOVA, the data was tested for normal distribution by Shapiro-Wilk test.

3 Results

3.1 STAT6 mutations in the GLSG2000 and BCCA cohort

I reanalyzed available sequencing data from Pastore *et al.* of 258 patients with advanced stage FL from the GLSG2000 and BCCA (appendix A.1 and A.2). Thirty-three cases (13%) carried STAT6 mutations in this cohort. All STAT6 mutations clustered within the DNA binding domain (35/35, 100%), including a hotspot at position D419 (figure 3.1). Additionally, there were three patients in our cohort who had a polymorphism-like variant at this position, which is listed in dbSNP (rs11172102, D419N). The variant allele frequency (VAF) of two of those cases suggested somatically acquired mutations (figure 3.2).

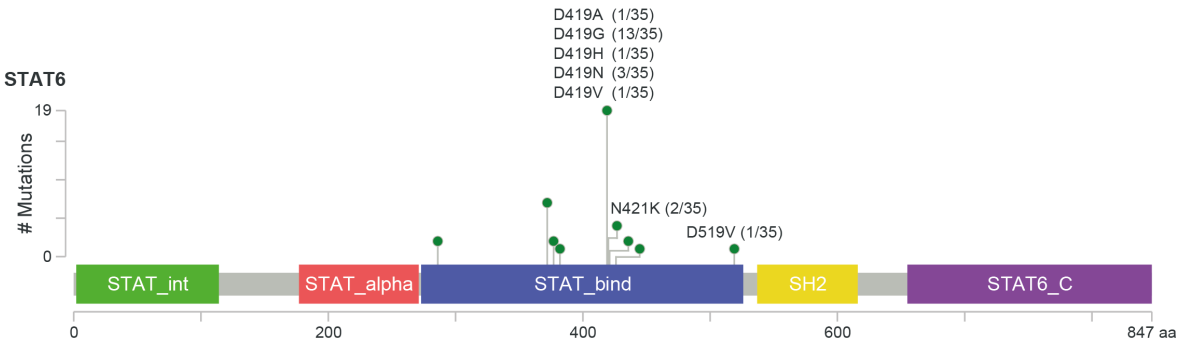

Figure 3.1
STAT6 mutations and polymorphism-like gene variations (D419N) in 258 patients from the GLSG2000 and BCCA cohort. STAT_int: protein interaction domain, STAT_alpha: all-alpha or coiled coil domain, STAT_bind: DNA-binding domain, SH2: src homology 2 domain, STAT6_C: C-terminal transactivation domain. Lollipop plot is visualized by Mutation Mapper from cBioPortal (`http://www.cbioportal.org/mutation_mapper.jsp`).

Two patients harbored two mutations each within the STAT6 DNA binding domain. In both cases, the two mutations were covered by the same sequencing read, i.e. they were located *in cis* on the same allele (appendix A.6).

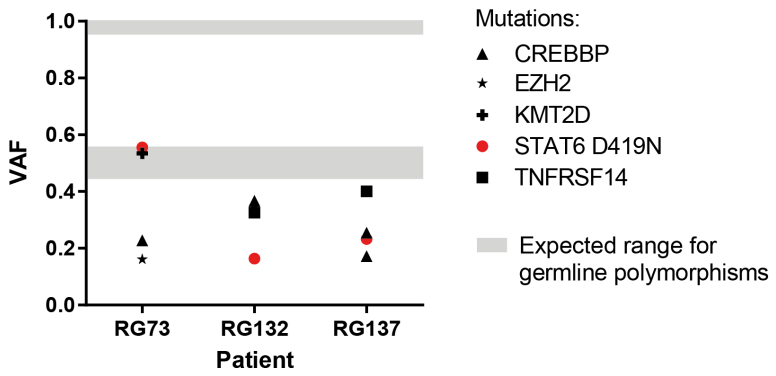

Figure 3.2
Variant allele frequencies of selected recurrent mutations from three patients carrying the D419N polymorphism-like variant. Grey area in the plot indicates the expected range for germline polymorphisms. VAF: Variant allele frequency.

3.2 Failure-free survival in the GLSG2000 and BCCA for patients with STAT6 DNA binding variations

I analyzed failure-free survival (FFS) of the 258 patients by STAT6 mutational status in a multivariate Cox regression model adjusting for high-risk FLIPI and ECOG performance status 2-4. All patients had advanced stage disease and received upfront immunochemotherapy. Patients with mutations in the DNA binding domain of STAT6 had shorter FFS (5-year FFS: 54.0% vs 64.2%), yet this did not reach statistical significance in this cohort (figure 3.3; hazard ratio 1.512, 95% confidence interval 0.939-2.435, P= 0.0888).

3.3 Gene expression data from primary FL samples

3.3.1 Genome-wide gene expression data from BCCA primary FL samples

I reanalyzed available genome-wide RNA profiling data (DASL, Illumina) from 106 diagnostic biopsies, including 89 wild-type and 17 mutant cases, to identify mutant *STAT6* specific gene expression patterns.

Several IL-4 regulated genes were significantly upregulated in STAT6 mutant cases (figure 3.4). The top most differentially expressed genes included *CCL17* (FC: 0.98, p-value: 0.0001), *CCL22* (FC: 0.73, p-value: 0.0381), and *FCER2* (FC: 1.04, p-value:

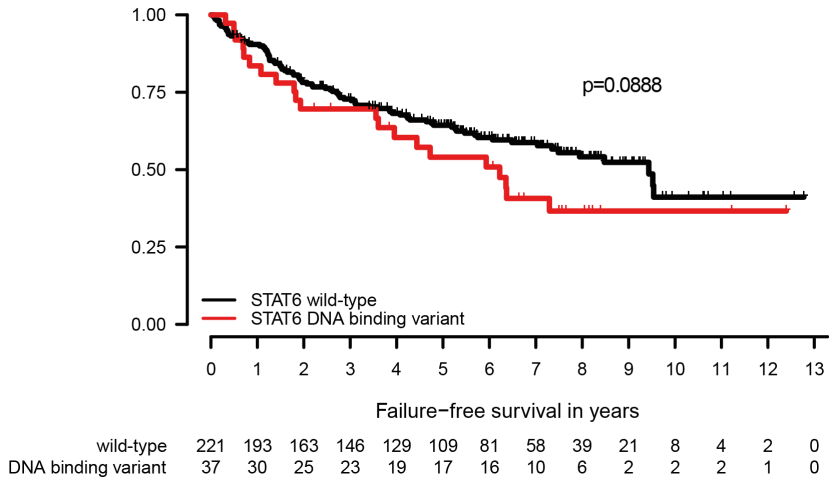

Figure 3.3
FFS in the GLSG2000 and BCCA cohort for patients with wild-type STAT6 or variations in the STAT6 DNA binding domain. Kaplan-Meier curve of 221 STAT6 wild-type patients and 37 patients with STAT6 DNA binding variants. Curves were compared using log-rank test and fitting the cox-regression model was done multivariate with adjustment for high-risk FLIPI and ECOG performance status 2-4.

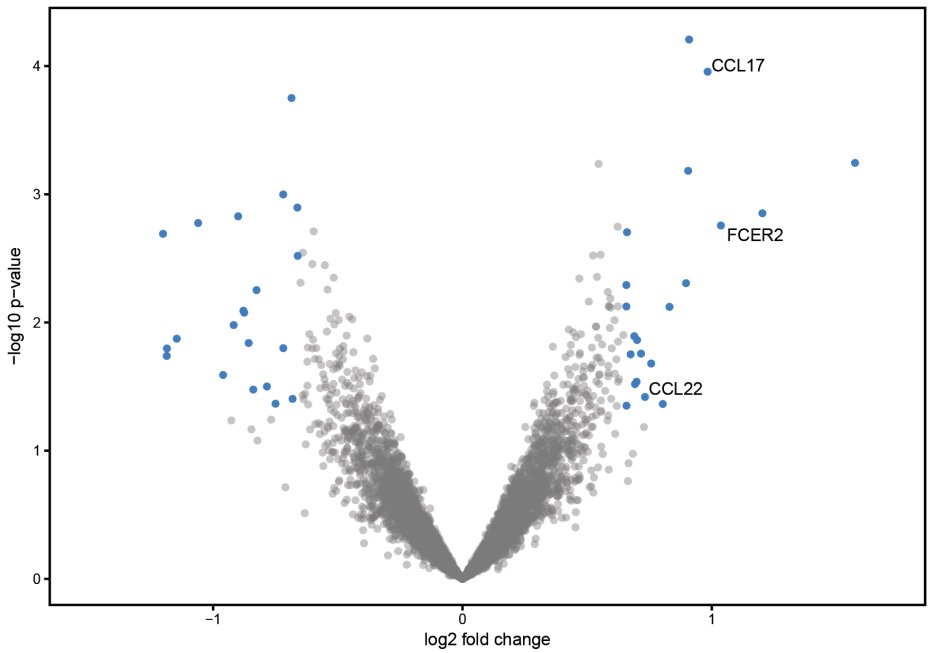

Figure 3.4
Volcano plot showing differentially expressed genes between STAT6 wild-type and mutant status in 106 patients of the BCCA. Among the top most differentially expressed genes were IL-4 regulated genes *FCER2*, *CCL17*, and *CCL22*. Cutoff: log2FC: ± 0.65, p-value: <0.05.

0.0018), which encodes for the low-affinity cell surface receptor for IgE (FcεRII), alias CD23. A complete list of differentially expressed genes is in the appendix (table A.2).

Unsupervised, hierarchical clustering of 106 BCCA patients significantly separated patients according to their STAT6 phenotype (figure 3.5). In the first cluster 9 out of 18 patients (50%) carried STAT6 mutations, whereas in the second cluster only 8 out of 88 patients (9%) had mutations in STAT6.

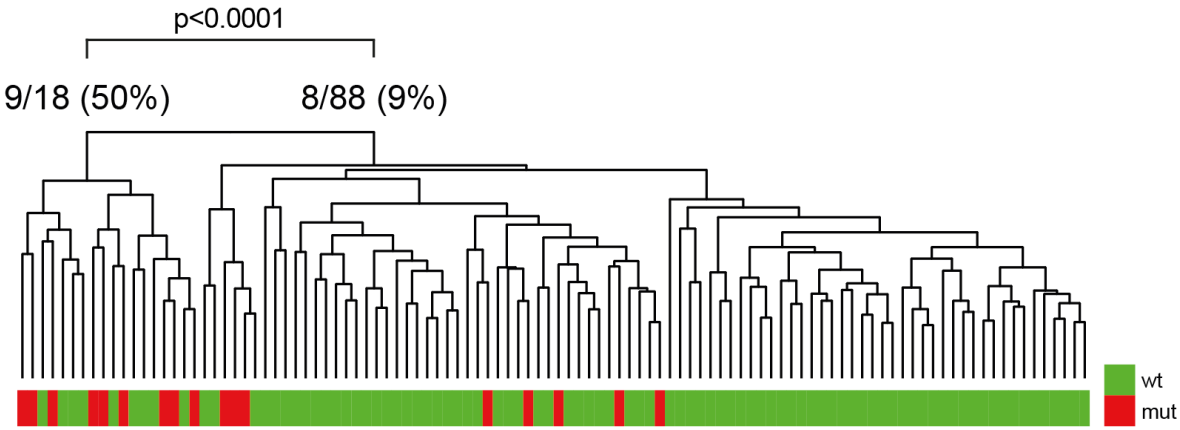

Figure 3.5
Dendrogram shows unsupervised, hierarchical clustering of 106 BCCA patients according to their STAT6 mutational status. Unpaired t test was used to determine the statistical difference between the two groups. wt: wild-type, mut: mutant.

To link this gene expression data to biological function, I performed GSEA with focus on IL-4/STAT6 signaling. GSEA showed significant enrichment of two distinct IL-4 gene signatures in STAT6 mutant cases (figure 3.6). The gene sets have been previously published by Schaefer *et al.* and by Zhang *et al.* One gene set includes genes upregulated by IL-4,[150] the other containing genes which are part of the IL-4 signaling cascade.[151]

3.3.2 CD23 expression in patients from the GLSG2000

As CD23 was among the top differentially expressed genes in patients with mutant STAT6 in the BCCA cohort, we aimed to validate this finding in an independent, second cohort. We used available data of 138 patients from the GLSG2000 with known STAT6 mutation status. Again, CD23 expression was significantly increased in patients having a STAT6 mutation compared to patients with wild-type STAT6 (figure 3.7).

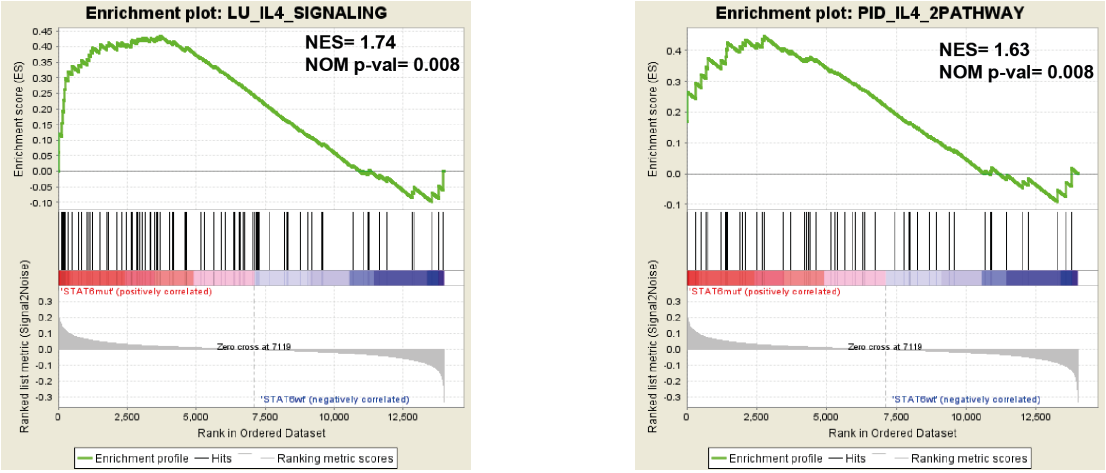

Figure 3.6
GSEA shows significant enrichment of gene sets with IL-4 regulated genes and genes involved in the IL-4 pathway in patients with mutated STAT6. NES: normalized enrichment score, NOM p-val: nominal p-value.

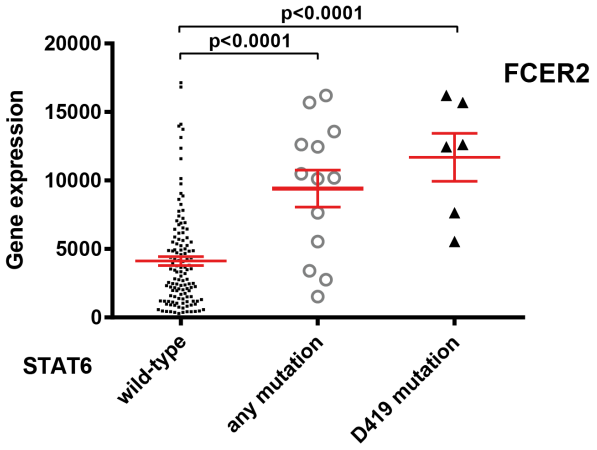

Figure 3.7
CD23 expression in 138 patient samples from the GLSG2000 cohort with known STAT6 mutation status.

3.4 CD23 and pSTAT6 immunohistochemistry in primary FL samples

To confirm enhanced IL-4 pathway activation in STAT6 mutant lymphomas, we performed IHC for pSTAT6 and CD23 on primary patient samples. We found increased pSTAT6 and CD23 staining in STAT6 mutant cases compared to wild-type. Moreover, pSTAT6 positive cells were forming clusters in STAT6 mutant patients compared to wild-type (figure 3.8).

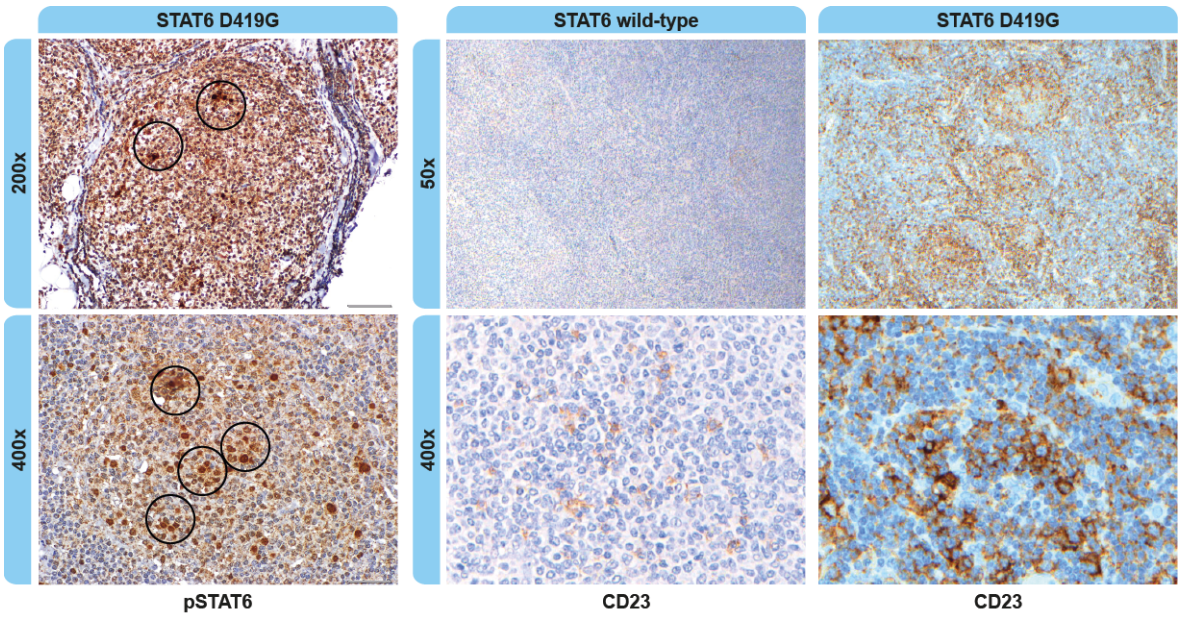

Figure 3.8
pSTAT6 and CD23 immunohistochemistry of FL primary patient samples. Left: representative pSTAT6 IHC stain showing cluster formation of pSTAT6 positive cells in patient with mutant STAT6. Right: representative CD23 IHC stain displaying enhanced CD23 expression in STAT6 mutant cases compared to wild-type.

3.5 Identification of an appropriate cell line model to functionally characterize *STAT6* mutations

3.5.1 CD23 expression in various B-NHL cell lines

To identify a suitable cell line model to investigate the biology of STAT6 mutants, available B-NHL cell lines were tested for membrane CD23 expression upon 48 h IL-4 stimulation by flow cytometry. The final concentration of IL-4 was 10 ng/ml. DG75, Karpas 422, OCI-Ly18, and SU-DHL-5 did not increase membrane CD23 expression upon IL-4 treatment, or only to a small extent. Namalwa and WSU-FSCCL already had a high baseline CD23 expression (data not shown). OCI-Ly1 and OCI-Ly8, two cell lines carrying the t(14;18)(q32;q21) translocation, had low baseline CD23 expression and responded to IL-4 stimulation with an upregulation of CD23. Therefore, they were selected for further analysis.

3.5.2 IL-4 time course experiment in OCI-Ly1 and OCI-Ly8 cell lines

To identify the optimal duration of IL-4 stimulation, a time course experiment was performed. OCI-Ly1 and OCI-Ly8 cell lines were treated with IL-4 (10 ng/ml) for 8 h, 24 h, 48 h, and 72 h, followed by membrane CD23 detection using flow cytometry. After 8 h IL-4 stimulation, there was an upregulation in CD23 expression which peaked after 24 h in both cell lines. In OCI-Ly1 cells, membrane CD23 expression was still at its maximum at the 48 h time point and declined almost back to baseline level after 72 h. In OCI-Ly8, CD23 expression already decreased after 48 h and was back to baseline level at the 72 h time point. Stimulation with IL-4 for 24 h showed significant upregulation of CD23 in both cell lines and was used in subsequent experiments (figure 3.9).

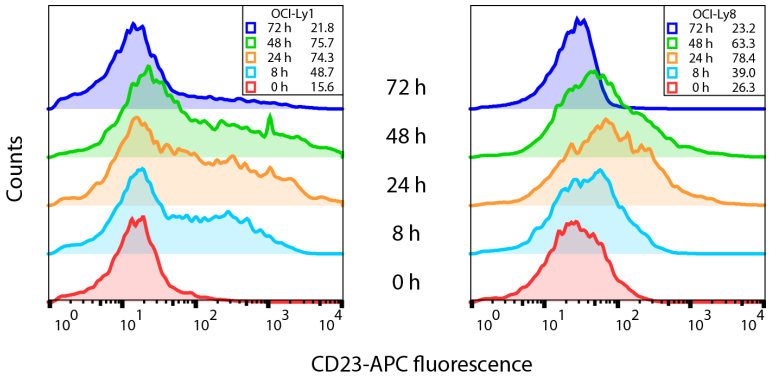

Figure 3.9
IL-4 time course experiment in OCI-Ly1 and OCI-Ly8 cell lines assessed by analysis of membrane CD23 expression by flow cytometry. Cells were stimulated with increasing duration of IL-4 (10 ng/ml) as indicated or were cultivated without IL-4 (red). Numbers in the legend indicate the geometric mean of the CD23-APC fluorescence.

3.5.3 *STAT6* mutations included for functional experiments

I selected the following STAT6 variants for further functional experiments. The STAT6 D419G point mutation was included, since it was the most frequent mutation detected in patients with FL. The D419N variant was included, because of the co-localization of this polymorphism with the mutational hotspot. Moreover, from all STAT6 mutations found in the GLSG2000 and BCCA cohort, N421K and D519V mutations were predicted to have a significant functional impact based on the MutationAssessor score. This score is based on the evolutionary conservation of protein residues within protein families and subfamilies (`http://mutationassessor.org/v1/`).[152]

3.5.4 Stable expression of STAT6 variants in OCI-Ly1 and OCI-Ly8 cell lines

OCI-Ly1 and OCI-Ly8 cell lines stably expressing STAT6 wild-type and STAT6 mutants were generated by lentiviral transduction. The used pCIG expression vector had a ZsGreen fluorescent marker and the ZsGreen positive population was sorted after transduction. A C-terminal 3xFlag tag allowed the detection of ectopic 3xFlag-tagged STAT6 next to endogenous STAT6. I confirmed the equal expression of STAT6 3xFlag in all cell lines by immunoblot analysis (figure 3.10). The simultaneous expression of endogenous wild-type STAT6 and ectopic mutant STAT6 in OCI-Ly1 and OCI-Ly8 makes them an ideal model system, since all mutations detected in our cohort were monoallelic.

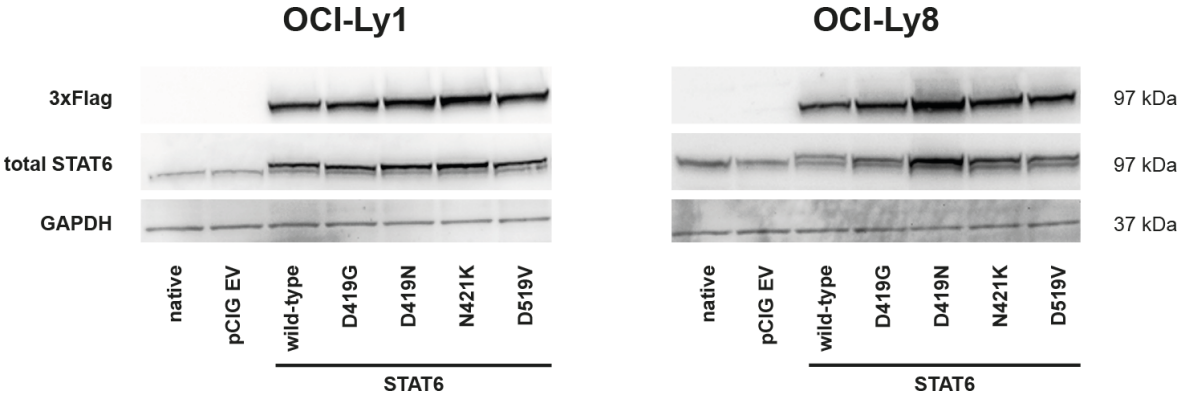

Figure 3.10
Immunoblot showing expression of ectopic, 3xFlag-tagged STAT6 and total STAT6 protein in stably transduced OCI-Ly1 and OCI-Ly8 cell lines. Below the STAT6 3xFlag band, endogenous STAT6 protein was detected. GAPDH was used as loading control.

3.6 CD23 expression in OCI-Ly1 and OCI-Ly8 cell lines stably expressing STAT6 variants

As CD23 is a known target gene of STAT6, plays a role in B cell biology,[153] and its surface expression can be determined by flow cytometry, we decided to use CD23 as a functional readout, for IL-4 mediated STAT6 activation.

3.6.1 CD23 surface expression on OCI-Ly1 and OCI-Ly8 STAT6 cell lines

OCI-Ly1 and OCI-Ly8 cell lines, stably expressing STAT6 wild-type as well as mutant STAT6, were used to check for membrane-bound CD23 levels upon 24 h IL-4 stimulation. STAT6 mutant (D419G, D419N, N421K, and D519V) cell lines showed significantly enhanced CD23 surface expression by FACS analysis compared to wild-type cell lines. Importantly, there was no effect of mutant *STAT6* in the absence of IL-4 (figure 3.11).

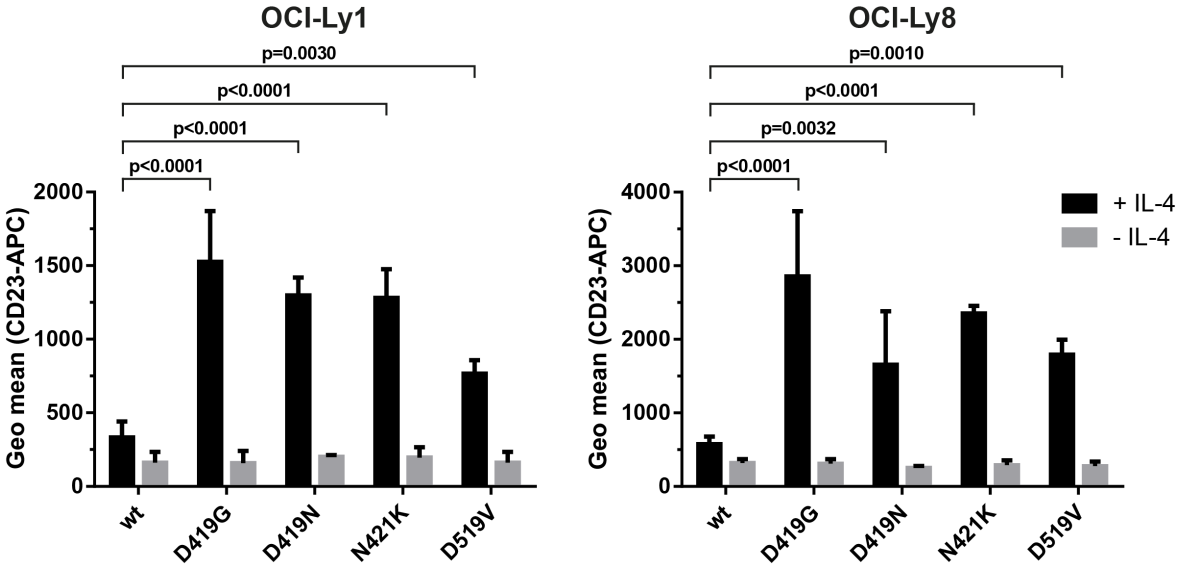

Figure 3.11
Membrane CD23 expression is augmented in lymphoma cell lines expressing mutant (D419G, N421K, and D519V) and polymorphism-like (D419N) STAT6 upon 24 h IL-4 stimulation. Depicted is the geometric mean of CD23-APC fluorescence detected by flow cytometry (N=3, mean±SD). wt: wild-type.

3.6.2 *FCER2* transcription in OCI-Ly1 and OCI-Ly8 STAT6 cell lines

To investigate if these findings result from enhanced transcription, qRT-PCR (SybrGreen) was performed. These experiments showed increased *FCER2* transcriptional levels for OCI-Ly1 expressing mutant STAT6, compared to STAT6 wild-type upon 24 h IL-4 stimulation. Similar results were observed in OCI-Ly8 cells. Again, there was no effect without IL-4 stimulation (figure 3.12).

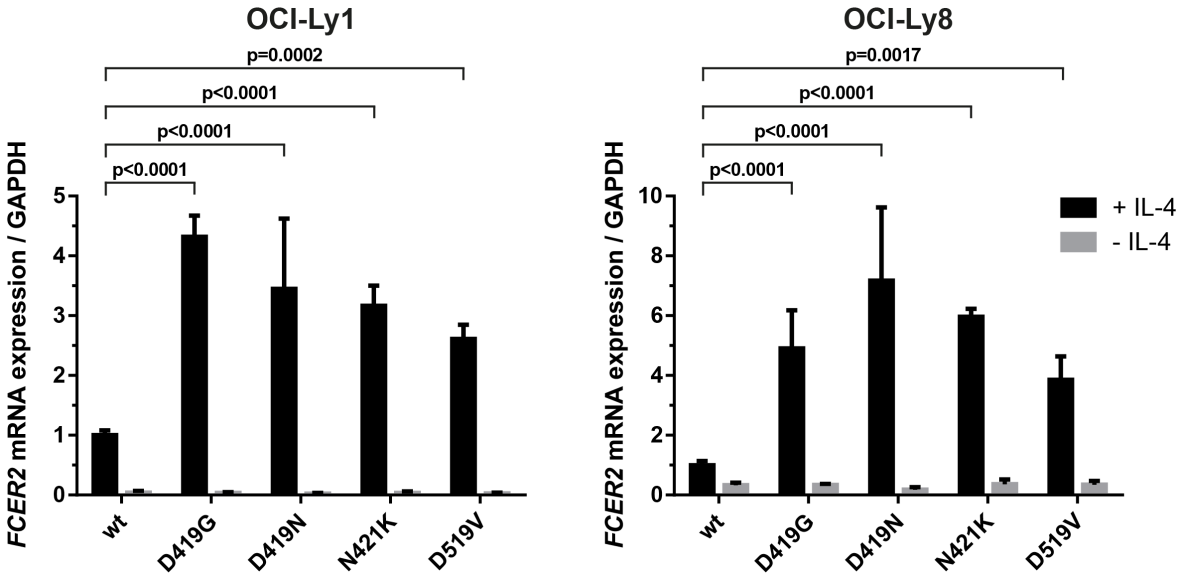

Figure 3.12
Relative *FCER2* mRNA transcript levels of STAT6 mutant and polymorphism-like cell lines are increased compared to STAT6 wild-type upon IL-4 stimulation for 24 h. Shown are 2^{-dCt} values relative to STAT6 wild-type of three independent quantitative RT-PCR experiments (mean±SD). wt: wild-type.

3.6.3 Analysis of soluble CD23 in cell culture supernatants

In addition to membrane-bound CD23, the soluble CD23 in the microenvironment might further contribute to FL biology. To address this, I performed sCD23 ELISA analyzing cell culture supernatants of OCI-Ly1 and OCI-Ly8 cells stably expressing wild-type or mutant STAT6 after 72 h IL-4 stimulation. sCD23 levels were significantly elevated in cell culture supernatants from cell lines expressing mutant STAT6 compared to STAT6 wild-type. Also in this experiment, there was no effect of mutant *STAT6* in the absence of IL-4 (figure 3.13).

Of note, the STAT6 variant with the highest abundance in patients with FL (D419G) had the most pronounced phenotype.

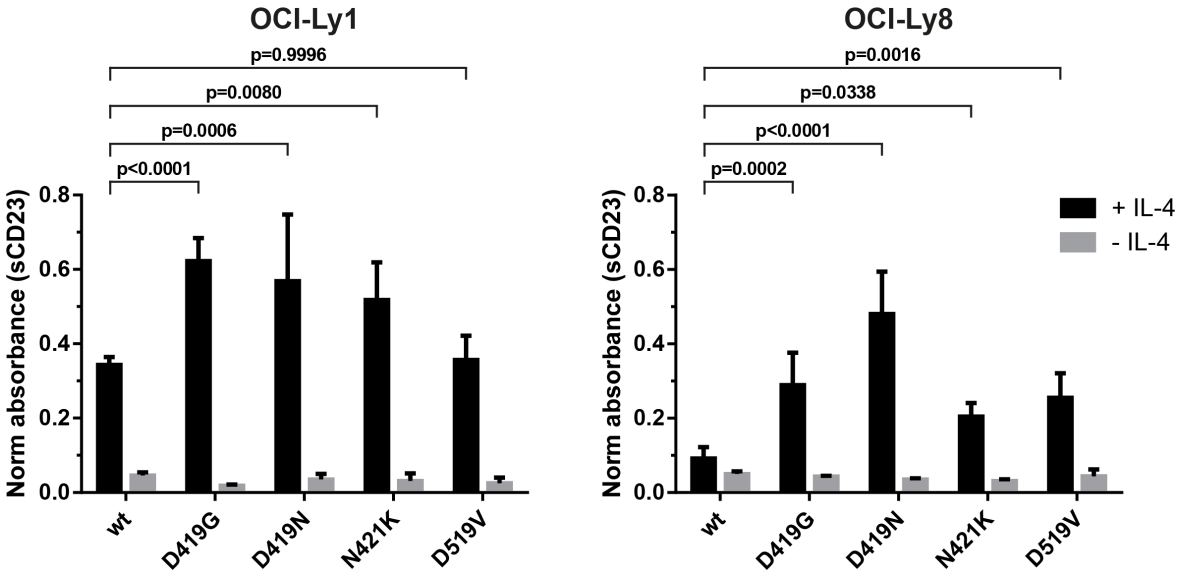

Figure 3.13
Relative soluble CD23 levels are enhanced after 72 h IL-4 stimulation in cell culture supernatants of STAT6 mutant cell lines compared to wild-type. sCD23 was measured by ELISA, and resulting absorbance values were normalized to the viable cell count. Data of three independent experiments is shown (mean±SD). wt: wild-type.

3.7 Underlying mechanism of enhanced transcriptional activity of mutant STAT6

3.7.1 Wild-type and mutant STAT6 dimerization

STAT6 transcriptional activity is initiated by phospho-STAT6 homodimers localized in the nucleus. To study the underlying mechanism of increased transcriptional activity of mutant STAT6 upon IL-4 stimulation, I studied the dimerization capabilities of STAT6 wild-type and mutant STAT6. In this study, pSTAT6 was analyzed after 20 min IL-4 stimulation. This time point was previously described in the literature.[53,154] HA-tagged STAT6 wild-type and 3xFlag-tagged STAT6 mutant constructs were co-transfected into 293T HEK cells, which do not express endogenous STAT6. For *in vitro* analysis of STAT6 dimerization, cells were stimulated with IL-4 (10 ng/ml) for 20 min, lysed, and Co-IPs were performed using anti-pSTAT6 antibody. The anti-pSTAT6 antibody used in this work was specific for the Y641 phosphorylation site. Eluates were analyzed by immunoblot using anti-Flag and anti-HA antibody. No differences in dimerization was detected between the various STAT6 constructs in this experiment (figure 3.14).

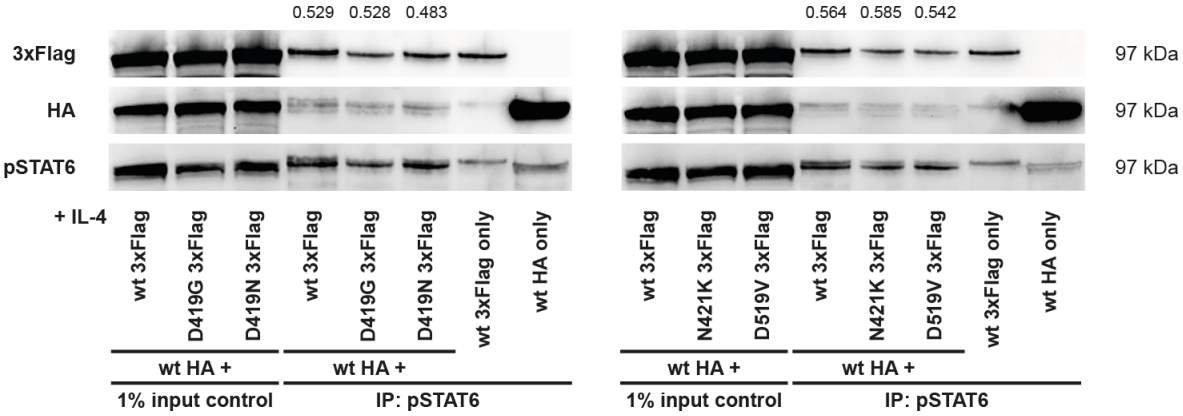

Figure 3.14
STAT6 dimerization assays performed in 293T HEK cells co-transfected with HA-tagged STAT6 wild-type and 3xFlag-tagged STAT6 mutant constructs. After IL-4 stimulation (20 min, 10 ng/ml) and subsequent cell lysis, Co-IPs were performed using anti-pSTAT6 antibody. Precipitated proteins were analyzed by immunoblot using anti-Flag and anti-HA antibody. pSTAT6 was detected as reference. Numbers on top indicate STAT6 3xFlag protein levels normalized to pSTAT6 signal. wt: wild-type.

3.7.2 Phospho-STAT6 levels in OCI-Ly1 and OCI-Ly8 STAT6 stable cell lines

To asses differences in STAT6 phosphorylation among cell lines stably expressing STAT6 wild-type and STAT6 variants, I measured pSTAT6 levels in whole cell lysates. Cells were stimulated with IL-4 for 20 min, or cultivated without IL-4. To model the transient exposure of malignant B-cells to TFH derived IL-4 within the dynamic microenvironment of FL, a third condition was included. Cell lines were stimulated with IL-4 (20 min) and cultured for additional 8 h in the absence of IL-4 (IL-4 *pulse* stimulation). Immunoblot analysis revealed that pSTAT6 levels were comparable across all cell lines. After 20 min IL-4 stimulation there was a strong pSTAT6 signal, which is decreased after further 8 h incubation (*pulse* condition). No pSTAT6 was detected in the absence of IL-4. Total STAT6, as well as STAT6 3xFlag levels were similar in all samples (figure 3.15).

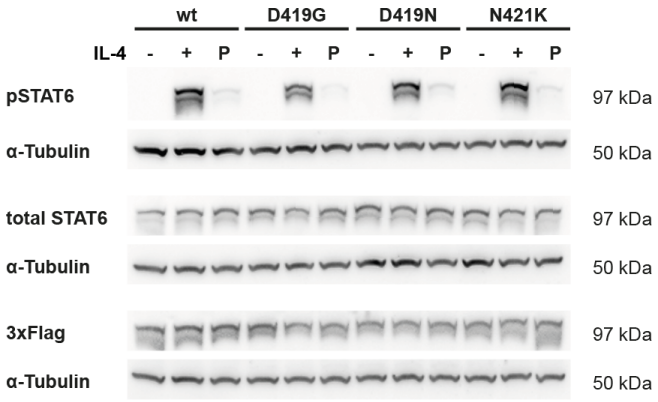

Figure 3.15
Immunoblots depicting comparable pSTAT6, total STAT6, as well as STAT6 3xFlag levels in whole cell lysates from OCI-Ly1 STAT6 wild-type and mutant cell lines treated with IL-4. α-Tubulin was used as loading control. Legend: "-" without IL-4, "+" 20 min IL-4, "P" *pulse* (20 min IL-4, removal of IL-4, further incubation for 8 h), wt: wild-type.

3.7.3 Nuclear accumulation of wild-type and mutant pSTAT6

Since there were no differences in total phospho-STAT6 levels in STAT6 wild-type and mutant whole cell lysates, I performed subcellular fractionations to test possible differences in the distribution of pSTAT6 in the nucleus and cytoplasm applying the same conditions as before. Following 20 min IL-4 stimulation, increased nuclear pSTAT6 levels in cell lines expressing D419G or D419N STAT6 as compared to wild-type STAT6 was detected. Accordingly, mutant pSTAT6 in cytoplasmic fractions was more depleted compared to STAT6 wild-type. After IL-4 *pulse*, higher levels of nuclear pSTAT6 in STAT6 mutant versus wild-type cell lines were detected, as well. Therefore, mutant and polymorphism-like pSTAT6 accumulated more effectively in the nucleus at an early time point (20 min) and were stronger retained there after 8 h compared to wild-type pSTAT6 (figure 3.16).

This data was confirmed by pSTAT6 immunohistochemistry in OCI-Ly1 STAT6 wild-type and STAT6 D419G cell lines. Again, increased pSTAT6 levels were detected in cell lines expressing mutant STAT6 compared to wild-type, after IL-4 *pulse* (figure 3.17).

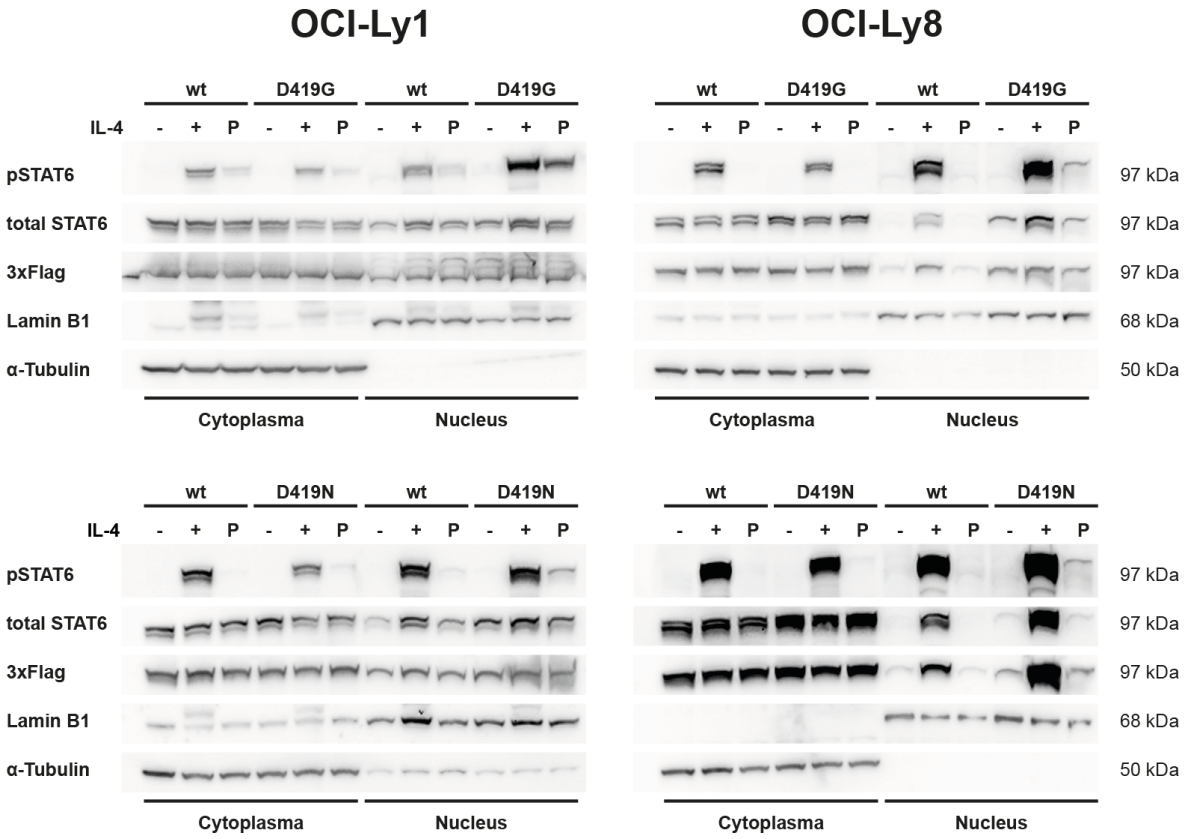

Figure 3.16
Immunoblots of subcellular fractions from OCI-Ly1 and OCI-Ly8 stably expressing either wild-type STAT6 (wt), mutant STAT6 (D419G), or polymorphism-like STAT6 (D419N). Following IL-4 stimulation, there is increased and prolonged nuclear accumulation of mutant pSTAT6. The anti-pSTAT6 antibody used in this study specifically detects STAT6 Y641 phosphorylation. Lamin B1: nuclear loading control, α-Tubulin: cytoplasmic loading control. Legend: "-" without IL-4, "+" 20 min IL-4, "P" *pulse* (20 min IL-4, removal of IL-4, further incubation for 8 h).

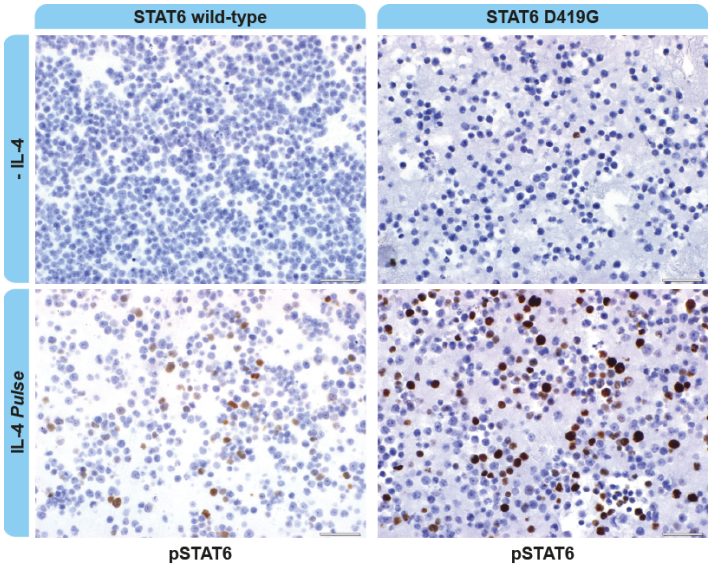

Figure 3.17
pSTAT6 immunohistochemistry in OCI-Ly1 STAT6 wild-type and STAT6 D419G cell lines. Representative picture showing enhanced pSTAT6 levels after IL-4 *pulse* in the STAT6 mutant cell line compared to wild-type.

3.7.4 CD23 expression in OCI-Ly1 and OCI-Ly8 STAT6 cell lines upon IL-4 *pulse*

To test whether *pulsed* IL-4 stimulation has an effect on STAT6 target gene expression, I analyzed CD23 levels after IL-4 *pulse*. In addition to increased levels of nuclear pSTAT6, significantly enhanced expression of membrane CD23 in STAT6 mutant and polymorphism-like versus wild-type cell lines was detected upon IL-4 *pulse* simulation (figure 3.18).

This result was confirmed on *FCER2* mRNA level by quantitative RT-PCR (figure 3.19). Thus, DNA binding site mutations in STAT6 lead to increased accumulation of pSTAT6 within the nucleus, and increased transcription and expression of STAT6 target genes.

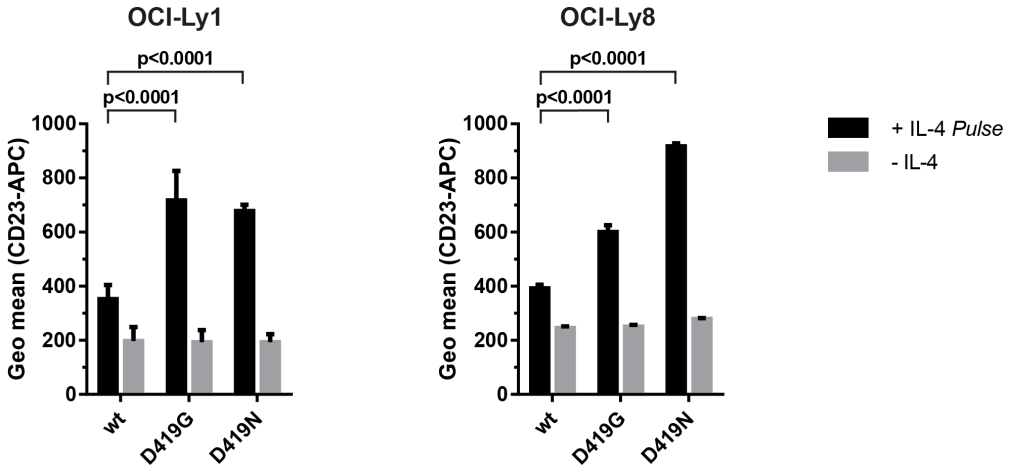

Figure 3.18
Membrane CD23 expression in OCI-Ly1 and OCI-Ly8 STAT6 cell lines upon IL-4 *pulse*. Before making subcellular fractions, an aliquot of cells was stained for CD23 and analyzed by flow cytometry. IL-4 *pulse* led to augmented membrane CD23 expression in STAT6 mutant and polymorphism-like cell lines compared to wild-type STAT6. The geometric mean of CD23-APC fluorescence from three independent experiments is shown (mean±SD). wt: wild-type.

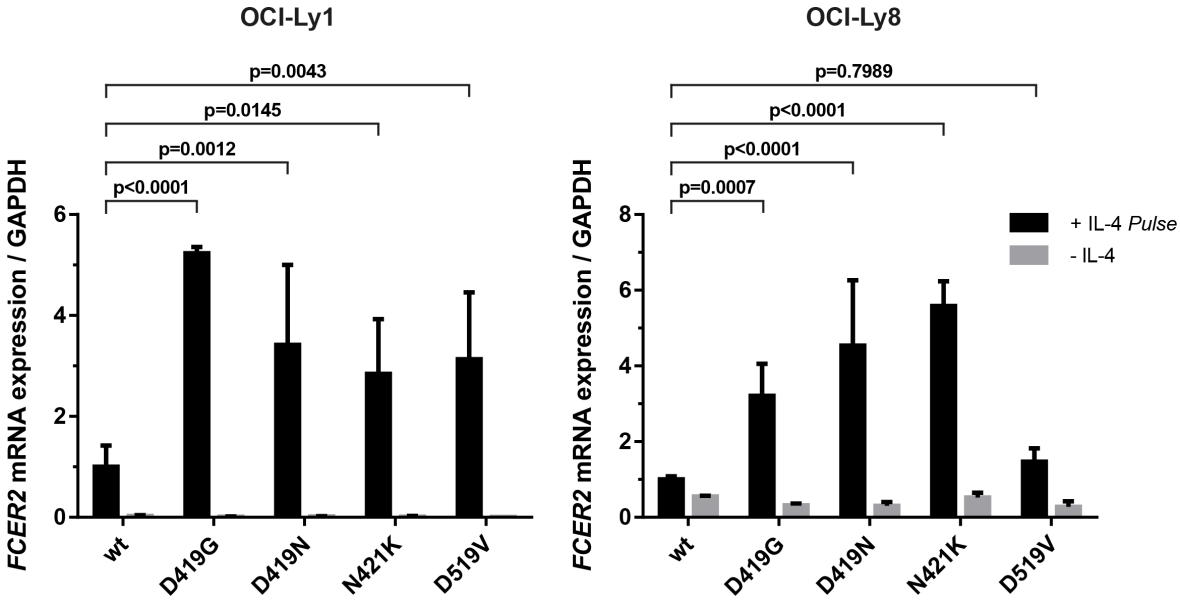

Figure 3.19
FCER2 mRNA levels in OCI-Ly1 and OCI-Ly8 STAT6 cell lines detected by quantitative RT-PCR. *FCER2* mRNA expression is increased in STAT6 mutant cell lines upon IL-4 *pulse*. Shown are 2^{-dCt} values relative to STAT6 wild-type of three independent quantitative RT-PCR experiments (mean±SD). wt: wild-type.

3.8 Whole transcriptome analysis of OCI-Ly1 STAT6 cell lines

To investigate mutant STAT6-specific differences and kinetics of IL-4-induced transcriptomes, RNA sequencing of OCI-Ly1 cell lines was performed. OCI-Ly1 cell lines were selected, because of their pronounced IL-4 responsiveness in the previous experiments. RNA from OCI-Ly1 STAT6 wild-type and mutant cell lines treated with IL-4 for 20 min, followed by 2 h, 4 h, and 8 h incubation in the absence of IL-4 was analyzed. Sample similarity was visualized by principal components analysis (PCA). PCA showed clustering of samples according to their STAT6 mutational status and different time points (figure 3.20). Due to the similar clustering of STAT6 D419G, D419N, and N421K samples, and because of their similar gain-of-function phenotype in previous experiments, the data of these cell lines were pooled in the subsequent bioinformatic analysis and compared to the STAT6 wild-type samples (STAT6 wild-type versus mutant) to gain more statistical power (figure 2.3).

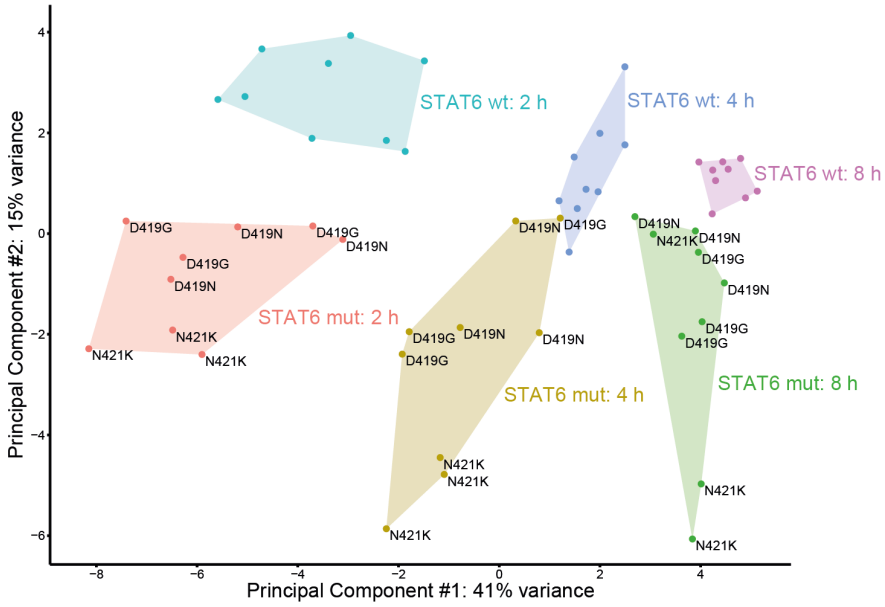

Figure 3.20
Principle component analysis of 54 samples from the RNA-seq experiment. Subgroups cluster according to STAT6 mutational status and the different time points. wt: wild-type, mut: mutant.

The expression levels of 54 genes were significantly different across all analyzed time points. Thereof, 44 genes were upregulated and 10 genes were downregulated in STAT6 mutant compared to wild-type samples (figure 3.21).

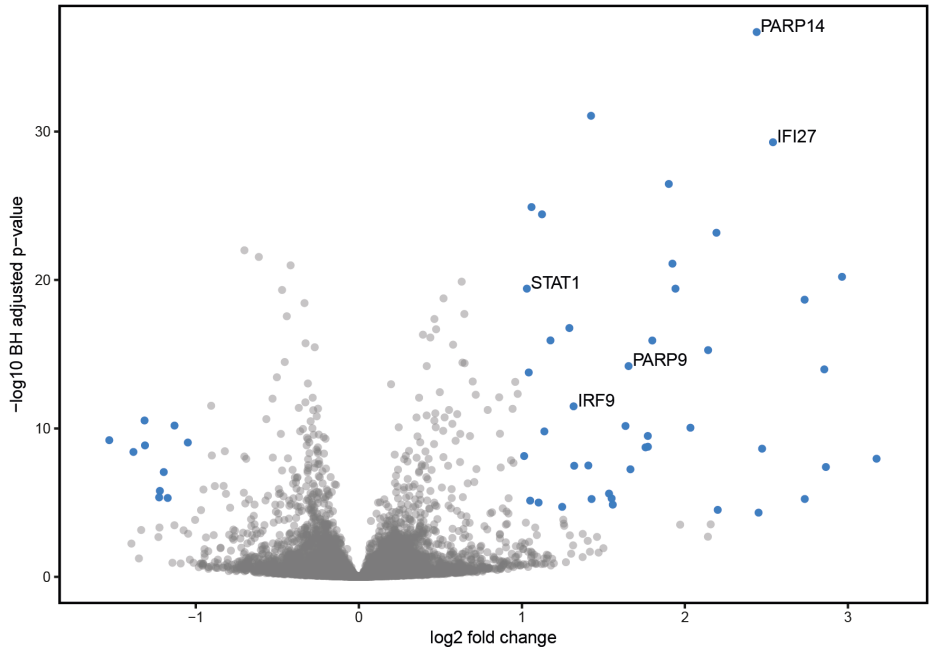

Figure 3.21
Volcano plot showing differentially expressed genes in IL-4 stimulated OCI-Ly1 STAT6 cell lines based on STAT6 mutational status including data from all time points. Among the most differentially expressed genes is PARP14, a co-activator of the STAT6 transcription complex. Cutoff: log2FC: $\pm$1.0, adjusted p-value: <0.0001.

The heatmaps generated from this data show the top differentially expressed genes for each time point and unsupervised clustering for STAT6 wild-type versus mutant STAT6 samples (figure 3.22).

Reassuringly, CD23 was differentially expressed in the 8 h time point, confirming my previous results. Other known IL-4 target genes e.g. the STAT inhibitors CISH and SOCS1, as well as IRF4 were also significantly upregulated in STAT6 mutant in comparison to STAT6 wild-type samples at one or more time points. Interestingly, the expression of IL4R alpha chain is significantly higher in STAT6 wild-type samples compared to STAT6 mutant at the 2 h time point (figure 3.23).

To validate the findings from the RNA sequencing experiment, I selected some top differentially expressed genes and performed quantitative RT-PCR. Results from the quantitative RT-PCR experiment matched the data from RNA sequencing for each analyzed gene and each time point (figure 3.24).

Furthermore, I tested PARP9 and STAT1 protein expression in OCI-Ly1 cell lines expressing wild-type or mutant STAT6 after 24 h IL-4 stimulation by immunoblot analysis.

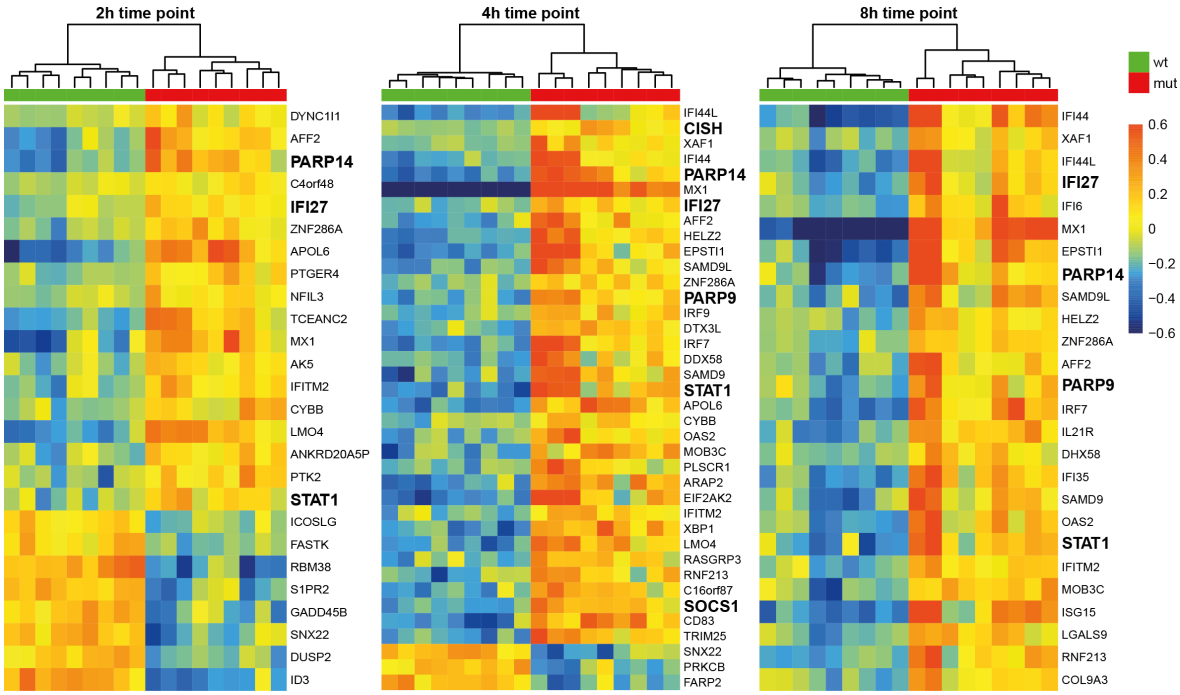

Figure 3.22
Heatmap representation of top differentially expressed genes in IL-4 stimulated OCI-Ly1 STAT6 cell lines between STAT6 wild-type and mutant samples for the 2 h, 4 h, and 8 h time point. Displayed are genes with log2 fold change above or below ±0.75 and adjusted p-value <0.0001. Unsupervised hierarchical clustering analysis is depicted by the dendrogram. wt: wild-type, mut: mutant.

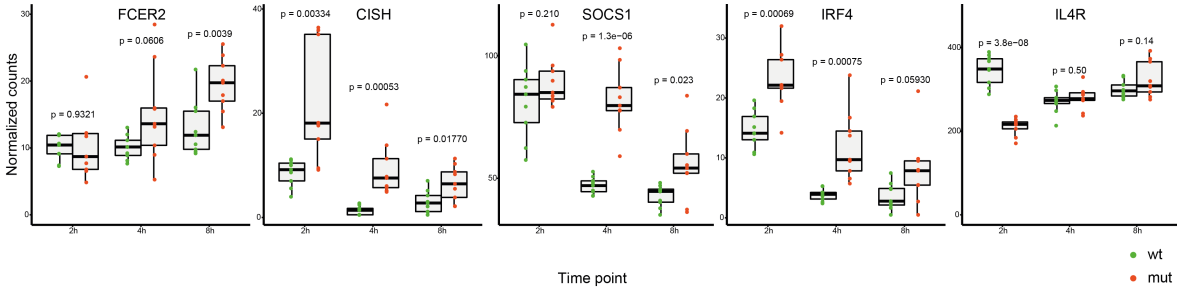

Figure 3.23
Changes in gene expression over time for genes involved in IL-4/STAT6 signaling or target genes of IL-4. Boxplots show normalized counts from the RNA-seq experiment for each time point comparing STAT6 wild-type (green) and mutant (red) cells.

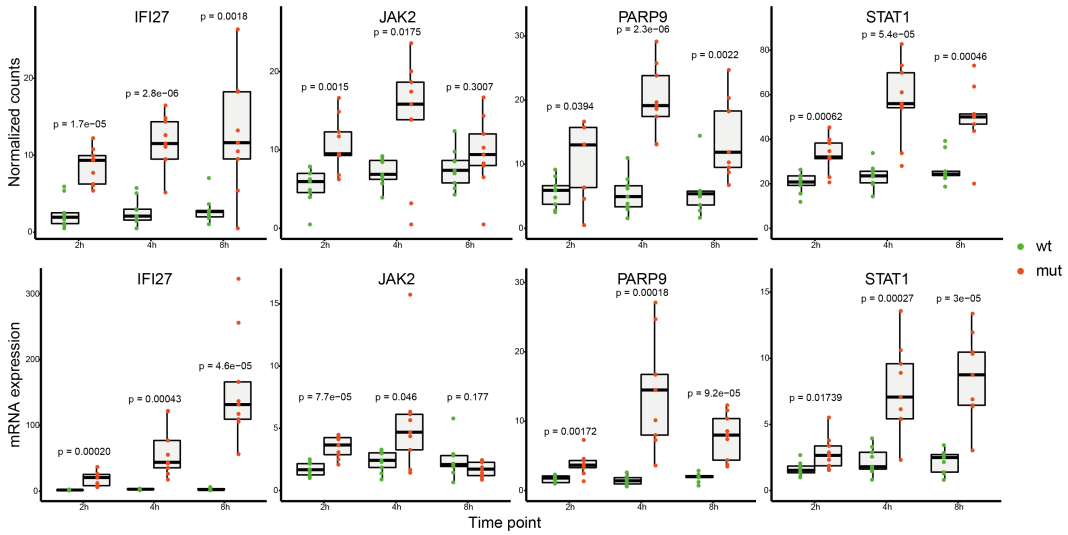

Figure 3.24
Validation of whole transcriptome data by quantitative RT-PCR. The top panel is displaying normalized counts from the RNA-seq experiment, the bottom panel is showing 2^{-dCt} values relative to STAT6 wild-type 2 h time point for IFI27, JAK2, PARP9, PARP14, and STAT1. Sample size and preparation is analog to the RNA-seq experiment. wt: wild-type, mut: mutant.

Protein levels were increased upon IL-4 stimulation in STAT6 mutant cell lines compared to wild-type. Of note, I did not detect an induction of PARP9 and STAT1 in STAT6 wild-type cell lines by IL-4 (figure 3.25).

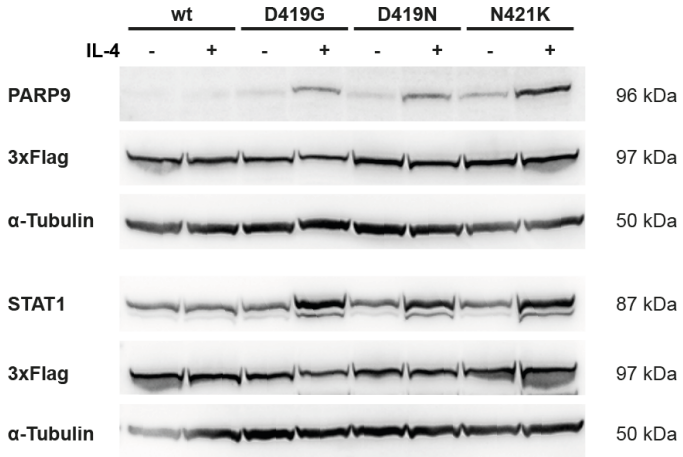

Figure 3.25
Immunoblot analysis of OCI-Ly1 STAT6 wild-type and mutant cell lines with and without IL-4 stimulation (24 h). Expression of PARP9 and STAT1 is augmented in mutant STAT6 cell lines upon IL-4 stimulation, which is in line with the RNA sequencing data. α-Tubulin was used as loading control. wt: wild-type.

3.9 STAT6 transcriptional co-activator PARP14

3.9.1 PARP14 expression in STAT6 mutant cell lines

Among the top most differentially expressed genes in all time points was poly ADP-ribose polymerase 14. PARP14 is part of the STAT6 transcriptional complex and previous studies have shown that PARP14 is a co-activator of IL-4 induced STAT6 transcription.[61] Therefore, the potential role of PARP14 in hyper-activated IL-4/STAT6 signaling was further studied. Again, PARP14 RNA-seq data was validated by performing quantitative RT-PCR (figure 3.26).

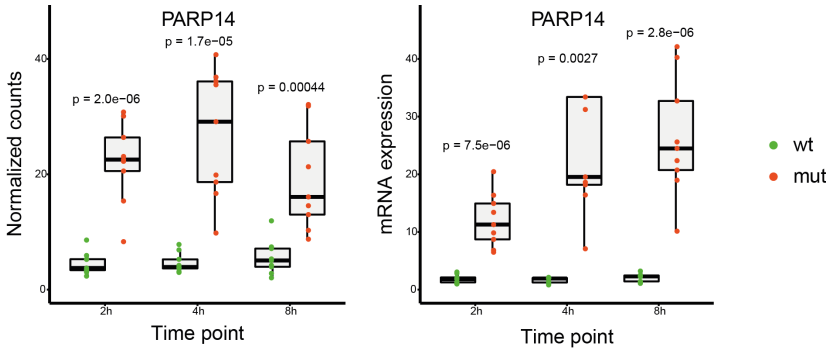

Figure 3.26
Validation of PARP14 whole transcriptome data by quantitative RT-PCR. The left graph is showing normalized counts from the RNA-seq experiment, the right graph is displaying 2^{-dCt} values relative to STAT6 wild-type 2 h time point. Sample size and preparation is analog to the RNA-seq experiment. wt: wild-type, mut: mutant.

Furthermore, PARP14 expression was increased on protein level in OCI-Ly1 cell lines expressing mutant STAT6 upon IL-4 stimulation, confirming the results from RNA-seq. Again, I did not detect an IL-4-mediated upregulation of PARP14 in STAT6 wild-type cell lines. These observations were confirmed in OCI-Ly8 STAT6 wild-type and STAT6 D419G cell lines (figure 3.27).

Moreover, increased PARP14 levels were detected, in cytoplasmic and nuclear fractions after IL-4 stimulation in STAT6 mutant cell lines (figure 3.28).

Overall, this data suggested a feed-forward loop of PARP14 expression and mutant STAT6 gain-of-function phenotype.

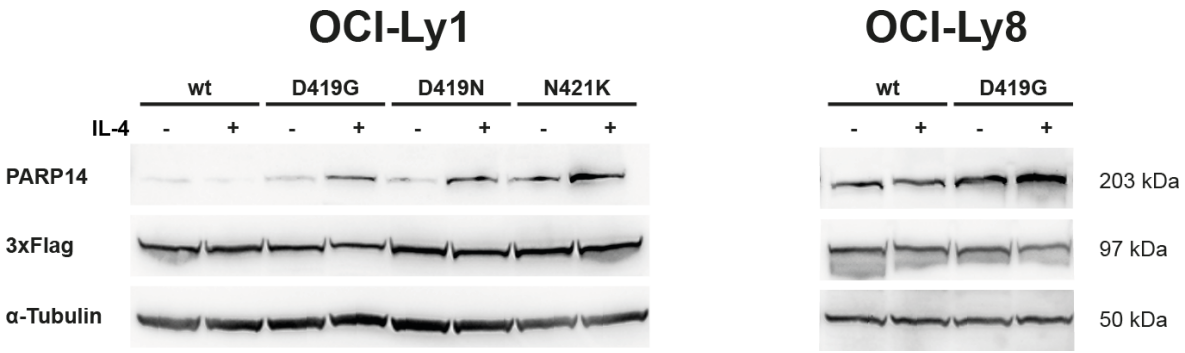

Figure 3.27
Immunoblot analysis displaying increased PARP14 protein expression in STAT6 mutant (D419G and N421K) or polymorphism-like (D419N) OCI-Ly1 and OCI-Ly8 cell lines compared to STAT6 wild-type (wt) cell lines upon 24 h IL-4 stimulation. STAT6 3xFlag expression is comparable in all cell lines. α-Tubulin was used as loading control.

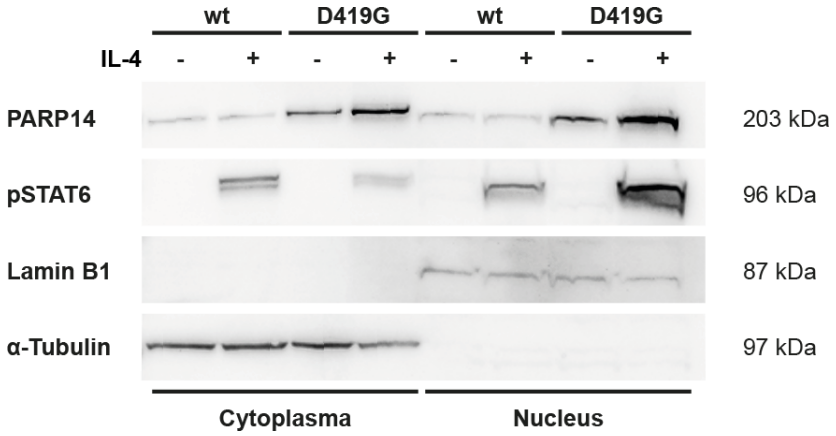

Figure 3.28
Subcellular fractions of OCI-Ly1 STAT6 wild-type and mutant cell line showing correlation of nuclear pSTAT6 and enhanced PARP14 protein expression after 24 h IL-4 stimulation. Lamin B1: nuclear loading control, α-Tubulin: cytoplasmic loading control, wt: wild-type.

3.9.2 PARP14 promoter luciferase reporter assay

I hypothesized that PARP14 itself is a previously unknown and potentially mutation-specific target gene of STAT6. The 5.4 kb PARP14 promoter region (ENSR00000305844) was analyzed using MatInspector software (Genomatix). This Bioinformatic analysis identified twelve putative STAT binding sites (figure 3.29).

After testing several fragments, luciferase reporter assays were performed by co-transfecting a 621 bp fragment (construct #3) of the PARP14 promoter, containing two potential STAT binding sites in close proximity to the PARP14 transcription start site (TSS) (figure 3.30), together with either STAT6 wild-type, mutant, or polymorphism-like constructs into 293T

Inspecting sequence ENSR00000305844 (1 - 5398):

1799 matches found in this sequence

Page 1 of 1 | 20 | View 1 - 12 of 12

Check transcription factor <-> matrix family assignment				Position			Strand	Matrix sim.	Sequence
Matrix Family	Detailed Family Information	Matrix	Detailed Matrix Information	from	to	anchor			
V$STAT							+		
V$STAT	Signal transducer and activator of transcription	V$STAT6.01	STAT6: signal transducer and activator of transcription 6	376	394	385	(+)	0.970	gtgcTTCCaggaagaaag
V$STAT	Signal transducer and activator of transcription	V$STAT6.01	STAT6: signal transducer and activator of transcription 6	445	463	454	(+)	0.858	attcTTCAagtgaacaagg
V$STAT	Signal transducer and activator of transcription	V$STAT3.02	Signal transducer and activator of transcription 3	1768	1786	1777	(+)	0.988	tctgTTCCaggaacacaag
V$STAT	Signal transducer and activator of transcription	V$STAT5A.01	Signal transducer and activator of transcription 5A	1791	1809	1800	(+)	0.863	ttctTTCCagagcaccta
V$STAT	Signal transducer and activator of transcription	V$STAT1.02	Signal transducer and activator of transcription 1	2394	2412	2403	(+)	0.994	agttttccaGGAAacgaaa
V$STAT	Signal transducer and activator of transcription	V$STAT3.02	Signal transducer and activator of transcription 3	2868	2886	2877	(+)	0.951	gcgcTTCCaggcgcttaat
V$STAT	Signal transducer and activator of transcription	V$STAT5B.01	Signal transducer and activator of transcription 5B	3471	3489	3480	(+)	0.929	gcagctcccAGAAtgggca
V$STAT	Signal transducer and activator of transcription	V$STAT5A.01	Signal transducer and activator of transcription 5A	3750	3768	3759	(+)	0.870	tgttTTCCtaggattaatt
V$STAT	Signal transducer and activator of transcription	V$STAT5B.01	Signal transducer and activator of transcription 5B	3776	3794	3785	(+)	0.953	ggagtgctcAGAAgggcaa
V$STAT	Signal transducer and activator of transcription	V$STAT5B.01	Signal transducer and activator of transcription 5B	4830	4848	4839	(+)	0.931	tgaagtcccAGAAgtgcat
V$STAT	Signal transducer and activator of transcription	V$STAT1.02	Signal transducer and activator of transcription 1	4878	4896	4887	(+)	0.889	tccatgccaGGAAgtggcc
V$STAT	Signal transducer and activator of transcription	V$STAT3.02	Signal transducer and activator of transcription 3	5140	5158	5149	(+)	0.942	ttggTTCCtggttgttgtc

Page 1 of 1 | 20 | View 1 - 12 of 12

Figure 3.29
Bioinformatic analysis of the PARP14 promoter region. Twelve potential STAT binding sites were identified by MatInspector software.

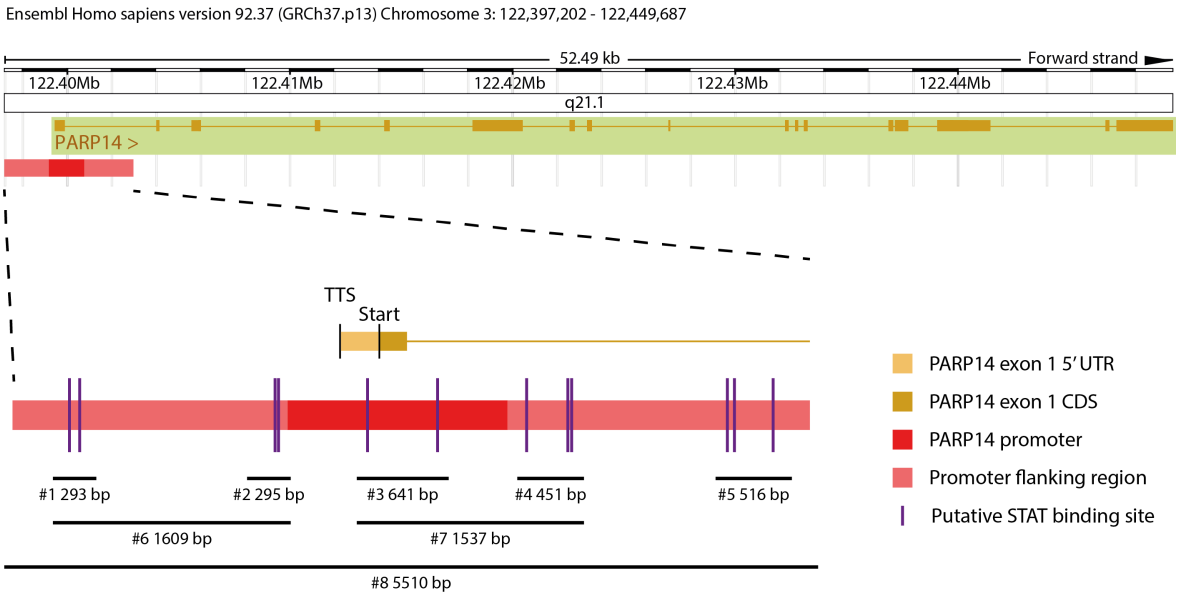

Figure 3.30
The *PARP14* gene and the PARP14 promoter region (ENSR00000305844). Depicted are the twelve potential STAT binding sites and eight constructs covering the twelve sites. Construct #3 (621 bp) was used in the subsequent luciferase reporter assay. The fragment included parts of the PARP14 promoter, with two putative STAT binding sites in close proximity to the PARP14 transcription start site, and the PARP14 exon 1 coding sequence. Upper part of the graphic from Ensembl genome browser.[155] TTS: transcription start site, Start: ATG start codon, 5' UTR: five prime untranslated region, CDS: coding sequence, kb: kilo base, Mb: mega base.

HEK cells. Moreover, different amounts (1 ng, 10 ng, or 50 ng) of STAT6 expression plasmids were transfected. 293T HEK cells were used, since they do not express endogenous STAT6. Although, the ATG codon is part of the PARP14 promoter fragment, it was not in frame with the start codon of the luciferase gene (*luc+*), and therefore not expected to interfere with the assay.

Twenty-four hours after transfection, cells were treated with IL-4 for 6 h. After IL-4 stimulation, a significant induction of luciferase reporter plasmid in all cell lines expressing STAT6 was detected. For STAT6 wild-type, I noticed a modest increase of luciferase activity with increasing amount of transfected expression plasmid. Importantly, mutated STAT6 had a significantly increased transactivation activity compared to STAT6 wild-type. In line with my previous experiments, the most pronounced effect was seen for STAT6 D419G (figure 3.31). I did not observe any transactivation activity in the absence of IL-4 (data not shown).

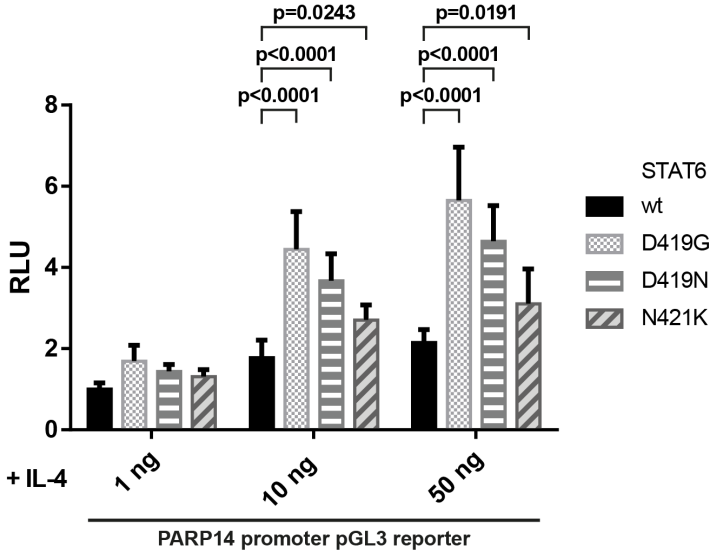

Figure 3.31
PARP14 promoter luciferase reporter assay demonstrating pSTAT6 binding to the PARP14 promoter. Significantly more luciferase is expressed in STAT6 mutant cell lines compared to STAT6 wild-type. Shown are fold change values of normalized ratios (normalized to Renilla luciferase control) based on STAT6 wild-type 1 ng sample (N=6, mean$\pm$SD). RLU: relative light units, wt: wild-type.

3.10 Targeting PARP14 in STAT6 mutant lymphoma

3.10.1 Inhibtion of PARP in OCI-Ly1 and OCI-Ly8 STAT6 cell lines

Previous experiments of this work suggested that PARP14 plays a central role in mutant STAT6 signaling, therefore the potential of PARP inhibition for therapeutic application was investigated. OCI-Ly1 and OCI-Ly8 STAT6 stable cell lines were treated with PJ34, an unselective PARP inhibitor, stimulated with IL-4, and membrane CD23 expression was analyzed by FACS. As observed before, CD23 expression was augmented in cell lines expressing mutant STAT6 compared to wild-type STAT6 after IL-4 stimulation. Inhibition of PARP in these cell lines resulted in diminished CD23 levels. Interestingly, CD23 expression was comparable between STAT6 wild-type and mutant cell lines after PJ34 treatment, suggesting that inhibition of PARP abrogates the gain-of-function phenotype of mutated and polymorphism-like STAT6 (figure 3.32).

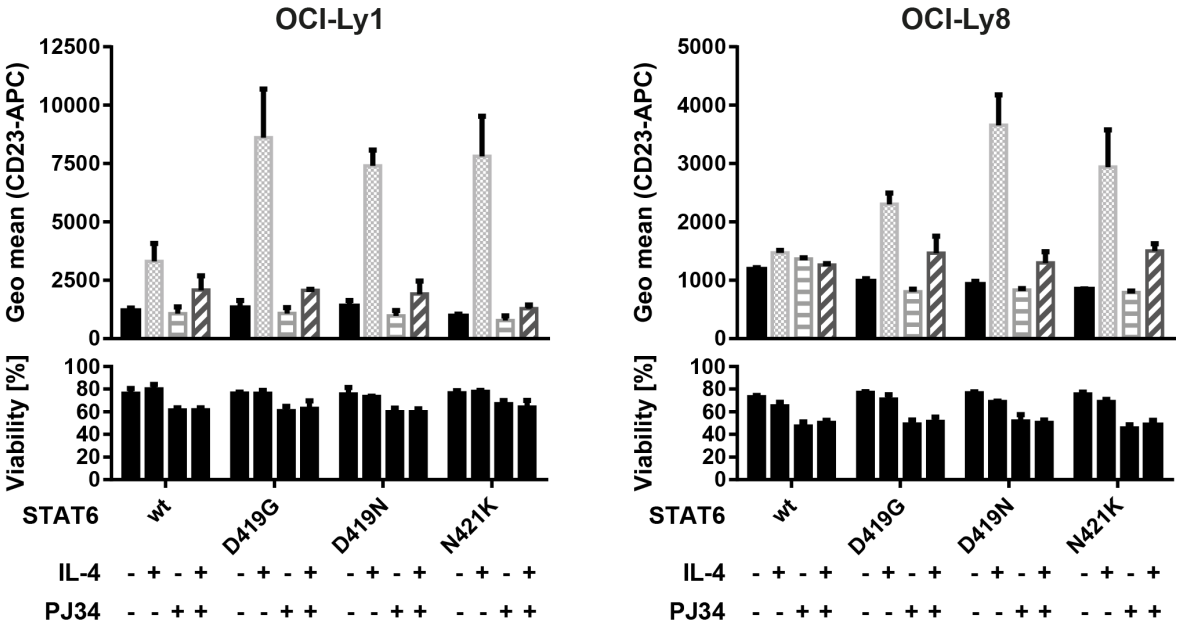

Figure 3.32
Top bar graph: CD23 expression in OCI-Ly1 and OCI-Ly8 STAT6 cell lines after treatment with PARP inhibitor and IL-4 stimulation. As before, increased CD23 expression was detected in STAT6 mutant cell lines upon IL-4 stimulation compared to cell lines expressing STAT6 wild-type. After treatment with PARP inhibitor PJ34, CD23 levels were decreased. Shown is the geometric mean of CD23-APC fluorescence detected by flow cytometry (N=3, mean$\pm$SD).
Bottom bar graph: cell viability for each sample in [%]. wt: wild-type.

3.10.2 Knockdown of PARP14 in OCI-Ly1 and OCI-Ly8 STAT6 cell lines

PJ34 is an unspecific inhibitor of the PARP protein family. To specifically target PARP14, knockdown experiments using PARP14-specific short hairpin RNA were performed. Five shRNAs targeting different regions of the PARP14 coding sequence were tested by transient transfection of Hela cells, which express endogenous PARP14 (figure 3.33). shRNA #4 and shRNA #5 showed best knockdown and were selected for further experiments.

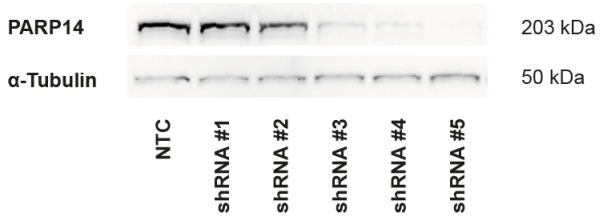

Figure 3.33
Immunoblot depicting PARP14 knockdown by transient transfection of five different shRNA plasmids and non-target control (NTC) in HeLa cells. shRNA #4 and shRNA #5 showed the best knockdown efficiency and were selected for use in subsequent experiments. α-Tubulin was used as loading control.

Luciferase reporter assays were performed as previously described (chapter 3.9.2), but additionally co-transfecting PARP14 shRNA plasmids #4, #5, as well as non-target control (NTC) and using HeLa cell line. 24 h after transfection cells were treated with IL-4 for 6 h. Similar to previous experiments, PARP14 knockdown resulted in reduced luciferase expression compared to samples transfected with NTC plasmid. When comparing samples transfected with shRNA #4 and shRNA #5, the more effective the knockdown (shown by the immunoblot), the more pronounced was the inhibiting effect on luciferase transactivation (figure 3.34). This demonstrates that PARP14 specifically mediates mutant STAT6 signaling.

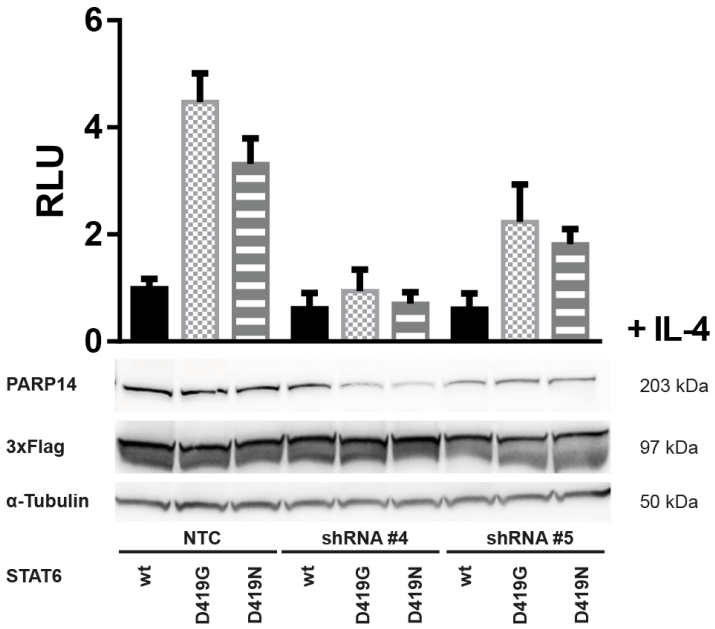

Figure 3.34
Reporter assays presenting the effects of PARP14 knockdown on STAT6-induced luciferase expression. PARP14 knockdown showed decreased induction of luciferase compared to non-target control. Shown are fold change values of normalized ratios (normalized to Renilla luciferase control) based on STAT6 wild-type NTC sample (N=3, mean$\pm$SD). The top immunoblot is showing the extent of the PARP14 knockdown. Also, equal expression of 3x-Flag tagged STAT6 constructs among all cell lines, and α-Tubulin as loading control is depicted. NTC: non-target control, RLU: relative light units, wt: wild-type.

4 Discussion

4.1 Proposed model of malignant IL-4/STAT6 signaling in *STAT6* mutant FL

Based on the results of this work, I propose the following concept of malignant IL-4/STAT6 signaling in *STAT6* mutant FL.

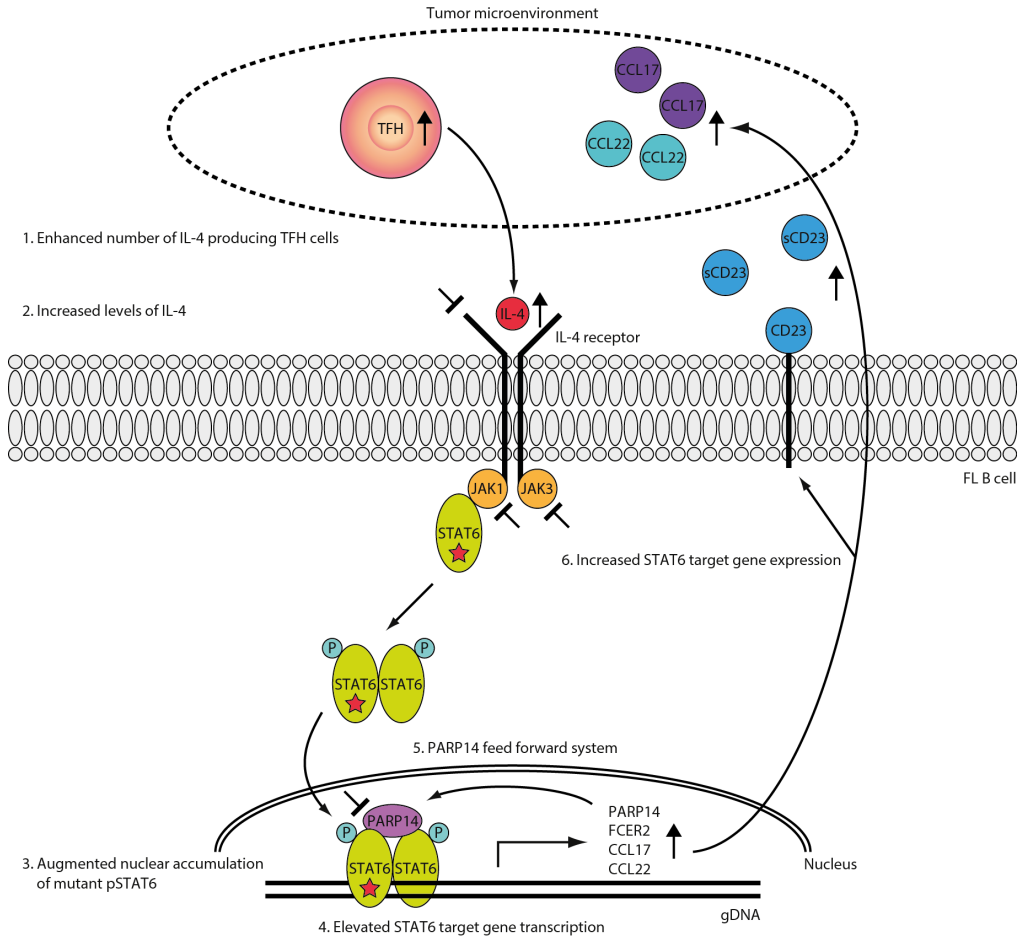

Figure 4.1
Proposed model of hyperactive IL-4/STAT6 signaling in *STAT6* mutant FL.

The details of this proposed model will be further discussed in the following sections.

4.2 STAT6 is recurrently and significantly mutated in follicular lymphoma

In this work, we identified that STAT6 was recurrently mutated in 13% of FL cases. The mutation frequency is in line with published data from other cohorts, e.g. Okosun *et al.* who found STAT6 mutated in 12% or Yildiz *et al.* who reported STAT6 mutations in 11% of FL cases.[31,53] Moreover, STAT6 was found to be significantly mutated by MutSigCV algorithm, which indicated functional relevance of these STAT6 variants.[87] All STAT6 mutations clustered within the DNA-binding domain, with a hotspot mutation at position D419. This clustering of STAT6 mutations suggested a gain-of-function phenotype.

Furthermore, all found mutations were monoallelic. This raises the question, if a wild-type *STAT6* allele is necessary for the observed mutant STAT6 gain-of-function phenotype or if a biallelic STAT6 mutation would further enhance this phenotype. In my OCI-Ly1 and OCI-Ly8 cell line models, endogenous wild-type STAT6 and ectopic mutant STAT6 were simultaneously expressed. In that, I tried to mimic the occurrence of mutant STAT6 as observed in patients with FL.

Three patients in our cohort were identified having a D419N variant. This variant has been reported to be a germline polymorphism and is listed in dbSNP (rs11172102). One percent of the global population carry this germline variant and it has not been linked to any disease so far.[156] Polymorphic gene variations, e.g. from dbSNP are often filtered out by sequencing analysis pipelines in an effort to focus on somatic gene alterations in cancer research. Of note, the VAF of two out of three cases suggested that the variants were somatically acquired. Furthermore, the polymorphism-like D419N had a similar gain-of-function phenotype in our assays, suggesting that this variant might actually contribute to the biology of FL, and should not be excluded from prognostic and functional studies.

4.3 Clinical impact of STAT6 DNA-binding variants

Clinical data from the GLSG2000 and BCCA cohort showed reduced FFS for patients with *STAT6* mutant FL. The analysis did not reach statistical significance. Yet, our data indicates that two factors are necessary for the mutant *STAT6* gain-of-function phenotype. In addition to the STAT6 mutations, it also requires upstream IL-4 produced by TFH cells. Without activation by IL-4, STAT6 mutants show no phenotype and this is not reflected in this analysis. Overall, the data further emphasizes the contribution of these variants to the complex malignant FL biology and therefore STAT6 variants are interesting candidates for further functional characterization.

4.4 IL-4 signaling activates mutant, hyperactive STAT6 in FL

GSEA of whole-genome gene expression data from the BCCA showed significant enrichment of gene sets with IL-4 regulated genes and genes involved in the IL-4 pathway in STAT6 mutant FL. This further supports the role of the IL-4 mediated activation of mutant STAT6 signaling. Work by Pangault *et al.* and by Amé-Thomas *et al.* previously demonstrated the IL-4-dependent interaction of TFH cells with FL B cells and identified an aberrant subset of TFH cells, which is enriched in the FL microenvironment and secretes higher levels of IL-4 compared to purified, non-malignant TFH cells derived from tonsils.[157,158] Our pSTAT6 immunohistochemistry data from primary patient samples presented here suggests that these IL-4 producing FL-TFH cells co-localize with pSTAT6 positive cells and form clusters with high IL-4 levels in STAT6 mutant cases, a phenomenon previously described by Pangault *et al.*[157]

Another mechanism of aberrant IL-4 signaling in lymphoma has been recently identified by Viganò *et al.* The group reported mutations in the IL4R alpha chain in 24.2% of PMBL cases. The mutations led to constitutive STAT6 activation and STAT6 target gene expression independent of IL-4 stimulation. Furthermore, whole-genome gene expression data from 42 PMBL samples showed that *FCER2* and *CCL17* were among the top upregulated genes in *IL4R* mutant tumors. Moreover, STAT6 mutations and other aberrations in the IL-4/JAK/STAT6 signaling cascade (e.g. inactivating mutations in *SOCS1*)

are frequent in PMBL, and co-occur in many PMBL cases (frequency of two or more mutations=63.3%).[154] Again, this supports the hypothesis that enhanced IL-4 signaling and hyperactive STAT6 mutants are synergistic and amplify the gain-of-function phenotype.

4.5 Consequences of enhanced STAT6 target gene expression in FL

Constitutive active IL-4 signaling through *IL4R* mutations or increased IL-4 levels in the FL microenvironment from TFH cells combined with hyperactive, mutant *STAT6* tumor cells result in increased STAT6 target gene expression. In this work, I noticed that *FCER2*, *CCL17*, and *CCL22* were among the top differentially expressed genes in STAT6 mutant patients from the BCCA cohort.

The role of CCL17 and CCL22 in FL microenvironment is well-characterized by work of Rawal *et al.* Both chemokines are produced by FL tumor cells upon stimulation with IL-4 (and CD40L), which are expressed by TFH cells. This attracts Tregs, which leads to tumor immune evasion, and attraction of more IL-4 producing T cells.[42] This work here suggests that hyperactive STAT6 variants might further augment this process by increased expression of CCL17 and CCL22.

On the other hand, CD23 and its soluble form promote growth of human B cell precursors and supports survival of germinal center B cells.[159,160] However, the functional relevance of enhanced CD23 in FL is still unclear. Data from Liu *et al.* showed that co-stimulation of germinal center cells with sCD23 and IL-1α leads to expression of antiapoptotic BCL2 protein.[161] Interestingly, Siddiqi *et al.* identified a small group (n=11) of patients with FL with mutations in STAT6 and high CD23 expression, who lack the t(14;18) IGH/BCL2 translocation.[86] Furthermore, many t(14;18) negative cases are indeed BCL2 positive by immunohistochemistry in the Siddiqi *et al.* study, which has also been reported by Leich *et al.*[162] This data raises the possibility that STAT6 mutations may be an alternative mechanism for upregulation of BCL2 in the absence of the t(14;18) in FL. Hence, the hyperactivation of the IL-4/mutant STAT6-axis in t(14;18) negative FL causes overexpression of CD23, which then leads to expression of BCL2.

Viganò *et al.* established xenografted mice by injection of DEV cell lines (a PMBL cell line) stably transduced with *IL4R* wild-type and *IL4R* mutant constructs into NOD scid gamma mice. *IL4R* mutant mice showed increased tumor volume and had inferior OS

compared to *IL4R* wild-type xenografts. Moreover, *ex-vivo* tumors excised from *IL4R* mutant mice expressed more *FCER2* and *CCL17* mRNA. Interestingly, the group also detected enhanced proliferation in *IL4R* mutant tumors assessed by Ki67 staining. However, the difference in proliferation did not occur *in vitro* at cell line level.[154] This data is in line with my results using OCI-Ly1 cell lines stably expressing STAT6 constructs. There was no significant difference in the growth kinetic of cell lines expressing wild-type or mutant STAT6 (figure A.7 in the appendix).

Taken together, TFH cells in the FL microenvironment produce increased levels of IL-4, which activate mutant STAT6 in FL cells. This leads to enhanced STAT6 target gene expression, which results in attraction of more IL-4 producing T cells as well as immunosuppressive Tregs (through CCL17 and CCL22), and potential growth and survival advantages through expression of CD23 and BCL2.

4.6 Aberrant nuclear accumulation of mutant pSTAT6 is associated with enhanced CD23 expression

The functional experiments in this study showed that STAT6 mutations and polymorphism-like variants are activating, which results in enhanced CD23 expression, a known STAT6 target gene. This is due to aberrant nuclear accumulation of mutant phospho-STAT6 (and not due to differences in dimerization), which is located in the nucleus to a greater extend and is retained longer inside the nucleus, compared to wild-type pSTAT6. However, does this also lead to increased STAT6 target gene transcription? Chen and Reich reported in 2010 that STAT6 nuclear shuttling is continuous and independent of Y641 phosphorylation. Moreover, pSTAT6 accumulation in the nucleus is due to its binding to the DNA.[59] Therefore, the data presented in this work suggests that increased mutant pSTAT6 inside the nucleus is caused by enhanced binding of mutant pSTAT6 to its DNA recognition sequences which results in augmented STAT6 target gene expression.

To this date, two studies previously reported functional data characterizing STAT6 mutations. Ritz *et al.* performed EMSAs, which showed reduced DNA binding activity of a N417Y/N430T double mutant to STAT6 binding sites upon IL-4 stimulation. Furthermore, they saw decreased transactivation of luciferase reporter constructs with artificial multiple STAT6 binding sites, when co-transfected with mutant STAT6 expression constructs (STAT6 N417Y/N430T, N417Y, D419H, N421K, and N430T) after IL-4 stimulation. This

data suggest that STAT6 DNA binding variants are loss-of-function. However, no decreased STAT6 target gene expression was detected in primary lymphoma samples.[84]

Yildiz *et al.* repeated the luciferase reporter assays performed by Ritz *et al.* using the same reporter constructs and STAT6 wild-type as well as STAT6 D419G expression vectors, and could confirm the previous results. However, when using reporter constructs with natural occurring STAT6 binding sites (of STAT6 target genes *AGAP9*, *CCL17*, *CISH*, *FCER2*, and *NFIL3*), Yildiz *et al.* observed enhanced induction of luciferase in cells expressing STAT6 D419G mutant compared to STAT6 wild-type upon IL-4 stimulation. Moreover, their EMSA showed increased binding of STAT6 D419G to DNA oligos containing STAT6 binding sites from the *CCL17* promoter or *FCER2* promoter compared to STAT6 wild-type. Overall, this data suggests that the synthetic STAT6 binding sites used in the Ritz *et al.* study have distinct features compared to natural occurring promoters with STAT6 binding sites, and that STAT6 mutations are indeed gain-of-function, which is further supported by the data presented in this work.

Importantly, the mutant STAT6 gain-of-function phenotype only occurred in the presence of IL-4 in this work. Yildiz *et al.* on the other hand also reported increased baseline expression of STAT6 target genes in *STAT6* mutant primary FL B cells. One possible explanation could be that these B cells were exposed to IL-4 prior to their purification. Other experiments performed by Yildiz *et al.* demonstrated that IL-4 was necessary to induce hyperactivated mutant STAT6, highlighting the essential role of IL-4 in this malignant pathway. Moreover, Yildiz *et al.* reported increased nuclear STAT6 D419G levels independent of IL-4 induced STAT6 phosphorylation, which has not been observed in this work. Yildiz *et al.* concluded form this data that nuclear localization of STAT6 D419G takes place through a novel mechansim. However, the underlying biology of this novel mechanism is still unaddressed.[53]

Of note, in all functional experiments performed in this study, the STAT6 D419G variant, which is the variant with the highest abundance in our cohort (n=19/35) shows the most distinct gain-of-function phenotype. The phenotype is less pronounced in the N421K mutation (n=2/35), and even more less in the D519V mutation (n=1/35). This indicates that STAT6 variants located close to the D419 hotspot have greatest impact. Overall, this adds another level of evidence for the contribution of mutant STAT6 to malignant FL biology.

4.7 Whole transcriptome analysis shows strong upregulation of STAT6 transcriptional co-activator PARP14 in STAT6 mutant samples

Whole transcriptome analysis of OCI-Ly1 STAT6 wild-type and mutant cell lines revealed that gene expression was skewed towards upregulation in STAT6 mutant expressing cell lines. Of 54 differentially expressed genes, 44 were significantly upregulated and only 10 genes were downregulated, which is consistent with the proposed gain-of-function phenotype of mutant STAT6. Differential gene expression was validated on RNA and protein level for several genes, among them was PARP14. PARP14 was the most significantly differentially expressed gene and PARP14 has been previously described as a co-activator of the STAT6 transcriptional complex, promoting IL-4 induced transcription of STAT6 target genes.[61] Therefore, PARP14 was a promising candidate for further functional experiments.

Among the top differentially expressed genes were other IL-4/STAT6 targets like FCER2, SOCS1, CISH, and IRF4. Surprisingly, the IL4R alpha chain, which is also regulated by STAT6, has higher expression levels at the 2 h time point in cell lines expressing STAT6 wild-type compared mutant STAT6. Viganò *et al.* observed a similar phenotype in their DEV cell lines transduced with *IL4R* wild-type and mutant *IL4R*. *IL4R* mutant cells, with constitutive active STAT6, did express significantly lower levels of the IL4R on protein level assessed by immunoblot and on the cell surface analyzed by flow cytometry.[154] This data suggests that hyperactive STAT6 signaling, caused by STAT6 mutations or IL4R mutations, results in a downregulation of the IL4R.

Interestingly, PARP14, PARP9, and STAT1 protein expression was not increased by IL-4 in cell lines expressing wild-type STAT6. One possible interpretation is that PARP14, PARP9, and STAT1 are mutation-specific targets of STAT6. This could explain why these genes were not previously identified as targets of STAT6, for example by Elo et al. who performed STAT6 chromatin immunoprecipitation (ChIP)-sequencing upon IL-4 stimulation.[58] Another possible interpretation is that induction of these genes by wild-type STAT6 occurs before my earliest time point (2 h after IL-4 *pulse*). To address this, one could analyze PARP14, PARP9, and STAT1 gene expression upon IL-4 *pulse* at earlier time points by quantitative RT-PCR.

4.8 PARP14 in STAT6 mutant FL

Upregulation of PARP14 in *STAT6* mutant lymphoma cell lines was not significant in whole-genome gene expression data from primary FL samples. The most likely explanation is the complex architecture of the FL tumor with its heterogeneous microenvironment. To isolate FL cells, one approach could be to perform laser capture microdissection. The human protein atlas reports that a majority of lymphoma specimens (8 out of 12 cases, 66.7%) stains positive for PARP14 (`https://www.proteinatlas.org/ENSG00000173193-PARP14/pathology`).[163,164] It would be of great interest to analyze more patient samples and to link this data to the mutational profile of the individual tumor, to examine the extent of PARP14 activity in lymphoma and the co-occurrence with STAT6 mutations.

Luciferase reporter assays at the PARP14 promoter revealed that PARP14 itself is a target gene of STAT6. Consequently, STAT6-induced expression of luciferase was significantly increased in cell lines expressing mutant STAT6 compared to wild-type STAT6 upon IL-4 stimulation. In this experiment, cell lines expressing STAT6 wild-type did induce the PARP14 reporter construct upon IL-4 stimulation to a small extent. However, luciferase assays were performed in HEK 293T cells, an artificial model. Further experiments have to be performed to finally answer the question whether the induction of PARP14 by STAT6 is mutation-specific (chapter 4.10).

Interestingly, the PARP14 promoter is partly located in exon 1 of PARP14. Stergachis *et al.* found that around 15% of human codons are genetic code specifying amino acids, as well as regulatory code specifying transcription factor binding sites. The group named this phenomenon dual-use codons or duons. Duons are highly conserved regions and exonic transcription factor binding sites are mostly located in the first coding exon.[165]

In conclusion, PARP14 is induced by mutated or polymorphism-like STAT6 upon IL-4 stimulation. As a co-activator of the STAT6 transcriptional complex, PARP14 amplifies the hyperactive mutant STAT6 target gene expression, creating a feed forward system. This data suggests that PARP14 is a promising therapeutic target in FL with mutant STAT6.

Mehrotra *et al.* showed previously that knockdown of PARP14 results in decreased binding of STAT6 to target gene promoters and inhibition of PARP14 by PARP inhibitor PJ34 showed reduced transcription of STAT6 target genes.[61] Therefore, the potential of PARP14 inhibition was tested in OCI-Ly1 and OCI-Ly8 expressing STAT6 wild-type and

STAT6 mutant constructs. Inhibition of PARP by PJ34 resulted in decreased CD23 expression upon IL-4 stimulation, abrogating the mutant STAT6 gain-of-function phenotype. PARP14-specific knockdown in a reporter assay using an independent cell line again dampened the mutant STAT6 gain-of-function phenotype and confirmed the previous results. Molecular targeted therapy of hyperactive IL-4/STAT6 signaling downstream of STAT6 bears great potential, is conceivably less toxic, and can complement other therapeutic approaches. Overall, inhibition of PARP14 could be a novel therapeutic strategy in STAT6 mutant lymphoma. PARP inhibitors are already in clinical use, primary in the treatment of BRCA-deficient cancer (mainly ovarian, breast, or prostate cancer). Inhibition of PARP1 impairs the repair of single strand brakes, which ultimately progress to double strand breaks. Repair of double strand breaks is dysfunctional due to BRCA-deficiency and this genomic instability leads to cell death.[166]

4.9 Summary of this work

In summary, this work presents aberrant activation of the STAT6 signaling cascade in a subgroup of patients with FL carrying variants in the STAT6 DNA-binding domain. Hyperactive STAT6 signaling is initiated by IL-4, which is mainly produced by TFH cells within the tumor microenvironment, and leads to overexpression of STAT6 target genes, e.g. *FCER2*, *CCL17*, and *CCL22*. Mechanistically, enhanced STAT6 target gene expression is caused by aberrant and prolonged nuclear accumulation of mutant phospho-STAT6. Moreover, this study identifies PARP14, a transcriptional co-activator of STAT6, as a novel, potentially mutant-specific target gene of STAT6. Finally, this study shows that inhibition of PARP14 dampens the mutant STAT6 gain-of-function phenotype and identifies PARP14 as a novel therapeutic target in STAT6 mutant FL.

4.10 Future perspective

In addition to PARP14 inhibtion, one could test other therapeutic targets within the IL-4/STAT6 pathway to block or diminish hyperactive STAT6 signaling. Upstream of STAT6, one could examine Dupilumab, which blocks the alpha chain of the IL4R, or JAK inhibitors like Tofacitinib, which is selective for JAK1 and JAK3. Downstream of STAT6, one could test two recently discovered selective PARP14 inhibitors.[167,168]

A *STAT6* wild-type and mutant xenograft mouse model, comparable to the model reported by Viganò *et al.*, would be a valuable tool for further investigation. In addition to tumor volume and proliferation, overall survival, as well as STAT6 target gene expression, one could test the therapeutic capabilities of various agents in *STAT6* mutant lymphoma *in vivo* (e.g. selective PARP14 inhibitors, which have not been tested *in vivo* so far).

To further investigate if enhanced, IL-4 induced STAT6 target gene expression in cell lines expressing mutant STAT6 is due to increased DNA binding of mutant STAT6 to its binding sites, STAT6 ChIP assays at the *FCER2* promoter region followed by qRT-PCR quantification could be performed to analyze the extent of mutant STAT6 DNA binding in comparison to wild-type STAT6.

Mechanistically, one could examine the potential role of PARP14 in the enhanced nuclear accumulation of mutant pSTAT6 upon IL-4 stimulation. To address this, one could test if the knockdown of PARP14 leads to decreased nuclear retention of mutant pSTAT6.

Finally, to verify if PARP14, PARP9, and STAT1 are mutant STAT6-specific targets, one could perform STAT6 ChIP-sequencing experiments including STAT6 wild-type and STAT6 mutant expressing cell lines after IL-4 stimulation.

5 References

[1] Morton, L. M., Wang, S. S., Devesa, S. S., Hartge, P., Weisenburger, D. D., and Linet, M. S.: *Lymphoma incidence patterns by WHO subtype in the United States, 1992-2001*. Blood, 107(1):265–76, 2006.

[2] Sant, M., Allemani, C., Tereanu, C., De Angelis, R., Capocaccia, R., Visser, O., Marcos-Gragera, R., Maynadie, M., Simonetti, A., Lutz, J. M., and Berrino, F.: *Incidence of hematologic malignancies in Europe by morphologic subtype: results of the HAEMACARE project*. Blood, 116(19):3724–34, 2010.

[3] Smith, A., Crouch, S., Lax, S., Li, J., Painter, D., Howell, D., Patmore, R., Jack, A., and Roman, E.: *Lymphoma incidence, survival and prevalence 2004-2014: subtype analyses from the UK's Haematological Malignancy Research Network*. Br J Cancer, 112(9):1575–84, 2015.

[4] Musshoff, K.: *Prognostic and therapeutic implications of staging in extranodal Hodgkin's disease*. Cancer Res, 31(11):1814–27, 1971.

[5] Weigert, O. and Weinstock, D. M.: *The promises and challenges of using gene mutations for patient stratification in follicular lymphoma*. Blood, 130(13):1491–1498, 2017.

[6] El-Galaly, Tarec Christoffer, Gormsen, Lars Christian, and Hutchings, Martin: *PET/CT for Staging; Past, Present, and Future*. Seminars in Nuclear Medicine, 2017.

[7] Tan, D., Horning, S. J., Hoppe, R. T., Levy, R., Rosenberg, S. A., Sigal, B. M., Warnke, R. A., Natkunam, Y., Han, S. S., Yuen, A., Plevritis, S. K., and Advani, R. H.: *Improvements in observed and relative survival in follicular grade 1-2 lymphoma during 4 decades: the Stanford University experience*. Blood, 122(6):981–7, 2013.

[8] Casulo, C., Byrtek, M., Dawson, K. L., Zhou, X., Farber, C. M., Flowers, C. R., Hainsworth, J. D., Maurer, M. J., Cerhan, J. R., Link, B. K., Zelenetz, A. D., and Friedberg, J. W.: *Early Relapse of Follicular Lymphoma After Rituximab Plus Cyclophosphamide, Doxorubicin, Vincristine, and Prednisone Defines Patients at High Risk for Death: An Analysis From the National LymphoCare Study*. J Clin Oncol, 33(23):2516–22, 2015.

[9] Tan, Daryl, Horning, Sandra J., Hoppe, Richard T., Levy, Ronald, Rosenberg, Saul A., Sigal, Bronislava M., Warnke, Roger A., Natkunam, Yasodha, Han, Summer S., Yuen, Alan, Plevritis, Sylvia K., and Advani, Ranjana H.: *Improvements in observed and relative survival in follicular grade 1-2 lymphoma during 4 decades: the Stanford University experience*. Blood, 122(6):981–987, 2013.

[10] Solal-Celigny, P., Roy, P., Colombat, P., White, J., Armitage, J. O., Arranz-Saez, R., Au, W. Y., Bellei, M., Brice, P., Caballero, D., Coiffier, B., Conde-Garcia, E., Doyen, C., Federico, M., Fisher, R. I., Garcia-Conde, J. F., Guglielmi, C., Hagenbeek, A., Haioun, C., LeBlanc, M., Lister, A. T., Lopez-Guillermo, A., McLaughlin, P., Milpied, N., Morel, P., Mounier, N., Proctor, S. J., Rohatiner, A., Smith, P., Soubeyran, P., Tilly, H., Vitolo, U., Zinzani, P. L., Zucca, E., and Montserrat, E.: *Follicular lymphoma international prognostic index*. Blood, 104(5):1258–65, 2004.

[11] Pastore, A., Jurinovic, V., Kridel, R., Hoster, E., Staiger, A. M., Szczepanowski, M., Pott, C., Kopp, N., Murakami, M., Horn, H., Leich, E., Moccia, A. A., Mottok, A., Sunkavalli, A., Van Hummelen, P., Ducar, M., Ennishi, D., Shulha, H. P., Hother, C., Connors, J. M., Sehn, L. H., Dreyling, M., Neuberg, D., Moller, P., Feller, A. C., Hansmann, M. L., Stein, H., Rosenwald, A., Ott, G., Klapper, W., Unterhalt, M., Hiddemann, W., Gascoyne, R. D., Weinstock, D. M., and Weigert, O.: *Integration of gene mutations in risk prognostication for patients receiving first-line immunochemotherapy for follicular lymphoma: a retrospective analysis of a prospective clinical trial and validation in a population-based registry*. Lancet Oncol, 16(9):1111–22, 2015.

[12] Pugh, T. J., Ballonoff, A., Newman, F., and Rabinovitch, R.: *Improved survival in patients with early stage low-grade follicular lymphoma treated with radiation: a Surveillance, Epidemiology, and End Results database analysis*. Cancer, 116(16):3843–51, 2010.

[13] Campbell, B. A., Voss, N., Woods, R., Gascoyne, R. D., Morris, J., Pickles, T., Connors, J. M., and Savage, K. J.: *Long-term outcomes for patients with limited stage follicular lymphoma: involved regional radiotherapy versus involved node radiotherapy*. Cancer, 116(16):3797–806, 2010.

[14] Dreyling, M., Ghielmini, M., Rule, S., Salles, G., Vitolo, U., Ladetto, M., and the, ESMO Guidelines Committee on behalf of: *Newly diagnosed and relapsed follicular lymphoma: ESMO Clinical Practice Guidelines for diagnosis, treatment and follow-up*. Annals of Oncology, 27(suppl_5):v83–v90, 2016.

[15] Hiddemann, W., Kneba, M., Dreyling, M., Schmitz, N., Lengfelder, E., Schmits, R., Reiser, M., Metzner, B., Harder, H., Hegewisch-Becker, S., Fischer, T., Kropff, M., Reis, H. E., Freund, M., Wormann, B., Fuchs, R., Planker, M., Schimke, J., Eimermacher, H., Trumper, L., Aldaoud, A., Parwaresch, R., and Unterhalt, M.: *Frontline therapy with rituximab added to the combination of cyclophosphamide, doxorubicin, vincristine, and prednisone (CHOP) significantly improves the outcome for patients with advanced-stage follicular lymphoma compared with therapy*

with CHOP alone: results of a prospective randomized study of the German Low-Grade Lymphoma Study Group. Blood, 106(12):3725–32, 2005.

[16] Marcus, R., Imrie, K., Solal-Celigny, P., Catalano, J. V., Dmoszynska, A., Raposo, J. C., Offner, F. C., Gomez-Codina, J., Belch, A., Cunningham, D., Wassner-Fritsch, E., and Stein, G.: *Phase III study of R-CVP compared with cyclophosphamide, vincristine, and prednisone alone in patients with previously untreated advanced follicular lymphoma*. J Clin Oncol, 26(28):4579–86, 2008.

[17] Salles, G., Seymour, J. F., Offner, F., Lopez-Guillermo, A., Belada, D., Xerri, L., Feugier, P., Bouabdallah, R., Catalano, J. V., Brice, P., Caballero, D., Haioun, C., Pedersen, L. M., Delmer, A., Simpson, D., Leppa, S., Soubeyran, P., Hagenbeek, A., Casasnovas, O., Intragumtornchai, T., Ferme, C., Silva, M. G. da, Sebban, C., Lister, A., Estell, J. A., Milone, G., Sonet, A., Mendila, M., Coiffier, B., and Tilly, H.: *Rituximab maintenance for 2 years in patients with high tumour burden follicular lymphoma responding to rituximab plus chemotherapy (PRIMA): a phase 3, randomised controlled trial*. Lancet, 377(9759):42–51, 2011.

[18] Murphy, Kenneth and Weaver, Casey: *Janeway's immunobiology*. Garland Science/Taylor & Francis Group, LLC, New York, NY, 9th edition. edition, 2016, ISBN 9780815345053 (PBK.).

[19] LeBien, Tucker W. and Tedder, Thomas F.: *B lymphocytes: how they develop and function*. Blood, 112(5):1570–1580, 2008.

[20] Crotty, Shane: *A brief history of T cell help to B cells*. Nature Reviews Immunology, 15:185, 2015.

[21] Tsujimoto, Y., Finger, L. R., Yunis, J., Nowell, P. C., and Croce, C. M.: *Cloning of the chromosome breakpoint of neoplastic B cells with the t(14;18) chromosome translocation*. Science, 226(4678):1097–9, 1984.

[22] Yunis, J. J., Frizzera, G., Oken, M. M., McKenna, J., Theologides, A., and Arnesen, M.: *Multiple recurrent genomic defects in follicular lymphoma. A possible model for cancer*. N Engl J Med, 316(2):79–84, 1987.

[23] Graninger, W. B., Seto, M., Boutain, B., Goldman, P., and Korsmeyer, S. J.: *Expression of Bcl-2 and Bcl-2-Ig fusion transcripts in normal and neoplastic cells*. J Clin Invest, 80(5):1512–5, 1987.

[24] Roulland, S., Navarro, J. M., Grenot, P., Milili, M., Agopian, J., Montpellier, B., Gauduchon, P., Lebailly, P., Schiff, C., and Nadel, B.: *Follicular lymphoma-like B cells in healthy individuals: a novel intermediate step in early lymphomagenesis*. J Exp Med, 203(11):2425–31, 2006.

[25] Egle, A., Harris, A. W., Bath, M. L., O'Reilly, L., and Cory, S.: *VavP-Bcl2 transgenic mice develop follicular lymphoma preceded by germinal center hyperplasia*. Blood, 103(6):2276–83, 2004.

[26] Horsman, D. E., Connors, J. M., Pantzar, T., and Gascoyne, R. D.: *Analysis of secondary chromosomal alterations in 165 cases of follicular lymphoma with t(14;18)*. Genes Chromosomes Cancer, 30(4):375–82, 2001.

[27] Pasqualucci, L., Bhagat, G., Jankovic, M., Compagno, M., Smith, P., Muramatsu, M., Honjo, T., Morse, H. C., 3rd, Nussenzweig, M. C., and Dalla-Favera, R.: *AID is required for germinal center-derived lymphomagenesis*. Nat Genet, 40(1):108–12, 2008.

[28] Weigert, O., Kopp, N., Lane, A. A., Yoda, A., Dahlberg, S. E., Neuberg, D., Bahar, A. Y., Chapuy, B., Kutok, J. L., Longtine, J. A., Kuo, F. C., Haley, T., Salois, M., Sullivan, T. J., Fisher, D. C., Fox, E. A., Rodig, S. J., Antin, J. H., and Weinstock, D. M.: *Molecular ontogeny of donor-derived follicular lymphomas occurring after hematopoietic cell transplantation*. Cancer Discov, 2(1):47–55, 2012.

[29] Weigert, O. and Weinstock, D. M.: *The evolving contribution of hematopoietic progenitor cells to lymphomagenesis*. Blood, 120(13):2553–61, 2012.

[30] Green, M. R., Gentles, A. J., Nair, R. V., Irish, J. M., Kihira, S., Liu, C. L., Kela, I., Hopmans, E. S., Myklebust, J. H., Ji, H., Plevritis, S. K., Levy, R., and Alizadeh, A. A.: *Hierarchy in somatic mutations arising during genomic evolution and progression of follicular lymphoma*. Blood, 121(9):1604–11, 2013.

[31] Okosun, J., Bodor, C., Wang, J., Araf, S., Yang, C. Y., Pan, C., Boller, S., Cittaro, D., Bozek, M., Iqbal, S., Matthews, J., Wrench, D., Marzec, J., Tawana, K., Popov, N., O'Riain, C., O'Shea, D., Carlotti, E., Davies, A., Lawrie, C. H., Matolcsy, A., Calaminici, M., Norton, A., Byers, R. J., Mein, C., Stupka, E., Lister, T. A., Lenz, G., Montoto, S., Gribben, J. G., Fan, Y., Grosschedl, R., Chelala, C., and Fitzgibbon, J.: *Integrated genomic analysis identifies recurrent mutations and evolution patterns driving the initiation and progression of follicular lymphoma*. Nat Genet, 46(2):176–81, 2014.

[32] Pasqualucci, L., Khiabanian, H., Fangazio, M., Vasishtha, M., Messina, M., Holmes, A. B., Ouillette, P., Trifonov, V., Rossi, D., Tabbo, F., Ponzoni, M., Chadburn, A., Murty, V. V., Bhagat, G., Gaidano, G., Inghirami, G., Malek, S. N., Rabadan, R., and Dalla-Favera, R.: *Genetics of follicular lymphoma transformation*. Cell Rep, 6(1):130–40, 2014.

[33] Green, M. R., Kihira, S., Liu, C. L., Nair, R. V., Salari, R., Gentles, A. J., Irish, J., Stehr, H., Vicente-Duenas, C., Romero-Camarero, I., Sanchez-Garcia, I., Plevritis, S. K., Arber, D. A., Batzoglou, S., Levy, R., and Alizadeh, A. A.: *Mutations in early follicular lymphoma progenitors are associated with suppressed antigen presentation*. Proc Natl Acad Sci U S A, 112(10):E1116–25, 2015.

[34] Kahl, B. S. and Yang, D. T.: *Follicular lymphoma: evolving therapeutic strategies*. Blood, 127(17):2055–63, 2016.

[35] Scott, D. W. and Gascoyne, R. D.: *The tumour microenvironment in B cell lymphomas*. Nat Rev Cancer, 14(8):517–34, 2014.

[36] Kridel, R., Sehn, L. H., and Gascoyne, R. D.: *Pathogenesis of follicular lymphoma*. J Clin Invest, 122(10):3424–31, 2012.

[37] Ame-Thomas, P. and Tarte, K.: *The yin and the yang of follicular lymphoma cell niches: role of microenvironment heterogeneity and plasticity*. Semin Cancer Biol, 24:23–32, 2014.

[38] Ame-Thomas, P., Maby-El Hajjami, H., Monvoisin, C., Jean, R., Monnier, D., Caulet-Maugendre, S., Guillaudeux, T., Lamy, T., Fest, T., and Tarte, K.: *Human mesenchymal stem cells isolated from bone marrow and lymphoid organs support tumor B-cell growth: role of stromal cells in follicular lymphoma pathogenesis*. Blood, 109(2):693–702, 2007.

[39] Pandey, S., Mourcin, F., Marchand, T., Nayar, S., Guirriec, M., Pangault, C., Monvoisin, C., Ame-Thomas, P., Guilloton, F., Dulong, J., Coles, M., Fest, T., Mottok, A., Barone, F., and Tarte, K.: *IL-4/CXCL12 loop is a key regulator of lymphoid stroma function in follicular lymphoma*. Blood, 129(18):2507–2518, 2017.

[40] Yang, Z. Z., Grote, D. M., Ziesmer, S. C., Niki, T., Hirashima, M., Novak, A. J., Witzig, T. E., and Ansell, S. M.: *IL-12 upregulates TIM-3 expression and induces T cell exhaustion in patients with follicular B cell non-Hodgkin lymphoma*. J Clin Invest, 122(4):1271–82, 2012.

[41] Ramsay, A. G., Clear, A. J., Kelly, G., Fatah, R., Matthews, J., Macdougall, F., Lister, T. A., Lee, A. M., Calaminici, M., and Gribben, J. G.: *Follicular lymphoma cells induce T-cell immunologic synapse dysfunction that can be repaired with lenalidomide: implications for the tumor microenvironment and immunotherapy*. Blood, 114(21):4713–20, 2009.

[42] Rawal, S., Chu, F., Zhang, M., Park, H. J., Nattamai, D., Kannan, S., Sharma, R., Delgado, D., Chou, T., Lin, H. Y., Baladandayuthapani, V., Luong, A., Vega, F., Fowler, N., Dong, C., Davis, R. E., and Neelapu, S. S.: *Cross talk between follicular Th cells and tumor cells in human follicular lymphoma promotes immune evasion in the tumor microenvironment*. J Immunol, 190(12):6681–93, 2013.

[43] Zou, W.: *Regulatory T cells, tumour immunity and immunotherapy*. Nat Rev Immunol, 6(4):295–307, 2006.

[44] Gobert, M., Treilleux, I., Bendriss-Vermare, N., Bachelot, T., Goddard-Leon, S., Arfi, V., Biota, C., Doffin, A. C., Durand, I., Olive, D., Perez, S., Pasqual, N., Faure, C., Ray-Coquard, I., Puisieux, A., Caux, C., Blay, J. Y., and Menetrier-Caux, C.: *Regulatory T cells recruited through CCL22/CCR4 are selectively activated in lymphoid infiltrates surrounding primary breast tumors and lead to an adverse clinical outcome*. Cancer Res, 69(5):2000–9, 2009.

[45] Mizukami, Y., Kono, K., Kawaguchi, Y., Akaike, H., Kamimura, K., Sugai, H., and Fujii, H.: *CCL17 and CCL22 chemokines within tumor microenvironment are related to accumulation of Foxp3+ regulatory T cells in gastric cancer*. Int J Cancer, 122(10):2286–93, 2008.

[46] Yang, Z. Z., Novak, A. J., Ziesmer, S. C., Witzig, T. E., and Ansell, S. M.: *Attenuation of CD8(+) T-cell function by CD4(+)CD25(+) regulatory T cells in B-cell non-Hodgkin's lymphoma*. Cancer Res, 66(20):10145–52, 2006.

[47] Galdiero, M. R., Garlanda, C., Jaillon, S., Marone, G., and Mantovani, A.: *Tumor associated macrophages and neutrophils in tumor progression*. J Cell Physiol, 228(7):1404–12, 2013.

[48] Guilloton, F., Caron, G., Menard, C., Pangault, C., Ame-Thomas, P., Dulong, J., De Vos, J., Rossille, D., Henry, C., Lamy, T., Fouquet, O., Fest, T., and Tarte, K.: *Mesenchymal stromal cells orchestrate follicular lymphoma cell niche through the CCL2-dependent recruitment and polarization of monocytes*. Blood, 119(11):2556–67, 2012.

[49] Gordon, S. and Martinez, F. O.: *Alternative activation of macrophages: mechanism and functions*. Immunity, 32(5):593–604, 2010.

[50] Lu, G., Middleton, R. E., Sun, H., Naniong, M., Ott, C. J., Mitsiades, C. S., Wong, K. K., Bradner, J. E., and Kaelin, W. G., Jr.: *The myeloma drug lenalidomide promotes the cereblon-dependent destruction of Ikaros proteins*. Science, 343(6168):305–9, 2014.

[51] Kronke, J., Udeshi, N. D., Narla, A., Grauman, P., Hurst, S. N., McConkey, M., Svinkina, T., Heckl, D., Comer, E., Li, X., Ciarlo, C., Hartman, E., Munshi, N., Schenone, M., Schreiber, S. L., Carr, S. A., and Ebert, B. L.: *Lenalidomide causes selective degradation of IKZF1 and IKZF3 in multiple myeloma cells*. Science, 343(6168):301–5, 2014.

[52] Fowler, Nathan Hale, Morschhauser, Franck, Feugier, Pierre, Bouabdallah, Reda, Tilly, Herve, Palomba, Maria Lia, Fruchart, Christophe, Libby, Edward N., Casasnovas, Olivier, Gomes, Maria Da Silva, Pranger, Delphine, Zachee, Pierre, Garcia-Sancho, Alejandro Martin, Lopez-Guillermo, Armando, Larouche, Jean Francois, Ando, Kiyoshi, Liu, Dongfang, Wang, Jianming, Xerri, Luc, and Salles, Gilles A.: *RELEVANCE: Phase III randomized study of lenalidomide plus rituximab (R2) versus chemotherapy plus rituximab, followed by rituximab maintenance, in patients with previously untreated follicular lymphoma.* J Clin Oncol, 36((suppl; abstr 7500)), 2018.

[53] Yildiz, M., Li, H., Bernard, D., Amin, N. A., Ouillette, P., Jones, S., Saiya-Cork, K., Parkin, B., Jacobi, K., Shedden, K., Wang, S., Chang, A. E., Kaminski, M. S., and Malek, S. N.: *Activating STAT6 mutations in follicular lymphoma*. Blood, 125(4):668–79, 2015.

[54] Lim, C. P. and Cao, X.: *Structure, function, and regulation of STAT proteins*. Mol Biosyst, 2(11):536–50, 2006.

[55] Hou, J., Schindler, U., Henzel, W. J., Ho, T. C., Brasseur, M., and McKnight, S. L.: *An interleukin-4-induced transcription factor: IL-4 Stat*. Science, 265(5179):1701–6, 1994.

[56] Goenka, S. and Kaplan, M. H.: *Transcriptional regulation by STAT6*. Immunol Res, 50(1):87–96, 2011.

[57] Ehret, G. B., Reichenbach, P., Schindler, U., Horvath, C. M., Fritz, S., Nabholz, M., and Bucher, P.: *DNA binding specificity of different STAT proteins. Comparison of in vitro specificity with natural target sites*. J Biol Chem, 276(9):6675–88, 2001.

[58] Elo, L. L., Jarvenpaa, H., Tuomela, S., Raghav, S., Ahlfors, H., Laurila, K., Gupta, B., Lund, R. J., Tahvanainen, J., Hawkins, R. D., Oresic, M., Lahdesmaki, H., Rasool, O., Rao, K. V., Aittokallio, T., and Lahesmaa, R.: *Genome-wide profiling of interleukin-4 and STAT6 transcription factor regulation of human Th2 cell programming*. Immunity, 32(6):852–62, 2010.

[59] Chen, Hui Chen and Reich, Nancy C.: *Live Cell Imaging Reveals Continuous STAT6 Nuclear Trafficking*. The Journal of Immunology, 185(1):64–70, 2010.

[60] Hebenstreit, D., Wirnsberger, G., Horejs-Hoeck, J., and Duschl, A.: *Signaling mechanisms, interaction partners, and target genes of STAT6*. Cytokine Growth Factor Rev, 17(3):173–88, 2006.

[61] Mehrotra, P., Riley, J. P., Patel, R., Li, F., Voss, L., and Goenka, S.: *PARP-14 functions as a transcriptional switch for Stat6-dependent gene activation*. J Biol Chem, 286(3):1767–76, 2011.

[62] Hanson, E. M., Dickensheets, H., Qu, C. K., Donnelly, R. P., and Keegan, A. D.: *Regulation of the dephosphorylation of Stat6. Participation of Tyr-713 in the interleukin-4 receptor alpha, the tyrosine phosphatase SHP-1, and the proteasome*. J Biol Chem, 278(6):3903–11, 2003.

[63] Zamorano, J., Rivas, M. D., Setien, F., and Perez, G. M.: *Proteolytic regulation of activated STAT6 by calpains*. J Immunol, 174(5):2843–8, 2005.

[64] Wang, D., Moriggl, R., Stravopodis, D., Carpino, N., Marine, J. C., Teglund, S., Feng, J., and Ihle, J. N.: *A small amphipathic alpha-helical region is required for transcriptional activities and proteasome-dependent turnover of the tyrosine-phosphorylated Stat5*. Embo j, 19(3):392–9, 2000.

[65] Croker, B. A., Kiu, H., and Nicholson, S. E.: *SOCS regulation of the JAK/STAT signalling pathway*. Semin Cell Dev Biol, 19(4):414–22, 2008.

[66] Wormald, S. and Hilton, D. J.: *Inhibitors of cytokine signal transduction*. J Biol Chem, 279(2):821–4, 2004.

[67] Krebs, D.L. and Hilton, D.J.: *SOCS: physiological suppressors of cytokine signaling*. Journal of Cell Science, 113(16):2813–2819, 2000.

[68] Calvo, K. R., Dabir, B., Kovach, A., Devor, C., Bandle, R., Bond, A., Shih, J. H., and Jaffe, E. S.: *IL-4 protein expression and basal activation of Erk in vivo in follicular lymphoma*. Blood, 112(9):3818–26, 2008.

[69] Ansel, K. M., Djuretic, I., Tanasa, B., and Rao, A.: *Regulation of Th2 differentiation and Il4 locus accessibility*. Annu Rev Immunol, 24:607–56, 2006.

[70] Messner, B., Stutz, A. M., Albrecht, B., Peiritsch, S., and Woisetschlager, M.: *Cooperation of binding sites for STAT6 and NF kappa B/rel in the IL-4-induced up-regulation of the human IgE germline promoter*. J Immunol, 159(7):3330–7, 1997.

[71] Iciek, L. A., Delphin, S. A., and Stavnezer, J.: *CD40 cross-linking induces Ig epsilon germline transcripts in B cells via activation of NF-kappaB: synergy with IL-4 induction*. J Immunol, 158(10):4769–79, 1997.

[72] Takeda, K., Tanaka, T., Shi, W., Matsumoto, M., Minami, M., Kashiwamura, S., Nakanishi, K., Yoshida, N., Kishimoto, T., and Akira, S.: *Essential role of Stat6 in IL-4 signalling*. Nature, 380(6575):627–30, 1996.

[73] Shimoda, K., Deursen, J. van, Sangster, M. Y., Sarawar, S. R., Carson, R. T., Tripp, R. A., Chu, C., Quelle, F. W., Nosaka, T., Vignali, D. A., Doherty, P. C., Grosveld, G., Paul, W. E., and Ihle, J. N.: *Lack of IL-4-induced Th2 response and IgE class switching in mice with disrupted Stat6 gene*. Nature, 380(6575):630–3, 1996.

[74] Kaplan, M. H., Schindler, U., Smiley, S. T., and Grusby, M. J.: *Stat6 is required for mediating responses to IL-4 and for development of Th2 cells*. Immunity, 4(3):313–9, 1996.

[75] Wirnsberger, G., Hebenstreit, D., Posselt, G., Horejs-Hoeck, J., and Duschl, A.: *IL-4 induces expression of TARC/CCL17 via two STAT6 binding sites*. Eur J Immunol, 36(7):1882–91, 2006.

[76] Liddiard, K., Welch, J. S., Lozach, J., Heinz, S., Glass, C. K., and Greaves, D. R.: *Interleukin-4 induction of the CC chemokine TARC (CCL17) in murine macrophages is mediated by multiple STAT6 sites in the TARC gene promoter*. BMC Mol Biol, 7:45, 2006.

[77] Kuperman, D. A. and Schleimer, R. P.: *Interleukin-4, interleukin-13, signal transducer and activator of transcription factor 6, and allergic asthma*. Curr Mol Med, 8(5):384–92, 2008.

[78] Sehra, S., Yao, Y., Howell, M. D., Nguyen, E. T., Kansas, G. S., Leung, D. Y., Travers, J. B., and Kaplan, M. H.: *IL-4 regulates skin homeostasis and the predisposition toward allergic skin inflammation*. J Immunol, 184(6):3186–90, 2010.

[79] Locksley, R. M.: *Asthma and allergic inflammation*. Cell, 140(6):777–83, 2010.

[80] Skinnider, B. F., Elia, A. J., Gascoyne, R. D., Patterson, B., Trumper, L., Kapp, U., and Mak, T. W.: *Signal transducer and activator of transcription 6 is frequently activated in Hodgkin and Reed-Sternberg cells of Hodgkin lymphoma*. Blood, 99(2):618–26, 2002.

[81] Mottok, A., Renne, C., Willenbrock, K., Hansmann, M. L., and Brauninger, A.: *Somatic hypermutation of SOCS1 in lymphocyte-predominant Hodgkin lymphoma is accompanied by high JAK2 expression and activation of STAT6*. Blood, 110(9):3387–90, 2007.

[82] Natoli, A., Lupertz, R., Merz, C., Muller, W. W., Kohler, R., Krammer, P. H., and Li-Weber, M.: *Targeting the IL-4/IL-13 signaling pathway sensitizes Hodgkin lymphoma cells to chemotherapeutic drugs*. Int J Cancer, 133(8):1945–54, 2013.

[83] Guiter, C., Dusanter-Fourt, I., Copie-Bergman, C., Boulland, M. L., Le Gouvello, S., Gaulard, P., Leroy, K., and Castellano, F.: *Constitutive STAT6 activation in primary mediastinal large B-cell lymphoma*. Blood, 104(2):543–9, 2004.

[84] Ritz, O., Guiter, C., Castellano, F., Dorsch, K., Melzner, J., Jais, J. P., Dubois, G., Gaulard, P., Moller, P., and Leroy, K.: *Recurrent mutations of the STAT6 DNA binding domain in primary mediastinal B-cell lymphoma*. Blood, 114(6):1236–42, 2009.

[85] Morin, R. D., Assouline, S., Alcaide, M., Mohajeri, A., Johnston, R. L., Chong, L., Grewal, J., Yu, S., Fornika, D., Bushell, K., Nielsen, T. H., Petrogiannis-Haliotis, T., Crump, M., Tosikyan, A., Grande, B. M., MacDonald, D., Rousseau, C., Bayat, M., Sesques, P., Froment, R., Albuquerque, M., Monczak, Y., Oros, K. K., Greenwood, C., Riazalhosseini, Y., Arseneault, M., Camlioglu, E., Constantin, A., Pan-Hammarstrom, Q., Peng, R., Mann, K. K., and Johnson, N. A.: *Genetic Landscapes of Relapsed and Refractory Diffuse Large B-Cell Lymphomas*. Clin Cancer Res, 22(9):2290–300, 2016.

[86] Siddiqi, I. N., Friedman, J., Barry-Holson, K. Q., Ma, C., Thodima, V., Kang, I., Padmanabhan, R., Dias, L. M., Kelly, K. R., Brynes, R. K., Kamalakaran, S., and Houldsworth, J.: *Characterization of a variant of t(14;18) negative nodal diffuse follicular lymphoma with CD23 expression, 1p36/TNFRSF14 abnormalities, and STAT6 mutations*. Mod Pathol, 29(6):570–81, 2016.

[87] Lawrence, M. S., Stojanov, P., Polak, P., Kryukov, G. V., Cibulskis, K., Sivachenko, A., Carter, S. L., Stewart, C., Mermel, C. H., Roberts, S. A., Kiezun, A., Hammerman, P. S., McKenna, A., Drier, Y., Zou, L., Ramos, A. H., Pugh, T. J., Stransky, N., Helman, E., Kim, J., Sougnez, C., Ambrogio, L., Nickerson, E., Shefler, E., Cortes, M. L., Auclair, D., Saksena, G., Voet, D., Noble, M., DiCara, D., Lin, P., Lichtenstein, L., Heiman, D. I., Fennell, T., Imielinski, M., Hernandez, B., Hodis, E., Baca, S., Dulak, A. M., Lohr, J., Landau, D. A., Wu, C. J., Melendez-Zajgla, J., Hidalgo-Miranda, A., Koren, A., McCarroll, S. A., Mora, J., Crompton, B., Onofrio, R., Parkin, M., Winckler, W., Ardlie, K., Gabriel, S. B., Roberts, C. W. M., Biegel, J. A., Stegmaier, K., Bass, A. J., Garraway, L. A., Meyerson, M., Golub, T. R., Gordenin, D. A., Sunyaev, S., Lander, E. S., and Getz, G.: *Mutational heterogeneity in cancer and the search for new cancer-associated genes*. Nature, 499(7457):214–218, 2013.

[88] Graham, F. L., Smiley, J., Russell, W. C., and Nairn, R.: *Characteristics of a human cell line transformed by DNA from human adenovirus type 5*. J Gen Virol, 36(1):59–74, 1977.

[89] DuBridge, R. B., Tang, P., Hsia, H. C., Leong, P. M., Miller, J. H., and Calos, M. P.: *Analysis of mutation in human cells by using an Epstein-Barr virus shuttle system*. Mol Cell Biol, 7(1):379–87, 1987.

[90] Pear, W. S., Nolan, G. P., Scott, M. L., and Baltimore, D.: *Production of high-titer helper-free retroviruses by transient transfection*. Proc Natl Acad Sci U S A, 90(18):8392–6, 1993.

[91] Ngo, V. N., Young, R. M., Schmitz, R., Jhavar, S., Xiao, W., Lim, K. H., Kohlhammer, H., Xu, W., Yang, Y., Zhao, H., Shaffer, A. L., Romesser, P., Wright, G., Powell, J., Rosenwald, A., Muller-Hermelink, H. K., Ott, G., Gascoyne, R. D., Connors, J. M., Rimsza, L. M., Campo, E., Jaffe, E. S., Delabie, J., Smeland, E. B., Fisher, R. I., Braziel, R. M., Tubbs, R. R., Cook, J. R., Weisenburger, D. D., Chan, W. C., and Staudt, L. M.: *Oncogenically active MYD88 mutations in human lymphoma*. Nature, 470(7332):115–9, 2011.

[92] Beckwith, M., Longo, D. L., O'Connell, C. D., Moratz, C. M., and Urba, W. J.: *Phorbol ester-induced, cell-cycle-specific, growth inhibition of human B-lymphoma cell lines*. J Natl Cancer Inst, 82(6):501–9, 1990.

[93] Morin, R. D., Johnson, N. A., Severson, T. M., Mungall, A. J., An, J., Goya, R., Paul, J. E., Boyle, M., Woolcock, B. W., Kuchenbauer, F., Yap, D., Humphries, R. K., Griffith, O. L., Shah, S., Zhu, H., Kimbara, M., Shashkin, P., Charlot, J. F., Tcherpakov, M., Corbett, R., Tam, A., Varhol, R., Smailus, D., Moksa, M., Zhao, Y., Delaney, A., Qian, H., Birol, I., Schein, J., Moore, R., Holt, R., Horsman, D. E., Connors, J. M., Jones, S., Aparicio, S., Hirst, M., Gascoyne, R. D., and Marra, M. A.: *Somatic mutations altering EZH2 (Tyr641) in follicular and diffuse large B-cell lymphomas of germinal-center origin*. Nat Genet, 42(2):181–5, 2010.

[94] Ben-Bassat, H., Goldblum, N., Mitrani, S., Goldblum, T., Yoffey, J. M., Cohen, M. M., Bentwich, Z., Ramot, B., Klein, E., and Klein, G.: *Establishment in continuous culture of a new type of lymphocyte from a "Burkitt like"malignant lymphoma (line D.G.-75)*. Int J Cancer, 19(1):27–33, 1977.

[95] Gabay, C., Ben-Bassat, H., Schlesinger, M., and Laskov, R.: *Somatic mutations and intraclonal variations in the rearranged Vkappa genes of B-non-Hodgkin's lymphoma cell lines*. Eur J Haematol, 63(3):180–91, 1999.

[96] Scherer, W. F., Syverton, J. T., and Gey, G. O.: *Studies on the propagation in vitro of poliomyelitis viruses. IV. Viral multiplication in a stable strain of human malignant epithelial cells (strain HeLa) derived from an epidermoid carcinoma of the cervix*. J Exp Med, 97(5):695–710, 1953.

[97] Macville, M., Schrock, E., Padilla-Nash, H., Keck, C., Ghadimi, B. M., Zimonjic, D., Popescu, N., and Ried, T.: *Comprehensive and definitive molecular cytogenetic characterization of HeLa cells by spectral karyotyping*. Cancer Res, 59(1):141–50, 1999.

[98] Adey, A., Burton, J. N., Kitzman, J. O., Hiatt, J. B., Lewis, A. P., Martin, B. K., Qiu, R., Lee, C., and Shendure, J.: *The haplotype-resolved genome and epigenome of the aneuploid HeLa cancer cell line*. Nature, 500(7461):207–11, 2013.

[99] Dyer, M. J., Fischer, P., Nacheva, E., Labastide, W., and Karpas, A.: *A new human B-cell non-Hodgkin's lymphoma cell line (Karpas 422) exhibiting both t (14;18) and t(4;11) chromosomal translocations*. Blood, 75(3):709–14, 1990.

[100] Stranks, G., Height, S. E., Mitchell, P., Jadayel, D., Yuille, M. A., De Lord, C., Clutterbuck, R. D., Treleaven, J. G., Powles, R. L., Nacheva, E., and al. et: *Deletions and rearrangement of CDKN2 in lymphoid malignancy*. Blood, 85(4):893–901, 1995.

[101] Mestre-Escorihuela, C., Rubio-Moscardo, F., Richter, J. A., Siebert, R., Climent, J., Fresquet, V., Beltran, E., Agirre, X., Marugan, I., Marin, M., Rosenwald, A., Sugimoto, K. J., Wheat, L. M., Karran, E. L., Garcia, J. F., Sanchez, L., Prosper, F., Staudt, L. M., Pinkel, D., Dyer, M. J., and Martinez-Climent, J. A.: *Homozygous deletions localize novel tumor suppressor genes in B-cell lymphomas*. Blood, 109(1):271–80, 2007.

[102] Li, C., Kim, S. W., Rai, D., Bolla, A. R., Adhvaryu, S., Kinney, M. C., Robetorye, R. S., and Aguiar, R. C.: *Copy number abnormalities, MYC activity, and the genetic fingerprint of normal B cells mechanistically define the microRNA profile of diffuse large B-cell lymphoma*. Blood, 113(26):6681–90, 2009.

[103] Inagaki, A., Ishida, T., Yano, H., Ishii, T., Kusumoto, S., Ito, A., Ri, M., Mori, F., Ding, J., Komatsu, H., Iida, S., and Ueda, R.: *Expression of the ULBP ligands for NKG2D by B-NHL cells plays an important role in determining their susceptibility to rituximab-induced ADCC*. Int J Cancer, 125(1):212–21, 2009.

[104] Zhang, J., Grubor, V., Love, C. L., Banerjee, A., Richards, K. L., Mieczkowski, P. A., Dunphy, C., Choi, W., Au, W. Y., Srivastava, G., Lugar, P. L., Rizzieri, D. A., Lagoo, A. S., Bernal-Mizrachi, L., Mann, K. P., Flowers, C., Naresh, K., Evens, A., Gordon, L. I., Czader, M., Gill, J. I., Hsi, E. D., Liu, Q., Fan, A., Walsh, K., Jima, D., Smith, L. L., Johnson, A. J., Byrd, J. C., Luftig, M. A., Ni, T., Zhu, J., Chadburn, A., Levy, S., Dunson, D., and Dave, S. S.: *Genetic heterogeneity of diffuse large B-cell lymphoma*. Proc Natl Acad Sci U S A, 110(4):1398–403, 2013.

[105] Iida, S., Saito, M., Okazaki, T., Seto, M., Yamamoto, K., Akao, Y., Ogura, M., Suzuki, H., Ariyoshi, Y., Koike, K., and al. et: *Phenotypic and genotypic characterization of 14 leukemia and lymphoma cell lines with 11q23 translocations*. Leuk Res, 16(12):1155–63, 1992.

[106] Siebert, R., Willers, C. P., Schramm, A., Fossa, A., Dresen, I. M., Uppenkamp, M., Nowrousian, M. R., Seeber, S., and Opalka, B.: *Homozygous loss of the MTS1/p16 and MTS2/p15 genes in lymphoma and lymphoblastic leukaemia cell lines*. Br J Haematol, 91(2):350–4, 1995.

[107] Takizawa, J., Suzuki, R., Kuroda, H., Utsunomiya, A., Kagami, Y., Joh, T., Aizawa, Y., Ueda, R., and Seto, M.: *Expression of the TCL1 gene at 14q32 in B-cell malignancies but not in adult T-cell leukemia*. Jpn J Cancer Res, 89(7):712–8, 1998.

[108] Morin, R. D., Mungall, K., Pleasance, E., Mungall, A. J., Goya, R., Huff, R. D., Scott, D. W., Ding, J., Roth, A., Chiu, R., Corbett, R. D., Chan, F. C., Mendez-Lago, M., Trinh, D. L., Bolger-Munro, M., Taylor, G., Hadj Khodabakhshi, A., Ben-Neriah, S., Pon, J., Meissner, B., Woolcock, B., Farnoud, N., Rogic, S., Lim, E. L., Johnson, N. A., Shah, S., Jones, S., Steidl, C., Holt, R., Birol, I., Moore, R., Connors, J. M., Gascoyne, R. D., and Marra, M. A.: *Mutational and structural analysis of diffuse large B-cell lymphoma using whole-genome sequencing*. Blood, 122(7):1256–65, 2013.

[109] Cao, S., Strong, M. J., Wang, X., Moss, W. N., Concha, M., Lin, Z., O'Grady, T., Baddoo, M., Fewell, C., Renne, R., and Flemington, E. K.: *High-throughput RNA sequencing-based virome analysis of 50 lymphoma cell lines from the Cancer Cell Line Encyclopedia project*. J Virol, 89(1):713–29, 2015.

[110] Klijn, C., Durinck, S., Stawiski, E. W., Haverty, P. M., Jiang, Z., Liu, H., Degenhardt, J., Mayba, O., Gnad, F., Liu, J., Pau, G., Reeder, J., Cao, Y., Mukhyala, K., Selvaraj, S. K., Yu, M., Zynda, G. J., Brauer, M. J., Wu, T. D., Gentleman, R. C., Manning, G., Yauch, R. L., Bourgon, R., Stokoe, D., Modrusan, Z., Neve, R. M., Sauvage, F. J. de, Settleman, J., Seshagiri, S., and Zhang, Z.: *A comprehensive transcriptional portrait of human cancer cell lines*. Nat Biotechnol, 33(3):306–12, 2015.

[111] Iorio, F., Knijnenburg, T. A., Vis, D. J., Bignell, G. R., Menden, M. P., Schubert, M., Aben, N., Goncalves, E., Barthorpe, S., Lightfoot, H., Cokelaer, T., Greninger, P., Dyk, E. van, Chang, H., Silva, H. de, Heyn, H., Deng, X., Egan, R. K., Liu, Q., Mironenko, T., Mitropoulos, X., Richardson, L., Wang, J., Zhang, T., Moran, S., Sayols, S., Soleimani, M., Tamborero, D., Lopez-Bigas, N., Ross-Macdonald, P., Esteller, M., Gray, N. S., Haber, D. A., Stratton, M. R., Benes, C. H., Wessels, L. F., Saez-Rodriguez, J., McDermott, U., and Garnett, M. J.: *A Landscape of Pharmacogenomic Interactions in Cancer*. Cell, 166(3):740–54, 2016.

[112] Li, J., Zhao, W., Akbani, R., Liu, W., Ju, Z., Ling, S., Vellano, C. P., Roebuck, P., Yu, Q., Eterovic, A. K., Byers, L. A., Davies, M. A., Deng, W., Gopal, Y. N., Chen, G., Euw, E. M. von, Slamon, D., Conklin, D., Heymach, J. V., Gazdar, A. F., Minna, J. D., Myers, J. N., Lu, Y., Mills, G. B., and Liang, H.: *Characterization of Human Cancer Cell Lines by Reverse-phase Protein Arrays*. Cancer Cell, 31(2):225–239, 2017.

[113] Nadkarni, J. S., Nadkarni, J. J., Clifford, P., Manolov, G., Fenyo, E. M., and Klein, E.: *Characteristics of new cell lines derived from Burkitt lymphomas*. Cancer, 23(1):64–79, 1969.

[114] Nyormoi, O., Klein, G., Adams, A., and Dombos, L.: *Sensitivity to EBV superinfection and IUdR inducibility of hybrid cells formed between a sensitive and a relatively resistant Burkitt lymphoma cell line*. Int J Cancer, 12(2):396–408, 1973.

[115] Klein, G., Dombos, L., and Gothoskar, B.: *Sensitivity of Epstein-Barr virus (EBV) producer and non-producer human lymphoblastoid cell lines to superinfection with EB-virus*. Int J Cancer, 10(1):44–57, 1972.

[116] Benjamin, D., Magrath, I. T., Maguire, R., Janus, C., Todd, H. D., and Parsons, R. G.: *Immunoglobulin secretion by cell lines derived from African and American undifferentiated lymphomas of Burkitt's and non-Burkitt's type*. J Immunol, 129(3):1336–42, 1982.

[117] Klein, F., Ricketts, R. T., Jones, W. I., DeArmon, I. A., Temple, M. J., Zoon, K. C., and Bridgen, P. J.: *Large-scale production and concentration of human lymphoid interferon*. Antimicrob Agents Chemother, 15(3):420–7, 1979.

[118] Tweeddale, M. E., Lim, B., Jamal, N., Robinson, J., Zalcberg, J., Lockwood, G., Minden, M. D., and Messner, H. A.: *The presence of clonogenic cells in high-grade malignant lymphoma: a prognostic factor*. Blood, 69(5):1307–14, 1987.

[119] Farrugia, M. M., Duan, L. J., Reis, M. D., Ngan, B. Y., and Berinstein, N. L.: *Alterations of the p53 tumor suppressor gene in diffuse large cell lymphomas with translocations of the c-MYC and BCL-2 proto-oncogenes*. Blood, 83(1):191–8, 1994.

[120] Chang, H., Blondal, J. A., Benchimol, S., Minden, M. D., and Messner, H. A.: *p53 mutations, c-myc and bcl-2 rearrangements in human non-Hodgkin's lymphoma cell lines*. Leuk Lymphoma, 19(1-2):165–71, 1995.

[121] Mehra, S., Messner, H., Minden, M., and Chaganti, R. S.: *Molecular cytogenetic characterization of non-Hodgkin lymphoma cell lines*. Genes Chromosomes Cancer, 33(3):225–34, 2002.

[122] Kuppers, R., Klein, U., Schwering, I., Distler, V., Brauninger, A., Cattoretti, G., Tu, Y., Stolovitzky, G. A., Califano, A., Hansmann, M. L., and Dalla-Favera, R.: *Identification of Hodgkin and Reed-Sternberg cell-specific genes by gene expression profiling*. J Clin Invest, 111(4):529–37, 2003.

[123] Chang, H., Messner, H. A., Wang, X. H., Yee, C., Addy, L., Meharchand, J., and Minden, M. D.: *A human lymphoma cell line with multiple immunoglobulin rearrangements*. J Clin Invest, 89(3):1014–20, 1992.

[124] Chang, H., Leeder, S., Cook, V. A., Patterson, B., Dosch, M., Minden, M. D., and Messner, H. A.: *Growth of human lymphoma cells in SCID mice*. Leuk Lymphoma, 8(1-2):129–36, 1992.

[125] Epstein, A. L., Herman, M. M., Kim, H., Dorfman, R. F., and Kaplan, H. S.: *Biology of the human malignant lymphomas. III. Intracranial heterotransplantation in the nude, athymic mouse*. Cancer, 37(5):2158–76, 1976.

[126] Epstein, A. L., Levy, R., Kim, H., Henle, W., Henle, G., and Kaplan, H. S.: *Biology of the human malignant lymphomas. IV. Functional characterization of ten diffuse histiocytic lymphoma cell lines*. Cancer, 42(5):2379–91, 1978.

[127] Epstein, A. L. and Kaplan, H. S.: *Feeder layer and nutritional requirements for the establishment and cloning of human malignant lymphoma cell lines*. Cancer Res, 39(5):1748–59, 1979.

[128] Hecht, B. K., Epstein, A. L., Berger, C. S., Kaplan, H. S., and Hecht, F.: *Histiocytic lymphoma cell lines: immunologic and cytogenetic studies*. Cancer Genet Cytogenet, 14(3-4):205–18, 1985.

[129] Winter, J. N., Variakojis, D., and Epstein, A. L.: *Phenotypic analysis of established diffuse histiocytic lymphoma cell lines utilizing monoclonal antibodies and cytochemical techniques*. Blood, 63(1):140–6, 1984.

[130] Bodor, C., O'Riain, C., Wrench, D., Matthews, J., Iyengar, S., Tayyib, H., Calaminici, M., Clear, A., Iqbal, S., Quentmeier, H., Drexler, H. G., Montoto, S., Lister, A. T., Gribben, J. G., Matolcsy, A., and Fitzgibbon, J.: *EZH2 Y641 mutations in follicular lymphoma*. Leukemia, 25(4):726–9, 2011.

[131] Mohammad, R. M., Mohamed, A. N., Smith, M. R., Jawadi, N. S., and Katib, A. al: *A unique EBV-negative low-grade lymphoma line (WSU-FSCCL) exhibiting both t(14;18) and t(8;11)*. Cancer Genet Cytogenet, 70(1):62–7, 1993.

[132] Mohammad, R., Abubakr, Y., Dan, M., Aboukameel, A., Chow, C., Mohamed, A., Hamdy, N., and Al-Katib, A.: *Bcl-2 antisense oligonucleotides are effective against systemic but not central nervous system disease in severe combined immunodeficient mice bearing human t(14;18) follicular lymphoma*. Clin Cancer Res, 8(4):1277–83, 2002.

[133] Smith, M. R., Jin, F., and Joshi, I.: *Enhanced efficacy of therapy with antisense BCL-2 oligonucleotides plus anti-CD20 monoclonal antibody in scid mouse/human lymphoma xenografts*. Mol Cancer Ther, 3(12):1693–9, 2004.

[134] Subramanian, Aravind, Tamayo, Pablo, Mootha, Vamsi K., Mukherjee, Sayan, Ebert, Benjamin L., Gillette, Michael A., Paulovich, Amanda, Pomeroy, Scott L., Golub, Todd R., Lander, Eric S., and Mesirov, Jill P.: *Gene set enrichment analysis: A knowledge-based approach for interpreting genome-wide expression profiles*. Proceedings of the National Academy of Sciences, 102(43):15545–15550, 2005.

[135] Mootha, Vamsi K., Lindgren, Cecilia M., Eriksson, Karl Fredrik, Subramanian, Aravind, Sihag, Smita, Lehar, Joseph, Puigserver, Pere, Carlsson, Emma, Ridderstråle, Martin, Laurila, Esa, Houstis, Nicholas, Daly, Mark J., Patterson, Nick, Mesirov, Jill P., Golub, Todd R., Tamayo, Pablo, Spiegelman, Bruce, Lander, Eric

S., Hirschhorn, Joel N., Altshuler, David, and Groop, Leif C.: *PGC-1α-responsive genes involved in oxidative phosphorylation are coordinately downregulated in human diabetes*. Nature Genetics, 34:267, 2003.

[136] Untergasser, A., Cutcutache, I., Koressaar, T., Ye, J., Faircloth, B. C., Remm, M., and Rozen, S. G.: *Primer3–new capabilities and interfaces*. Nucleic Acids Res, 40(15):e115, 2012.

[137] Koressaar, T. and Remm, M.: *Enhancements and modifications of primer design program Primer3*. Bioinformatics, 23(10):1289–91, 2007.

[138] Chomczynski, P. and Sacchi, N.: *Single-step method of RNA isolation by acid guanidinium thiocyanate-phenol-chloroform extraction*. Anal Biochem, 162(1):156–9, 1987.

[139] Chomczynski, P. and Sacchi, N.: *The single-step method of RNA isolation by acid guanidinium thiocyanate-phenol-chloroform extraction: twenty-something years on*. Nat Protoc, 1(2):581–5, 2006.

[140] Ziegenhain, C., Vieth, B., Parekh, S., Reinius, B., Guillaumet-Adkins, A., Smets, M., Leonhardt, H., Heyn, H., Hellmann, I., and Enard, W.: *Comparative Analysis of Single-Cell RNA Sequencing Methods*. Mol Cell, 65(4):631–643.e4, 2017.

[141] Soumillon, Magali, Cacchiarelli, Davide, Semrau, Stefan, Oudenaarden, Alexander van, and Mikkelsen, Tarjei S: *Characterization of directed differentiation by high-throughput single-cell RNA-Seq*. bioRxiv, 2014.

[142] Kivioja, T., Vaharautio, A., Karlsson, K., Bonke, M., Enge, M., Linnarsson, S., and Taipale, J.: *Counting absolute numbers of molecules using unique molecular identifiers*. Nat Methods, 9(1):72–4, 2011.

[143] Macosko, E. Z., Basu, A., Satija, R., Nemesh, J., Shekhar, K., Goldman, M., Tirosh, I., Bialas, A. R., Kamitaki, N., Martersteck, E. M., Trombetta, J. J., Weitz, D. A., Sanes, J. R., Shalek, A. K., Regev, A., and McCarroll, S. A.: *Highly Parallel Genome-wide Expression Profiling of Individual Cells Using Nanoliter Droplets*. Cell, 161(5):1202–1214, 2015.

[144] Renaud, G., Stenzel, U., Maricic, T., Wiebe, V., and Kelso, J.: *deML: robust demultiplexing of Illumina sequences using a likelihood-based approach*. Bioinformatics, 31(5):770–2, 2015.

[145] Martin, Marcel: *Cutadapt removes adapter sequences from high-throughput sequencing reads*. 2011, 17(1), 2011.

[146] Dobin, Alexander, Davis, Carrie A., Schlesinger, Felix, Drenkow, Jorg, Zaleski, Chris, Jha, Sonali, Batut, Philippe, Chaisson, Mark, and Gingeras, Thomas R.: *STAR: ultrafast universal RNA-seq aligner*. Bioinformatics, 29(1):15–21, 2013.

[147] Love, M. I., Huber, W., and Anders, S.: *Moderated estimation of fold change and dispersion for RNA-seq data with DESeq2*. Genome Biol, 15(12):550, 2014.

[148] Hadley, Wickham: *ggplot2*. Springer Science+Business Media, LLC, New York, NY, 2016, ISBN 9783319242750.

[149] Mikita, T., Campbell, D., Wu, P., Williamson, K., and Schindler, U.: *Requirements for interleukin-4-induced gene expression and functional characterization of Stat6*. Mol Cell Biol, 16(10):5811–20, 1996.

[150] Lu, X., Nechushtan, H., Ding, F., Rosado, M. F., Singal, R., Alizadeh, A. A., and Lossos, I. S.: *Distinct IL-4-induced gene expression, proliferation, and intracellular signaling in germinal center B-cell-like and activated B-cell-like diffuse large-cell lymphomas*. Blood, 105(7):2924–32, 2005.

[151] Schaefer, C. F., Anthony, K., Krupa, S., Buchoff, J., Day, M., Hannay, T., and Buetow, K. H.: *PID: the Pathway Interaction Database*. Nucleic Acids Res, 37(Database issue):D674–9, 2009.

[152] Reva, Boris, Antipin, Yevgeniy, and Sander, Chris: *Predicting the functional impact of protein mutations: application to cancer genomics*. Nucleic Acids Research, 39(17):e118–e118, 2011.

[153] Acharya, M., Borland, G., Edkins, A. L., Maclellan, L. M., Matheson, J., Ozanne, B. W., and Cushley, W.: *CD23/FcepsilonRII: molecular multi-tasking*. Clin Exp Immunol, 162(1):12–23, 2010.

[154] Viganò, Elena, Gunawardana, Jay, Mottok, Anja, Van Tol, Tessa, Mak, Katina, Chan, Fong Chun, Chong, Lauren, Chavez, Elizabeth, Woolcock, Bruce, Takata, Katsuyoshi, Twa, David, Shulha, Hennady P., Telenius, Adèle, Kutovaya, Olga, Hung, Stacy S., Healy, Shannon, Ben-Neriah, Susana, Leroy, Karen, Gaulard, Philippe, Diepstra, Arjan, Kridel, Robert, Savage, Kerry J., Rimsza, Lisa, Gascoyne, Randy, and Steidl, Christian: *Somatic IL4R Mutations in Primary Mediastinal Large B-cell lymphoma lead to constitutive JAK-STAT signaling activation*. Blood, 2018.

[155] Zerbino, D. R., Achuthan, P., Akanni, W., Amode, M. R., Barrell, D., Bhai, J., Billis, K., Cummins, C., Gall, A., Giron, C. G., Gil, L., Gordon, L., Haggerty, L., Haskell, E., Hourlier, T., Izuogu, O. G., Janacek, S. H., Juettemann, T., To, J. K., Laird, M. R., Lavidas, I., Liu, Z., Loveland, J. E., Maurel, T., McLaren, W., Moore, B., Mudge, J., Murphy, D. N., Newman, V., Nuhn, M., Ogeh, D., Ong, C. K., Parker, A., Patricio, M., Riat, H. S., Schuilenburg, H., Sheppard, D., Sparrow, H., Taylor, K., Thormann, A., Vullo, A., Walts, B., Zadissa, A., Frankish, A., Hunt, S. E., Kostadima, M., Langridge, N., Martin, F. J., Muffato, M., Perry, E., Ruffier, M., Staines, D. M., Trevanion, S. J., Aken, B. L., Cunningham, F., Yates, A., and Flicek, P.: *Ensembl 2018*. Nucleic Acids Res, 46(D1):D754–d761, 2018.

[156] The International HapMap, Consortium: *Integrating common and rare genetic variation in diverse human populations*. Nature, 467:52, 2010.

[157] Pangault, C., Ame-Thomas, P., Ruminy, P., Rossille, D., Caron, G., Baia, M., De Vos, J., Roussel, M., Monvoisin, C., Lamy, T., Tilly, H., Gaulard, P., Tarte, K., and Fest, T.: *Follicular lymphoma cell niche: identification of a preeminent IL-4-dependent TFH-B cell axis*. Leukemia, 24(12):2080–2089, 2010.

[158] Ame-Thomas, P., Hoeller, S., Artchounin, C., Misiak, J., Braza, M. S., Jean, R., Le Priol, J., Monvoisin, C., Martin, N., Gaulard, P., and Tarte, K.: *CD10 delineates a subset of human IL-4 producing follicular helper T cells involved in the survival of follicular lymphoma B cells*. Blood, 125(15):2381–5, 2015.

[159] Borland, G., Edkins, A. L., Acharya, M., Matheson, J., White, L. J., Allen, J. M., Bonnefoy, J. Y., Ozanne, B. W., and Cushley, W.: *alphavbeta5 integrin sustains growth of human pre-B cells through an RGD-independent interaction with a basic domain of the CD23 protein*. J Biol Chem, 282(37):27315–26, 2007.

[160] Liu, Y. J., Cairns, J. A., Holder, M. J., Abbot, S. D., Jansen, K. U., Bonnefoy, J. Y., Gordon, J., and MacLennan, I. C.: *Recombinant 25-kDa CD23 and interleukin 1 alpha promote the survival of germinal center B cells: evidence for bifurcation in the development of centrocytes rescued from apoptosis*. Eur J Immunol, 21(5):1107–14, 1991.

[161] Liu, Y. J., Mason, D. Y., Johnson, G. D., Abbot, S., Gregory, C. D., Hardie, D. L., Gordon, J., and MacLennan, I. C.: *Germinal center cells express bcl-2 protein after activation by signals which prevent their entry into apoptosis*. Eur J Immunol, 21(8):1905–10, 1991.

[162] Leich, E., Salaverria, I., Bea, S., Zettl, A., Wright, G., Moreno, V., Gascoyne, R. D., Chan, W. C., Braziel, R. M., Rimsza, L. M., Weisenburger, D. D., Delabie, J., Jaffe, E. S., Lister, A., Fitzgibbon, J., Staudt, L. M., Hartmann, E. M., Mueller-Hermelink, H. K., Campo, E., Ott, G., and Rosenwald, A.: *Follicular lymphomas with and without translocation t(14;18) differ in gene expression profiles and genetic alterations*. Blood, 114(4):826–34, 2009.

[163] Uhlen, M., Fagerberg, L., Hallstrom, B. M., Lindskog, C., Oksvold, P., Mardinoglu, A., Sivertsson, A., Kampf, C., Sjostedt, E., Asplund, A., Olsson, I., Edlund, K., Lundberg, E., Navani, S., Szigyarto, C. A., Odeberg, J., Djureinovic, D., Takanen, J. O., Hober, S., Alm, T., Edqvist, P. H., Berling, H., Tegel, H., Mulder, J., Rockberg, J., Nilsson, P., Schwenk, J. M., Hamsten, M., Feilitzen, K. von, Forsberg, M., Persson, L., Johansson, F., Zwahlen, M., Heijne, G. von, Nielsen, J., and Ponten, F.: *Proteomics. Tissue-based map of the human proteome*. Science, 347(6220):1260419, 2015.

[164] Uhlen, M., Zhang, C., Lee, S., Sjostedt, E., Fagerberg, L., Bidkhori, G., Benfeitas, R., Arif, M., Liu, Z., Edfors, F., Sanli, K., Feilitzen, K. von, Oksvold, P., Lundberg, E., Hober, S., Nilsson, P., Mattsson, J., Schwenk, J. M., Brunnstrom, H., Glimelius, B., Sjoblom, T., Edqvist, P. H., Djureinovic, D., Micke, P., Lindskog, C., Mardinoglu, A., and Ponten, F.: *A pathology atlas of the human cancer transcriptome*. Science, 357(6352), 2017.

[165] Stergachis, A. B., Haugen, E., Shafer, A., Fu, W., Vernot, B., Reynolds, A., Raubitschek, A., Ziegler, S., LeProust, E. M., Akey, J. M., and Stamatoyannopoulos, J. A.: *Exonic transcription factor binding directs codon choice and affects protein evolution*. Science, 342(6164):1367–72, 2013.

[166] Fong, Peter C., Boss, David S., Yap, Timothy A., Tutt, Andrew, Wu, Peijun, Mergui-Roelvink, Marja, Mortimer, Peter, Swaisland, Helen, Lau, Alan, O'Connor, Mark J., Ashworth, Alan, Carmichael, James, Kaye, Stan B., Schellens, Jan H.M., and Bono, Johann S. de: *Inhibition of Poly(ADP-Ribose) Polymerase in Tumors from BRCA Mutation Carriers*. New England Journal of Medicine, 361(2):123–134, 2009.

[167] Peng, B., Thorsell, A. G., Karlberg, T., Schuler, H., and Yao, S. Q.: *Small Molecule Microarray Based Discovery of PARP14 Inhibitors*. Angew Chem Int Ed Engl, 56(1):248–253, 2017.

[168] Yoneyama-Hirozane, M., Matsumoto, S. I., Toyoda, Y., Saikatendu, K. S., Zama, Y., Yonemori, K., Oonishi, M., Ishii, T., and Kawamoto, T.: *Identification of PARP14 inhibitors using novel methods for detecting auto-ribosylation*. Biochem Biophys Res Commun, 486(3):626–631, 2017.

A Appendix

A.1 The GLSG2000 and BCCA study groups

	GLSG2000 training cohort	BCCA validation cohort	p value
Patients			
Number of assessable patients	151	107	
Male	78 (52%)	59 (55%)	0·67
Female	73 (48%)	48 (45%)	
Clinical risk factors			
>60 years	57 (38%)	59 (55%)	0·0083
>4 nodal sites	106 (70%)	78 (73%)	0·74
Lactate dehydrogenase elevate	49 (32%)	22 (21%)	0·074
Haemoglobin <120 g/L	32 (21%)	12 (11%)	0·062
ECOG performance status >1	8 (5%)	16 (15%)	0·016
FLIPI high-risk	77 (51%)	53 (50%)	0·92
Treatment			
First-line treatment	R-CHOP	R-CVP	
Maintenance treatment	IFNα	Rituximab	
Number of patients intended for maintenance treatment	151	93	
Outcome			
5-year failure-free survival (95% CI; number of events)	66·22% (58·63–74·79; 63)	58·43% (49·73–68·66; 48)	
5-year overall survival (95% CI; number of deaths)	83·25% (77·20–89·78; 33)	74·40% (66·50–83·23; 32)	
Median (IQR) follow-up for overall survival, years	7·7 (5·5–9·3)	6·7 (5·7–7·6)	

Figure A.1
Patient and disease attributes. Figure from Pastore *et al.*[11]

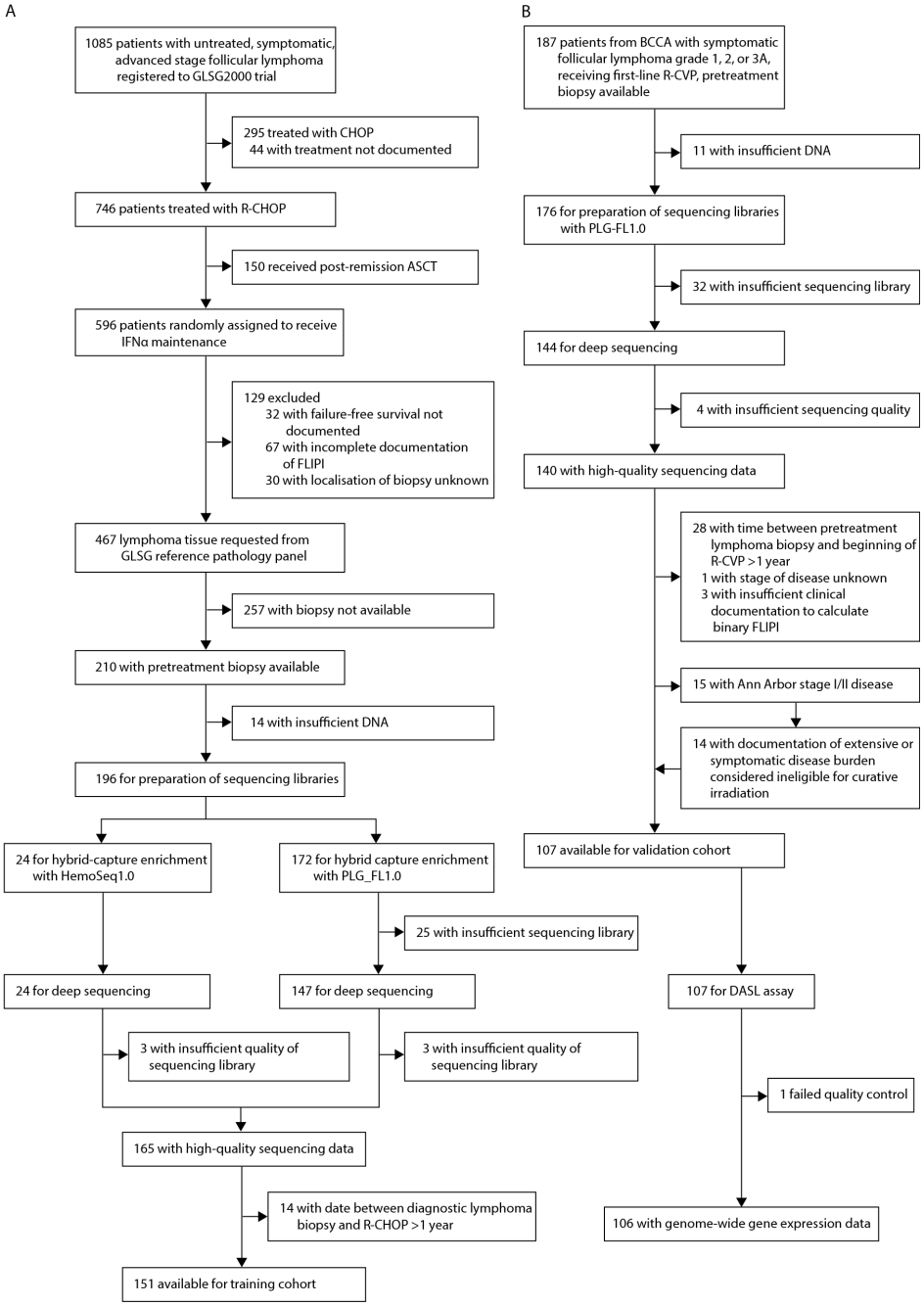

Figure A.2
Patient flow of GLSG2000 (A) and BCCA (B) cohort. Figure adapted from Pastore *et al.*[11]

A.2 Vector maps

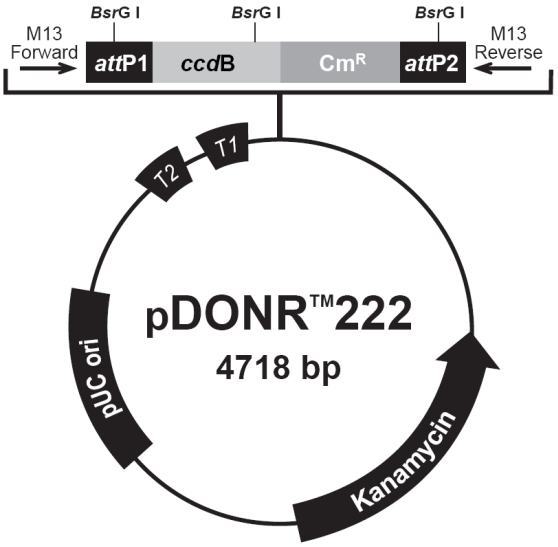

*rrn*B T2 transcription termination sequence: bases 58-85 (c)
rrnB T1 transcription termination sequence: bases 217-260 (c)
M13 Forward (-20) priming site: bases 327-342
*att*P1: bases 360-591
*Bsr*G I restriction sites: bases 442, 1232, 2689
*ccd*B gene: bases 987-1292 (c)
Chloramphenicol resistance gene: bases 1612-2295 (c)
*att*P2: bases 2543-2774 (c)
M13 Reverse priming site: bases 2816-2832
Kanamycin resistance gene: bases 2899-3714 (c)
pUC origin: bases 4045-4718
(c) = complementary strand

Figure A.3
Map of pDONR^{TM}222 (Invitrogen)

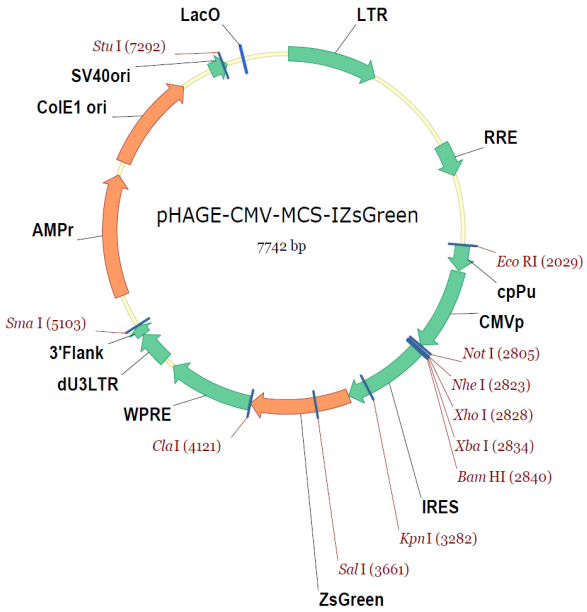

Figure A.4
Map of pHAGE-CMV-MCS-IRES-ZsGreen (Plasmid, Harvard Medical School)

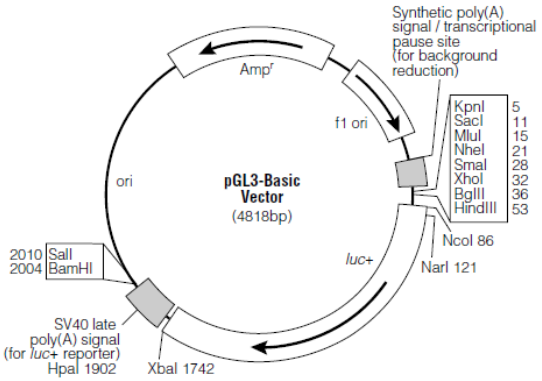

pGL3-Basic Vector Sequence Reference Points:

Promoter	(none)
Enhancer	(none)
Multiple cloning region	1–58
Luciferase gene (*luc*+)	88–1740
GLprimer2 binding site	89–111
SV40 late poly(A) signal	1772–1993
RVprimer4 binding site	2080–2061
ColE1-derived plasmid replication origin	2318
β-lactamase gene (Amp^r)	3080–3940
f1 origin	4072–4527
upstream poly(A) signal	4658–4811
RVprimer3 binding site	4760–4779

Figure A.5
Map of pGL3-Basic luciferase reporter vector (Promega)

A.3 Flow cytometer configuration

Table A.1
Flow cytometer configuration. ELLF of 3 laser, 8 color (4-2-2)

Laser Name	Wave-length	Power	Detector Array	Detec-tor	Chan-nel	Mirror	Filter	Parameter
Blue	488	20	Octagon	A	1	735 LP	780/60 BP	PE-Cy7
				B	2	655 LP	670 LP	7-AAD
								PerCP
								PerCP-Cy5-5
								PI (670nm)
				C		610 LP		
				D	3	556 LP	585/42 BP	PE
								PI (585nm)
								RFP
				E	4	502 LP	530/30 BP	AlexaFluor488
								FITC
								GFP
								YFP
				F	5		488/10 BP	SSC
				G				
				H				
Red	633	17	Trigon	A	6	735 LP	780/60 BP	APC-Cy7
								APC-H7
				B		685 LP		
				C	7		660/20 BP	AlexaFluor647
								APC
Violet	405	25	Trigon	A	9	502 LP	510/50 BP	AmCyan
								BV510
								V500
				B	8		450/50 BP	BV421
								DAPI
								Pacific Blue
								V450
				C				

A.4 STAT6 variants in the GLSG2000 and BCCA cohort are monoallelic

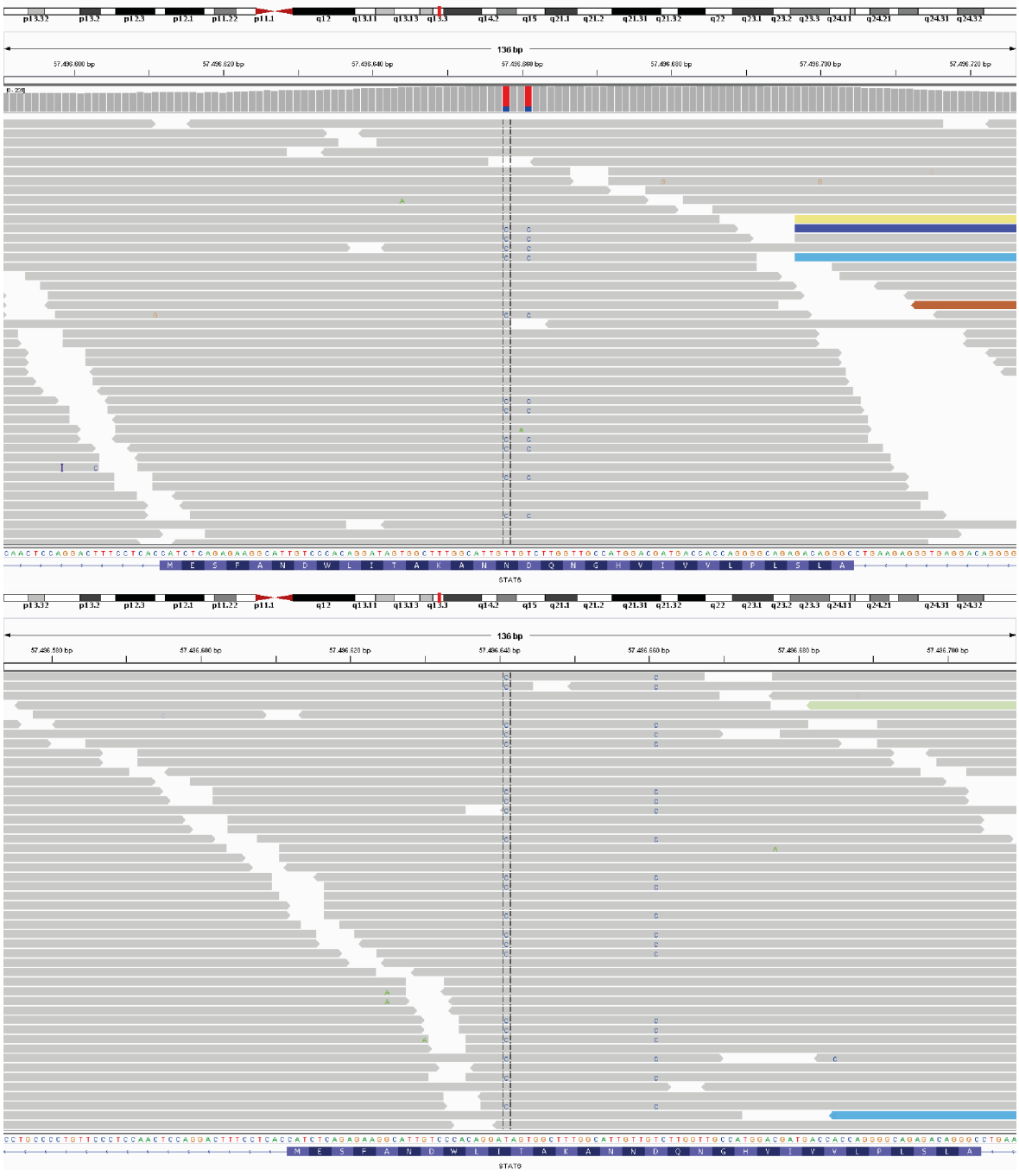

Figure A.6
Sequencing results of patient 1738 (top) and RG071 (bottom), each with two distinct STAT6 mutations. Both mutations are covered by the same read. Displayed is the BAM sequencing file by IGV browser (Broad institute).

A.5 Lists of differentially expressed genes

Table A.2
List of differentially expressed genes in the BCCA cohort based on STAT6 mutational status. Cutoff: log2FC: ±0.65, p-value: <0.05.

PROBE_ID	SYMBOL	logFC	AveExpr	t	P.Value	adj.P.Val	B
ILMN_1667756	DMD	1,57428378	6,23779305	3,52280592	0,0005693	0,83001963	-3,35028332
ILMN_1701170	BARX2	1,20291021	7,16752011	3,25510804	0,00140695	0,96482818	-3,54004875
ILMN_1662451	FCER2	1,03635352	12,0337774	3,18778123	0,00175191	0,96482818	-3,5859921
ILMN_1710186	CCL17	0,98310369	6,3952192	3,9735099	0,00011061	0,41969279	-3,00696461
ILMN_1760065	OR2T11	0,90886824	7,2158312	4,12396611	6,21E-05	0,41969279	-2,88625783
ILMN_1671486	HOMER2	0,90505855	6,63257436	3,48175918	0,00065623	0,83001963	-3,38009712
ILMN_1719677	MOBKL2C	0,89645628	8,69965737	2,85427357	0,00493722	0,99940501	-3,80240187
ILMN_1679011	SLC12A3	0,83020147	9,56110727	2,70887895	0,00755304	0,99940501	-3,89067678
ILMN_2391400	PITX2	0,80335793	8,48243255	2,03922386	0,04321944	0,99940501	-4,24577632
ILMN_1790843	NLRP11	0,75685708	6,56691641	2,33499746	0,02089663	0,99940501	-4,09970467
ILMN_2160476	CCL22	0,73193194	7,60609529	2,09262036	0,03810178	0,99940501	-4,22071085
ILMN_2105441	IGJ	0,71614761	10,5419729	2,40334459	0,01749248	0,99940501	-4,06348339
ILMN_1782729	CLECL1	0,70021567	8,86759175	2,49486247	0,01370683	0,99940501	-4,01356982
ILMN_1653434	DMD	0,69820174	6,31935743	2,2051301	0,02899872	0,99940501	-4,16600096
ILMN_1658247	OAS1	0,69184125	8,48158135	2,18802012	0,03024773	0,99940501	-4,17448545
ILMN_2196642	AGBL4	0,68897835	8,0051858	2,52025233	0,01279517	0,99940501	-3,99943887
ILMN_1794552	GAP43	0,67454868	9,58100699	2,39836282	0,01772288	0,99940501	-4,06615419
ILMN_1663858	ZNF286A	0,6599209	7,31265	3,15019672	0,00197714	0,96482818	-3,61131775
ILMN_1653687	GALNT9	0,65793013	6,64882268	2,02610541	0,04456301	0,99940501	-4,25184497
ILMN_1754921	FAM43B	0,65737959	6,63934788	2,71111726	0,0075047	0,99940501	-3,88934672
ILMN_2335398	CECR5	0,65716661	6,50909092	2,84310893	0,00510401	0,99940501	-3,80931435
ILMN_1779241	CRYM	-0,66096851	5,93637676	-3,01552805	0,00302326	0,99940501	-3,70013145
ILMN_2110422	PKD1L1	-0,66213669	7,92009629	-3,28643681	0,00126902	0,96482818	-3,51842085
ILMN_1680192	APOBEC3A	-0,68147805	10,5333715	-2,0783813	0,03941285	0,99940501	-4,22745196
ILMN_1711470	UBE2T	-0,68569563	9,23603068	-3,84718364	0,00017758	0,44921447	-3,10603608
ILMN_3245564	RICH2	-0,71852851	10,3102096	-2,44024518	0,01586686	0,99940501	-4,04355129
ILMN_1699610	CCT6B	-0,71906806	7,25561191	-3,35706957	0,00100297	0,96482818	-3,46908664
ILMN_1693119	LYPD6B	-0,74989144	7,19322789	-2,04138295	0,04300166	0,99940501	-4,24477412
ILMN_1657643	KCNIP2	-0,7842672	9,01683857	-2,17050873	0,03157412	0,99940501	-4,18310816
ILMN_1688103	CTNNBIP1	-0,82592341	8,18689185	-2,8121649	0,00559352	0,99940501	-3,82835744
ILMN_2361614	CCDC85A	-0,83905821	6,7449583	-2,14764846	0,03338129	0,99940501	-4,19427181
ILMN_2371079	HTR3A	-0,85754159	12,3955565	-2,47499807	0,01446005	0,99940501	-4,02454007
ILMN_2376859	PDGFD	-0,87525295	8,31243982	-2,6725563	0,008378	0,99940501	-3,91213247
ILMN_1770505	BIK	-0,87867171	9,34691547	-2,68472048	0,00809308	0,99940501	-3,90497403
ILMN_1699623	FAM81A	-0,8995933	10,6556591	-3,23849863	0,00148562	0,96482818	-3,55145113
ILMN_2206009	FCAMR	-0,91776824	9,78428615	-2,59315524	0,01047125	0,99940501	-3,95818806
ILMN_1674580	TRIM36	-0,96017068	8,29005776	-2,25396946	0,02567711	0,99940501	-4,14146086
ILMN_1709173	HMHB1	-1,06030534	8,46083322	-3,20160851	0,00167522	0,96482818	-3,57661657
ILMN_1670193	ACY3	-1,14586142	9,28271159	-2,50372765	0,01338213	0,99940501	-4,00864972
ILMN_2376194	CAMK2B	-1,18526058	8,31951107	-2,43838967	0,01594528	0,99940501	-4,04455982
ILMN_2159694	HLA-DRB4	-1,18604872	10,0814603	-2,38769032	0,01822555	0,99940501	-4,07185969
ILMN_1662070	HTR3A	-1,20089459	8,57123951	-3,14131413	0,00203416	0,96482818	-3,61726913

Table A.3
List of differentially expressed genes of IL-4 treated OCI-Ly1 STAT6 cell lines based on STAT6 mutational status. Cutoff: log2FC: ±1.0, adj. p-value: <0.0001.

baseMean	log2FoldChange	lfcSE	stat	pvalue	padj	ensembl	hgnc_symbol
1,26826295	3,175329549	0,49018155	6,47786433	9,30E-11	1,10E-08	ENSG00000221867	MAGEA3
8,74609604	2,963651073	0,29327705	10,105295	5,23E-24	6,13E-21	ENSG00000137965	IFI44
1,40595348	2,864617176	0,45771483	6,25851953	3,89E-10	3,97E-08	ENSG00000119917	IFIT3
8,0485527	2,85482033	0,33748499	8,45910317	2,69E-17	1,05E-14	ENSG00000137959	IFI44L
1,06954297	2,735053523	0,51161852	5,34588455	9,00E-08	5,66E-06	ENSG00000166450	PRTG
3,9618332	2,734062065	0,28149624	9,7126061	2,66E-22	2,13E-19	ENSG00000132530	XAF1
6,32166534	2,540108468	0,21031705	12,0775204	1,39E-33	5,28E-30	ENSG00000165949	IFI27
1,91485685	2,473248177	0,36731326	6,73334851	1,66E-11	2,32E-09	ENSG00000134326	CMPK2
0,80064898	2,451688739	0,50087794	4,89478283	9,84E-07	4,71E-05	ENSG00000186472	PCLO
13,3715004	2,440095849	0,18126238	13,4616787	2,63E-41	2,00E-37	ENSG00000173193	PARP14
1,07056679	2,201175376	0,44111532	4,99002251	6,04E-07	3,06E-05	ENSG00000128040	SPINK2
10,3131866	2,193429276	0,20310963	10,7992381	3,47E-27	6,60E-24	ENSG00000155966	AFF2
3,41312034	2,142221555	0,24290692	8,81910462	1,15E-18	5,32E-16	ENSG00000243449	C4orf48
81,8346567	2,084180674	0,14936287	13,9538072	2,98E-44	4,54E-40	ENSG00000157601	MX1
3,00029721	2,033850398	0,28112037	7,23480274	4,66E-13	8,98E-11	ENSG00000158560	DYNC1I1
15,6101786	1,941934028	0,19610256	9,90264487	4,05E-23	3,86E-20	ENSG00000133106	EPSTI1
8,89935896	1,923468975	0,18639246	10,3194571	5,75E-25	7,96E-22	ENSG00000130589	HELZ2
7,61891002	1,901106427	0,16511019	11,5141676	1,12E-30	3,41E-27	ENSG00000187607	ZNF286A
9,51513809	1,799888355	0,20000934	8,99902144	2,28E-19	1,20E-16	ENSG00000177409	SAMD9L
8,86603631	1,77277972	0,26145199	6,78051721	1,20E-11	1,72E-09	ENSG00000171476	HOPX
5,3747446	1,772374988	0,25169915	7,04164073	1,90E-12	3,21E-10	ENSG00000126709	IFI6
7,89714108	1,758256441	0,25988005	6,76564604	1,33E-11	1,88E-09	ENSG00000114737	CISH
2,48579707	1,665767394	0,26879967	6,19705885	5,75E-10	5,65E-08	ENSG00000249459	ZNF286B
9,66043477	1,654311226	0,19414578	8,52097433	1,58E-17	6,34E-15	ENSG00000138496	PARP9
3,6489482	1,635581866	0,22478416	7,27623261	3,43E-13	6,88E-11	ENSG00000144642	RBMS3
2,19729189	1,557345347	0,30167741	5,16228684	2,44E-07	1,36E-05	ENSG00000152778	IFIT5
2,59698524	1,550413501	0,28910702	5,3627668	8,20E-08	5,20E-06	ENSG00000138642	HERC6
2,30447398	1,534554285	0,27827771	5,51447076	3,50E-08	2,45E-06	ENSG00000129116	PALLD
2,8637722	1,427503559	0,2671008	5,34443751	9,07E-08	5,68E-06	ENSG00000185885	IFITM1
20,3345066	1,424167623	0,11454386	12,4333823	1,72E-35	8,74E-32	ENSG00000185507	IRF7
3,49137994	1,407496308	0,22340558	6,30018435	2,97E-10	3,14E-08	ENSG00000232920	LINC01400
3,98382714	1,320805111	0,20997674	6,29024475	3,17E-10	3,28E-08	ENSG00000142089	IFITM3
7,07705179	1,317066744	0,17068614	7,71630771	1,20E-14	3,26E-12	ENSG00000213928	IRF9
10,111431	1,291359027	0,13992481	9,22894968	2,73E-20	1,73E-17	ENSG00000163840	DTX3L
3,1984477	1,247131287	0,2451181	5,08787923	3,62E-07	1,92E-05	ENSG00000160255	ITGB2
21,996204	1,175392164	0,13053433	9,00446794	2,17E-19	1,18E-16	ENSG00000205413	SAMD9
8,36872772	1,137818371	0,15916634	7,14861173	8,77E-13	1,59E-10	ENSG00000108771	DHX58
37,6317091	1,123388548	0,10147398	11,0707054	1,74E-28	3,78E-25	ENSG00000221963	APOL6
3,84114585	1,10246598	0,21066503	5,23326524	1,67E-07	9,83E-06	ENSG00000172345	STARD5
18,6612066	1,05903285	0,09468747	11,1845093	4,86E-29	1,23E-25	ENSG00000185201	IFITM2
4,53213623	1,050849727	0,19866117	5,28965834	1,23E-07	7,32E-06	ENSG00000160062	ZBTB8A
12,3032113	1,042078934	0,12405768	8,39995499	4,47E-17	1,70E-14	ENSG00000165168	CYBB
34,5948058	1,030614913	0,10405254	9,90475536	3,97E-23	3,86E-20	ENSG00000115415	STAT1
12,438649	1,013936506	0,15486087	6,54740267	5,85E-11	7,25E-09	ENSG00000107201	DDX58
60,3729838	-1,048939845	0,15245319	-6,88040597	5,97E-12	8,91E-10	ENSG00000119888	EPCAM
7,49206437	-1,130721086	0,15516439	-7,28724594	3,16E-13	6,42E-11	ENSG00000074416	MGLL
4,04494517	-1,172431971	0,21794442	-5,3794998	7,47E-08	4,84E-06	ENSG00000154319	FAM167A
5,51613992	-1,19652736	0,19547703	-6,12106384	9,30E-10	8,68E-08	ENSG00000232677	LINC00665
4,45739629	-1,220393493	0,21805273	-5,59678146	2,18E-08	1,61E-06	ENSG00000047597	XK
4,30365614	-1,224821382	0,22690051	-5,3980547	6,74E-08	4,42E-06	ENSG00000135074	ADAM19
6,21747011	-1,311720974	0,19250987	-6,81378571	9,51E-12	1,39E-09	ENSG00000227051	C14orf132
6,01978477	-1,314467014	0,17762981	-7,40003596	1,36E-13	2,92E-11	ENSG00000105810	CDK6
4,80416805	-1,382633462	0,20787561	-6,65125387	2,91E-11	3,85E-09	ENSG00000110427	KIAA1549L
4,28905443	-1,530703986	0,22059278	-6,93904829	3,95E-12	6,19E-10	ENSG00000081913	PHLPP1

A.6 Proliferation of OCI-Ly1 STAT6 cell lines

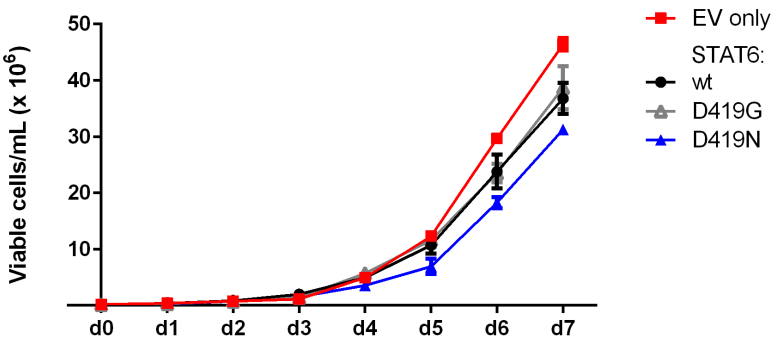

Figure A.7
Growth curves of OCI-Ly1 STAT6 cell lines. No significant differences in proliferation were observed between cell lines *in vitro*. The experiment was performed in biological duplicates and technical duplicates. Viable cell count was analyzed using the Vi-CELL^{TM} XR every 24 h. Moreover, cell lines were stimulated every 24 h with IL-4 for 20 min, followed by one-time washing, and further incubation for 24 h in absence of IL-4. EV: empty vector, wt: wild-type.

B Acknowledgement

My special thanks goes to PD Dr. Ursula Zimber-Strobl for being my supervisor and giving me the opportunity to perform my PhD program. Her vision and encouragement greatly formed this work. Moreover, her guidance taught me how to tackle the challenges ahead and helped me to become more self-reliant and well-structured.

Additionally, I want to express my thanks to Dr. Oliver Weigert and Dr. Deepak Bararia for their great scientific advice and their mentorship. Their outstanding knowledge and experience in so many techniques helped me to succeed this project.

Dr. Lothar Strobl for his scientific input and helpful discussions. His interest in this project provided new ideas and perspectives.

Michael Heide and Sebastian Tschuri for introducing me to the laboratory and to many techniques. Their hints and help made the big difference in the end.

Will Keay for great company during late hours and weekend work, as well as Stefan Alig, Sarah Häbe, Verena Passerini, and Elisabeth Silkenstedt for making my lab life much more enjoyable.

Furthermore, I want to thank all the collaborators of this project for their contributions: Dr. Robert Kridel, Prof. Dr. Randy Gascoyne, Dr. Anette Staiger, and Prof. Dr. German Ott for providing patient gene expression data.

Christoph Ziegenhain and Prof. Dr. Wolfgang Enard for their help and advice regarding the RNA sequencing experiment.

Prof. Dr. Wolfram Klapper for performing immunohistochemistry.

Finally, I want to thank my wife Hannah for her constant support, patience, and importantly her motivation in difficult times.